

## Accepted Manuscript

The crustal architecture of Myanmar imaged through zircon U-Pb, Lu-Hf and O isotopes: Tectonic and metallogenic implications

Nicholas J. Gardiner, Michael P. Searle, Christopher K. Morley, Laurence J. Robb, Martin J. Whitehouse, Nick M.W. Roberts, Christopher L. Kirkland, Christopher J. Spencer



PII: S1342-937X(18)30049-2  
DOI: doi:[10.1016/j.gr.2018.02.008](https://doi.org/10.1016/j.gr.2018.02.008)  
Reference: GR 1925

To appear in:

Received date: 22 January 2018  
Revised date: 28 February 2018  
Accepted date: 28 February 2018

Please cite this article as: Nicholas J. Gardiner, Michael P. Searle, Christopher K. Morley, Laurence J. Robb, Martin J. Whitehouse, Nick M.W. Roberts, Christopher L. Kirkland, Christopher J. Spencer , The crustal architecture of Myanmar imaged through zircon U-Pb, Lu-Hf and O isotopes: Tectonic and metallogenic implications. The address for the corresponding author was captured as affiliation for all authors. Please check if appropriate. Gr(2018), doi:[10.1016/j.gr.2018.02.008](https://doi.org/10.1016/j.gr.2018.02.008)

This is a PDF file of an unedited manuscript that has been accepted for publication. As a service to our customers we are providing this early version of the manuscript. The manuscript will undergo copyediting, typesetting, and review of the resulting proof before it is published in its final form. Please note that during the production process errors may be discovered which could affect the content, and all legal disclaimers that apply to the journal pertain.

*GR Focus Review: Special Issue on Tethyan Orogenesis and Metallogeny*

## **The crustal architecture of Myanmar imaged through zircon U-Pb, Lu-Hf and O isotopes: Tectonic and metallogenic implications**

Nicholas J. Gardiner<sup>1,2,3,4\*</sup>, Michael P. Searle<sup>4</sup>, Christopher K. Morley<sup>5</sup>, Laurence J. Robb<sup>4</sup>, Martin J. Whitehouse<sup>6</sup>, Nick M.W. Roberts<sup>7</sup>, Christopher L. Kirkland<sup>1,2,3</sup>, Christopher J. Spencer<sup>2</sup>

1. Centre for Exploration Targeting – Curtin Node, Department of Applied Geology, Western Australian School of Mines, Curtin University, Perth, WA 6102, Australia.

2. The Institute for Geoscience Research (TIGeR), Department of Applied Geology, Curtin University, GPO Box U1987, Perth WA 6845, Australia.

3. Australian Research Council Centre of Excellence for Core to Crust Fluid Systems, Australia.

4. Department of Earth Sciences, University of Oxford, Oxford OX1 3AN, United Kingdom.

5. Department of Geological Sciences, Chiang Mai University, Thailand.

6. Swedish Museum of Natural History, Box 50007, SE-104 05 Stockholm, Sweden.

7. NERC Isotope Geosciences Laboratory, British Geological Survey, Keyworth, Nottingham NG12 5GG, United Kingdom.

\*Corresponding author. E-mail address: [nicholas.gardiner@curtin.edu.au](mailto:nicholas.gardiner@curtin.edu.au)



## Abstract

The Tethys margin in central and eastern Asia is comprised of continental terranes separated by suture zones, some of which remain cryptic. Determining the crustal architecture, and therefore the geological history, of the Eastern Tethyan margin remains challenging. Sited in the heart of this region, Myanmar is a highly prospective but poorly explored minerals jurisdiction. A better understanding of Myanmar's mineralization can only be realized through a better understanding of its tectonic history, itself reflected in at least four major magmatic belts. The Eastern and the Main Range Provinces are associated with the Late Permian to Early Triassic closure of Palaeo-Tethys. The Mogok–Mandalay–Mergui Belt and Wuntho–Popa Arc are a response to the Eocene closure of Neo-Tethys. However, magmatic ages outside these two orogenic events are also recorded. We present new zircon U-Pb, Lu-Hf and O isotope data from magmatic rocks across Myanmar, which we append to the existing dataset to isotopically characterize Myanmar's magmatic belts. Eastern Province Permian I-type magmatism has evolved  $\epsilon_{\text{Hf}}$  (-10.9 to -6.4), while Main Range Province Triassic S-type magmatism also records evolved  $\epsilon_{\text{Hf}}$  (-13.5 to -8.8). The Mogok-Mandalay-Mergui Belt is here divided into the Tin Province and the Mogok Metamorphic Belt. The Tin Province hosts ca. 77–50 Ma magmatism with evolved  $\epsilon_{\text{Hf}}$  (-1.2 to -15.2), and  $\delta^{18}\text{O}$  of 5.6–8.3 ‰. The Mogok Metamorphic Belt exhibits a more complex magmatic and metamorphic history, and granitoids record Jurassic, Late Cretaceous, and Eocene to Miocene phases of magmatism, all of which exhibit evolved  $\epsilon_{\text{Hf}}$  values between -4.6 and -17.6, and  $\delta^{18}\text{O}$  between 6.3 and

9.2 ‰. From the Tagaung-Myitkyina Belt, we report a magmatic age of 172 Ma and  $\epsilon_{\text{Hf}}$  of 18.1 to 10.8. To accommodate the geological evidence, we propose a tectonic model for Myanmar involving a greater Sibumasu – where the documented zircon isotopic variations reflect compositional variations in magmatic source – and invoke the role of the Tengchong Block. The Baoshan Block and Greater Sibumasu were likely assembled on or before the Triassic, a former Andean margin and suture which may lie across the Northern Shan Plateau, and reflected in isotopic differences between the northern and southern parts of the Mogok Metamorphic Belt. This contiguous Sibumasu–Baoshan Block then sutured onto the Indochina margin in the Late Triassic. We propose that a Tengchong Block within Myanmar provides for a southerly termination of the Meso-Tethys suture immediately north of the Mogok area. A discrete Tengchong Block may explain a discontinuous arc of Late Triassic to Jurassic I-type magmatism in central Myanmar, representing an Andean-type margin sited above a subducting Meso-Tethys on the margin of Sibumasu. The Tengchong Block sutured onto Greater Sibumasu before the Late Cretaceous, after which subduction of Neo-Tethys drove the magmatism of the Wuntho-Popa Arc and ultimately that of the Tin Province. The metallogenic character of granite belts in Myanmar reflects the crustal architecture of the region, which is remarkable for its prolific endowment of granite-hosted Sn-W mineralization in two quite distinct granite belts related to sequential Indosinian and Himalayan orogenesis.

**Keywords** Myanmar Burma; Tethys tectonics; zircon U-Pb Hf O; Himalayas; Indosinian; Yunnan

## 1. Introduction

Isotope geochemistry and geochronology are techniques particularly applicable to deciphering the crustal architecture of cryptic terranes. They can provide information both on the timing, and style, of magmatism whose genesis may be driven through tectonic processes. Isotope geochemistry may also give insight into the geochemical nature of the underlying continental crust which provides a source component to that magmatism. The geological architecture of the Mesozoic to Cenozoic Eastern Tethyan margin within central–eastern Asia is highly complex. The margin is comprised of continental ribbon terranes which accreted onto the Asian continent during the closure of the various ocean basins of Tethys (Gardiner et al., 2015; Hall, 2012; Metcalfe, 2013; Searle and Morley, 2011). The modern Tethyan margin in central and eastern Asia is thus a collage of continental and island arc terranes separated by suture zones. Some of these suture zones remain cryptic in places, in that there is no direct geological evidence of a former ocean basin in the form of, for example, ophiolitic material, or deep oceanic sediments such as cherts, whose presence may represent the surface expression of the suture. Determining the crustal architecture, and therefore the geological history, of the Eastern Tethyan margin within Southeast Asia remains challenging.

The main Tethyan-related suture zones in Asia extend east–west across the Tibetan Plateau (Hodges, 2000; Searle et al., 2011). These sutures turn south into Southeast Asia around the Eastern Himalayan Syntaxis at Namche Barwa (Searle et al., 2017). Myanmar (Burma) lies at the heart of this key

tectonic region, and many of the Tethyan suture zones, and associated magmatic-metamorphic belts, recognized in Tibet, may be traced south through Myanmar into Thailand and the Malay Peninsula (Gardiner et al., 2016c; Searle and Morley, 2011; Searle et al., 2007; Sone and Metcalfe, 2008; Wai-Pan Ng et al., 2015a; Wai-Pan Ng et al., 2015b) (Figure 1). However, some suture zones interpreted as relating to the closure of Tethys, and which are identifiable within Tibet, remain unconstrained within Southeast Asia, particularly within Myanmar, rendering their precise location, or even their existence, equivocal. To further hinder geological restoration, some of the crustal units within Southeast Asia have experienced Cenozoic clockwise rotation and an oblique tectonic history of collision due to the northwards motion of India (e.g., Replumaz and Tapponnier, 2003). This rotation has been accommodated by the development of major strike-slip faults in the region.

Myanmar is a highly prospective minerals jurisdiction. It contains significant known deposits of tin, tungsten, copper, gold, zinc, lead, nickel, silver, jade and gemstones (Barber et al., 2017a; Chhibber, 1934; Gardiner et al., 2014; Khin Zaw, 2017; Soe Win and Malar Myo Myint, 1998), the metallogensis of much of which is tied to its Mesozoic to Cenozoic tectonic history. However, the country remains relatively poorly explored, at least with modern exploration methods. A better understanding of both the genesis of Myanmar's mineralization, and thus of its mineral potential, can only be fully realized with an understanding of its tectonic history.

In this contribution, we present new zircon U-Pb, Lu-Hf and O isotope data from magmatic rocks sampled from across Myanmar. We append this data to an existing published dataset, to provide an isotopic characterization through zircon geochemistry, of the major magmatic belts of Myanmar. This dataset is interpreted in order to provide an account of the nature of crust and the architecture of the major tectonic blocks of the region, and to inform on the timing and style of accretion and collision. In doing so, we aim to bring some clarity both about what is currently understood but, perhaps more pertinently, about what questions still remain open.

### 1.1. Zircon Isotopes: A Users Guide

The accessory mineral zircon provides an exceptional record of magmatic evolution (Belousova et al., 2010; Kemp et al., 2007; Roberts and Spencer, 2015; Scherer et al., 2007). Modern *in-situ* analytical techniques such as secondary ionization mass spectrometry (SIMS), and laser-ablation (multi-collector) inductively coupled plasma mass spectrometry (LA-(MC)-ICP-MS), allow the precise measurement of U-Pb, Lu-Hf, and O isotope ratios, and of trace element concentrations, within zoned zircon grains, which arguably exhibit greater fidelity to magmatic source and differentiation processes than whole-rock isotope analysis. Zircon grains are robust and survive weathering processes, thus even highly degraded outcrops of magmatic rocks, such as those found in monsoonal southeast Asia, may offer zircon crystals from which useful information may be derived.

Zircon crystals can be precisely dated through U-Pb geochronology, yielding a magmatic age, and in some cases an inherited age, for the host rock. The

Lu–Hf isotopic system, commonly measured in zircons, is highly sensitive to crustal differentiation processes (Hawkesworth and Kemp, 2006; Scherer et al., 2007). The Hf isotopic signature, expressed as  $\epsilon_{\text{Hf}}$ , provides a measure of magma source composition. It may indicate the extent to which the melt was either comprised of juvenile material, i.e. close to mantle value and enriched in radiogenic  $^{176}\text{Hf}$ , or was derived from an evolved, typically dominantly crustal source. Hf isotopes can also be used to calculate a two-stage Hf model age ( $T_{\text{DM}^2}$ ), which may give some indication of the timing of original extraction of that crustal packet from the mantle. The stable isotopes of O (usually  $^{18}\text{O}/^{16}\text{O}$  ratio, expressed as  $\delta^{18}\text{O}_{\text{V-SMOW}}$ ) are also sensitive to magma source. Values above a mantle signature of  $\delta^{18}\text{O} = 5.3 \pm 0.6 \text{ ‰}$  ( $2\sigma$ , Valley, 2003) fingerprint a contribution from  $^{18}\text{O}$ -enriched material which has experienced (low-temperature) surface processes, thereby indicating a greater supracrustal component in the melt. Oxygen isotope analysis in zircon can therefore be used to “screen” Hf isotope data for such supracrustal contamination of the magma, and to identify where a Hf model age may represent a mixing of source materials, rather than yielding a discrete crust-forming episode (Dhuime et al., 2012; Kemp et al., 2006).

Thus, a combination of zircon U–Pb, Lu–Hf and O isotope analysis from magmatic rocks allows the measurement of the age of magmatism, the characterization of magma source, and the determination of a Hf model age. These parameters permit the comparison of rocks which may have different magmatic ages but which are ultimately derived from the same crustal block, and vice-versa. We apply these techniques to samples of magmatic rocks from across Myanmar.

## 2. Geological Background

Myanmar has been affected by at least two major Tethyan-related suturing events. The closure of Palaeo-Tethys, interpreted as occurring in the Late Permian to Early Triassic, involved the collision of the Sibumasu block with Indochina and resulted in the Indosinian Orogeny and associated magmatism found in Eastern Myanmar, Northern Thailand, and further south in the Malay Peninsula (Gardiner et al., 2016c; Macdonald et al., 1993a; Metcalfe, 2000; Mitchell, 1977; Searle et al., 2012; Sone and Metcalfe, 2008; Wai-Pan Ng et al., 2015b). The Early Eocene closure of Neo-Tethys initiated the collision of India with Asia and resulted in the Himalayan Orogeny (Mitchell, 1993; Morley, 2012; Searle and Morley, 2011). The Neo-Tethys suture zone wraps around the Eastern Himalayan Syntaxis, and may reappear along the western Mount Victoria-Kawlung Belt (Searle et al., 2017). As a result of these orogenic events, major Tethyan-related metamorphic belts extend south from the Eastern Himalayan Syntaxis across Myanmar, and which may be correlated with those lying further west along the main India-Asia collision zone. The Himalayan Orogeny in particular is associated with significant regional crustal thickening and metamorphism (Morley, 2012; Searle and Morley, 2011; Searle et al., 2017; Searle et al., 2007; Sone and Metcalfe, 2008).

The major magmatic belts outcropping within Myanmar are, from east to west (Figure 2A) (a) the Eastern Province and (b) the Main Range Province, or Central Belt, associated with the closure of Palaeo-Tethys and the Indosinian Orogeny, a result of which collision granite magmatism peaked at ca. 220 Ma; (c) the Mogok–Mandalay–Mergui Belt and (d) the Wuntho–Popa, or Popa–

Loimye, Arc, which are both related to the subduction of Neo-Tethys which closed ca. 50 Ma, and the Himalayan Orogeny (Cobbing et al., 1986; Gardiner et al., 2015; Khin Zaw, 1990; Mitchell, 1977). The Mogok–Mandalay–Mergui Belt is here subdivided into, and discussed as, the northern Mogok Metamorphic Belt and the southern Tin Province. However, magmatic ages from across Myanmar have been recorded outside the two major Tethyan suturing events and ensuing periods of orogeny (e.g., Barley et al., 2003; Mitchell et al., 2012). Open questions therefore remain regarding the geological events to which their timing relates.

### **3. Samples, Analytical Methods and Results**

#### **3.1. Samples**

In this study we report new zircon U-Pb, Hf and O isotope data from magmatic rock samples sourced from three of Myanmar's magmatic belts: (a) the Mogok–Mandalay–Mergui Belt (Mogok Metamorphic Belt and Tin Province); (b) the Wuntho–Popa Arc; and (c) a sample from the Tagaung-Myitkyina Belt, taken from near Myitkyina, in Kachin State, northern Myanmar. Samples are detailed in Table 1, and Figure 2B shows a map of sample localities.

Samples MY1, MY4, MY9 and MY106 are taken from granitoids intruding into the Mogok Metamorphic Belt, central Myanmar (Figure 2B). Sample MY1 is of the Payangazu Granite, which outcrops ~150 km south of Mandalay, and which is a biotite-bearing granite which locally intrudes the sillimanite-grade metamorphic rocks of the Mogok Metamorphic Belt (Mitchell et al., 2012). Sample MY4 is taken from the Nattaung Granite, located in Nattaung Quarry



~200 km south of Mandalay. The Nattaung Granite outcrops as weakly foliated biotite granite sheets which intrude the schists and augen gneiss of the Mogok Metamorphic Belt (Mitchell et al., 2007). Sample MY106 was taken from the Kabaing Granite, a biotite microgranite outcropping immediately west of Mogok town. The Kabaing Granite intrudes the high-grade marbles of the Mogok Metamorphic Belt, and hosts numerous topaz-bearing pegmatites. This granite has previously been dated through SIMS zircon U-Pb geochronology, recording a magmatic age of  $16.8 \pm 0.5$  Ma (Gardiner et al., 2016a), and which compares well with an Ar-Ar cooling age of 15.8 Ma (Bertrand et al., 2001). Sample MY1 is the Byingye Granite, and records a complex magmatic history, as discussed below.

Samples MY34, MY37 and MYYAD are of granites located within the Tin Province, southern Myanmar (Figure 2B). Samples MY34 and MY37 were taken from roadside quarries on the main Dawei to Myeik road. Sample MYYAD is from the host granite outcropping within the Yadanabon tin mine in southern Myanmar, close to the Thai border. All these Tin Province samples have Cenozoic magmatic ages (MY34:  $62.3 \pm 0.6$  Ma; MY37:  $69.5 \pm 1.0$  Ma; MYYAD:  $50.3 \pm 0.6$  Ma) previously determined through SIMS zircon U-Pb geochronology (Gardiner et al., 2016a).

MY145 is a diorite porphyry sampled from the Shangalon Cu–Au district, situated within the northern part of the Wuntho–Popa Arc. The diorite intrudes into the mid-Cretaceous (ca. 105–95 Ma) granodiorite which predominates the Wuntho Massif (Figure 2B), and has a zircon U-Pb magmatic age of  $40.0 \pm 0.2$  Ma (Gardiner et al., 2016a). Sample MY182 is a dacite porphyry from

Kachin State, and is located within the Tagaung-Myitkyina Belt. The sample location of MY182 lies on the eastern bank of the Irrawaddy, immediately east of the Myitkyina ophiolite, and north of Myitkyina town (Figure 2B).

### 3.2. Analytical Methodology

Zircon crystals from all samples were separated by crushing and then a combination of magnetic and heavy liquids techniques on the sub 500 micron fraction. Selected zircon grains were mounted in epoxy resin and polished. Grains were imaged under cathodoluminescence to reveal internal textures. U-Pb geochronology on zircon from samples MY1, MY4 and MY9 was undertaken using the large geometry Cameca IMS1280 ion microprobe at the NordSIMS facility, Swedish Museum of Natural History, Stockholm. Analytical methodology is found in Appendix A. U-Pb analysis of zircon from sample MY182 was undertaken using the Laser Ablation Inductively Coupled Plasma Mass Spectrometry (LA-ICP-MS) GeoHistory Facility at the John De Laeter Centre, Curtin University, Perth, as detailed in Appendix B.

All zircon Lu-Hf isotope analyses were undertaken via Laser Ablation Multi-Collector Inductively Coupled Plasma Mass Spectrometry (LA-MC-ICP-MS). Lu-Hf isotope analysis of zircon from samples MY1, MY4, MY9, MY106, MY34, MY37, MYYAD, and MY145 was undertaken at the NERC (Natural Environment Research Council) Isotope Geosciences Laboratory (NIGL), British Geological Survey, Keyworth, UK. A detailed description of the methodology is provided in Appendix C. Lu-Hf isotope analysis of zircon from sample MY180 was undertaken at the Geohistory Facility at Curtin University, Perth, Australia, and follows the procedures outlined in Appendix B. Zircon O

isotope analysis for samples MY1, MY4, MY106, MY145 was also undertaken using the Cameca IMS1280 ion probe facility at NordSIMS following the method outlined in Appendix D. Full analytical results are presented in Tables 2, 3 and 4.

For each main group of zircon U-Pb age analyses, a U-Pb concordia age is calculated from the  $^{204}\text{Pb}$ -corrected isotopic ratios, and is reported along with the MSWD of combined equivalence and concordance as calculated using Isoplot (Ludwig, 2004). In addition for those analyses, which scatter away from the main population,  $^{207}\text{Pb}$ -corrected ages are provided as a means to discuss the dissimilarity of analyses from the main population. All calculated U-Pb ages are presented at the  $2\sigma$  level. Terra-Wasserburg U-Pb concordia plots for those samples with new age data reported here are presented in Figure 3. Initial  $^{176}\text{Hf}/^{177}\text{Hf}$  ratios were calculated using the decay constant of Scherer et al. (2001). All two-stage Hf model ages ( $T_{\text{DM}^2}$ ) are calculated using the calculated concordia age and a  $^{176}\text{Lu}/^{177}\text{Hf}$  of 0.015.

### 3.3. Zircon U-Pb, Lu-Hf and O Isotope Results

#### 3.3.1. Mogok–Mandalay–Mergui Belt (MMM)

Eight U-Pb analyses from discrete zircon grains separated from sample MY1 (Payangazu Granite) yielded a concordia age of  $55.02 \pm 0.53$  Ma (MSWD = 1.7) (Figure 3A). Three older analyses with  $^{207}\text{Pb}$ -corrected ages ranging from 63.2–64.8 Ma, and one younger analysis with a  $^{207}\text{Pb}$ -corrected age of 49.8 Ma, interpreted to reflect minor inheritance or radiogenic-Pb loss respectively, were excluded from the concordia age calculation. This age of 55 Ma for MY1

is similar to the 50 Ma date reported for a dacite dyke from the same area, and younger than the ca. 121–128 Ma age from an adjacent granodiorite intrusion (Barley et al., 2003; Mitchell et al., 2012). Eight zircon Hf isotope analysis of MY1 yield a mean  $\epsilon_{\text{Hf}}$  of -13.3, with a maximum and minimum  $\epsilon_{\text{Hf}}$  of -9.68 and -15.30 respectively. These Hf isotope data resolve to two-stage Hf model ages ( $T_{\text{DM}^2}$ ) of 1.74–2.09 Ga, with a mean of 1.97 Ga. Thirteen zircon O isotope analyses of sample MY1 range in  $\delta^{18}\text{O}$  from 6.14–8.03 ‰, with a mean  $\delta^{18}\text{O}$  of  $7.3 \pm 0.3$  ‰.

Ten zircon U-Pb analyses from Sample MY4 (Nattaung Granite) yield a concordia age of  $71.12 \pm 0.55$  Ma (MSWD 1.5) (Figure 3B). This is interpreted as the magmatic age, and is identical to that of 71.8 Ma reported from the same granite outcrop by Mitchell et al. (2012). Ten zircon Hf isotope analyses from MY4 range in  $\epsilon_{\text{Hf}}$  from -17.56 to -14.80, with a mean  $\epsilon_{\text{Hf}}$  of -15.9. These data resolve to two-stage Hf model ages ( $T_{\text{DM}^2}$ ) of 2.07–2.24 Ga, with a mean of 2.14 Ga. The evolved Hf isotope signal (negative  $\epsilon_{\text{Hf}}$ ) of MY4 is consistent with the reworking of an older crustal source as also implied by a whole-rock  $\epsilon_{\text{Nd}}$  value of -7.1 from the same locality (Mitchell et al., 2012). Thirteen zircon O isotope analyses from MY4 range in  $\delta^{18}\text{O}$  from 8.70–9.09 ‰ with a mean  $\delta^{18}\text{O}$  of  $8.9 \pm 0.3$  ‰.

Sample MY9 (Bying Granite) records a complex magmatic history. Three distinct zircon U-Pb age clusters from different zircon domains range from the Late Triassic through to the Late Cretaceous. Nine analyses have  $^{207}\text{Pb}$ -corrected ages of 54–81 Ma, of which five give a calculated concordia age of  $71.84 \pm 1.1$  Ma (MSWD 2.1) (Figure 3C). Four analyses give a calculated

concordia age of  $123.4 \pm 2.0$  Ma (MSWD 2.2) (Figure 3D). Twelve analysis resolve to a calculated concordia age of  $218.9 \pm 2.5$  Ma (MSWD 1.9) (Figure 3E). Four zircon Hf isotope analysis corresponding to the 72 Ma age group in MY4 range in  $\epsilon\text{Hf}$  from -15.01 to -13.03, with a mean  $\epsilon\text{Hf}$  of -15.0, corresponding to  $T_{\text{DM}^2}$  of 1.96–2.14 Ga with a mean of 2.08 Ga. Three zircon Hf isotope analysis corresponding to the 123 Ma age grouping range in  $\epsilon\text{Hf}$  from -10.15 to -9.30, with a mean  $\epsilon\text{Hf}$  of -9.7, corresponding to  $T_{\text{DM}^2}$  of 1.77–1.82 Ga, mean 1.79 Ga. Eleven zircon Hf isotope analysis corresponding to the 219 Ma age grouping range in  $\epsilon\text{Hf}$  from -17.15 to -12.26, with a mean  $\epsilon\text{Hf}$  of -13.4, corresponding to  $T_{\text{DM}^2}$  of 2.03–2.33 Ga, mean 2.10 Ga.

Sample MY106, the Kabaing Granite, yields one of the youngest magmatic ages reported within the Mogok Metamorphic Belt at  $16.8 \pm 0.5$  Ma (Gardiner et al., 2016a). Ten zircon Hf isotope analysis from previously dated grains in MY106 range in  $\epsilon\text{Hf}$  from -9.25 to -4.56, with a mean  $\epsilon\text{Hf}$  of -7.3. These data resolve to  $T_{\text{DM}^2}$  of 1.38–1.68 Ga, with a mean of 1.56 Ga. Twelve zircon O isotope analyses from MY106 range in  $\delta^{18}\text{O}$  from 7.81–9.02 ‰ with a mean  $\delta^{18}\text{O}$  of  $8.5 \pm 0.3$  ‰. In summary, zircon U-Pb isotopes on samples sourced from granites which intrude the Mogok Metamorphic Belt yield zircon U-Pb magmatic ages ranging from 218–17 Ma. They have uniformly evolved (i.e. negative)  $\epsilon\text{Hf}$ , and heavy (greater than mantle value)  $\delta^{18}\text{O}$ .

Zircon crystals taken from granites found within the Tin Province have U-Pb magmatic ages reported in Gardiner et al. (2016a). Sample MY34 has a magmatic age of  $62.3 \pm 0.6$  Ma. Fifteen zircon Hf isotope analyses on this previously dated sample reveal a spread in  $\epsilon\text{Hf}$  from -12.29 to -10.64, with a

mean of -11.4. These data give  $T_{DM}^2$  of 1.80–1.90 Ga with a mean of 1.85 Ga. Sample MY37 yielded a magmatic age of  $69.5 \pm 1.0$  Ma. Six zircon Hf isotope analyses indicate a spread in  $\epsilon_{Hf}$  from -14.09 to -9.21, with a mean  $\epsilon_{Hf}$  of -11.8. These data yield  $T_{DM}^2$  of 1.72–2.02 Ga with a mean of 1.88 Ga. A sample of the Yadanabon Granite, MYYAD, has a previously reported magmatic age of  $50.3 \pm 0.6$  Ma. Eleven zircon Hf isotope analyses from MYYAD range in  $\epsilon_{Hf}$  from -11.38 to -9.27, with a mean  $\epsilon_{Hf}$  of -10.3. These data indicate  $T_{DM}^2$  of 1.71–1.84 Ga and a mean of 1.78 Ga. Thus, samples from granites found within the Tin Province also yield highly evolved zircon Hf isotope signatures.

### 3.3.2. *Wuntho-Popa Arc (WPA)*

We present new data on one diorite sample (MY145) from the Wuntho Popa Arc, which has a reported Eocene zircon U-Pb magmatic age of  $40.0 \pm 0.2$  Ma (Gardiner et al., 2016a). Fourteen zircon Hf isotope analysis range in  $\epsilon_{Hf}$  from -0.03 to 5.32, with a mean  $\epsilon_{Hf}$  of 1.9. These data yield  $T_{DM}^2$  of 0.77–1.12 Ga and a mean of 0.99 Ga. Sixteen zircon O isotope analyses from MY145 give a spread in  $\delta^{18}O$  values from 5.31–5.79 ‰ with a mean  $\delta^{18}O$  of  $5.5 \pm 0.4$  ‰, all within uncertainty of the mantle value (Valley, 2003).

### 3.3.3. *Tagaung-Myitkyina Belt (Kachin State)*

Eighteen zircon U-Pb analyses sited on oscillatory zoned zircon grains from sample MY182 analysis yield a concordia age of  $172.0 \pm 1.3$  Ma (MSWD 0.55) (Figure 3F). Four zircon U-Pb analyses with both younger  $^{207}Pb$ -corrected ages (164 and 170 Ma) and older (187 and 191 Ma) ages were

excluded from the calculated concordia age. These older and younger dates are interpreted to reflect minor inheritance and radiogenic Pb loss respectively. Eighteen zircon Hf isotope analyses range in  $\epsilon\text{Hf}$  from 10.84 to 18.06, with a mean  $\epsilon\text{Hf}$  of 15.3. These data indicate  $T_{\text{DM}^2}$  of 0.06–0.52 Ga and a mean of 0.24 Ga.

#### 4. Isotopic Trends of Myanmar's Magmatic Belts

##### 4.1. Isotopic Characteristics and Geodynamic Implications

A space-time diagram of ages of magmatism derived from zircon U-Pb ages from across the major magmatic belts outcropping within Myanmar (Wuntho-Popa Arc, Mogok-Mandalay-Mergui Belt, Tagaung-Myitkyina Belt, Main Range Province and Eastern Province) is shown in Figure 4. To the isotope data presented in this paper we add previously reported zircon U-Pb, Lu-Hf and O isotope data, and use this dataset to isotopically characterize Myanmar's magmatic belts (summarized in Table 5), to frame the discussion. We also provide an outline geological map of Myanmar in Figure 5.

##### 4.1.1. *Palaeo-Tethyan Magmatic Belts*

The Eastern Province and the Main Range Province, the two magmatic belts associated with the Late Permian to Early Triassic suturing of Palaeo-Tethys and the ensuing Indosinian Orogeny, record the collision of the Sibumasu Block with Indochina (Cobbing, 2005; Cobbing et al., 1986; Gardiner et al., 2016c; Metcalfe, 2000; Sone and Metcalfe, 2008). These two magmatic belts outcrop within eastern Myanmar (Figure 2) (Gardiner et al., 2016c), and

extend southwards into northern Thailand and the Malay Peninsula (Searle et al., 2012; Wai-Pan Ng et al., 2015a; Wai-Pan Ng et al., 2015b). Magmatic belts with similar mineralogical characteristics and magmatic ages are reported further north in Yunnan, where they are collectively termed the Nujiang–Lancanjiang–Jishajiang Belts (Dong et al., 2013; Zi et al., 2012). An accreted terrane, termed the Sukothai Arc, is interpreted as having developed on the western flanks of Indochina (Barr and Macdonald, 1991). The Sukothai Arc is bounded by Palaeo-Tethys suture zones on either side (Sone and Metcalfe, 2008).

The granitoids which make up the Main Range Province are dominantly S-type (Cobbing et al., 1986; Wai-Pan Ng et al., 2015a), and have been dated in Thailand and Malaysia at 220–200 Ma (Figure 4) (Ahrendt et al., 1997; Dunning et al., 1995; Gardiner et al., 2016c; Wang et al., 2016), and in eastern Myanmar at ca. 220 Ma (Gardiner et al., 2016c), interpreted as peak post-collisional magmatism, and providing a minimum age of ocean closure. These ages are similar to those interpreted for the Bentong–Raub suture in Malaysia (Wai-Pan Ng et al., 2015a; Wai-Pan Ng et al., 2015b).

In northern Thailand, the Main Range Province exhibits a core of strongly-deformed mid-crustal gneisses and migmatites, termed the “North Thailand Migmatite Complex” (Dunning et al., 1995; Macdonald et al., 1993b) (the high-grade metamorphics indicated in Figure 5). Late Cretaceous (ca. 80–70 Ma), and Oligocene (34–24 Ma) ages calculated from both zircon and monazite U-Pb dating have also been recorded in granites and gneisses within the



Inthanon Zone, reflecting minor magmatism likely related to the era of Neo-Tethys (Figure 4) (Dunning et al., 1995; Gardiner et al., 2016b).

In contrast to the Main Range Province, Eastern Province granitoids are of I-type affinity, and record older U-Pb magmatic ages of Permian-Mid Triassic (290–220 Ma) (Wai-Pan Ng et al., 2015a; Wai-Pan Ng et al., 2015b); review in Morley (2012)). An outcrop of the Tachileik Granite in Myanmar, interpreted as part of the Eastern Province, has a zircon U-Pb magmatic age of 266 Ma (Gardiner et al., 2016c).

Limited zircon Hf and O isotope data have been reported from across the Eastern Province and the Main Range Province. Two granite samples from the Main Range Province in eastern Myanmar have a measured zircon  $\epsilon\text{Hf}$  of -9.6 and -10.5 (Gardiner et al., 2016c). The Tachileik Granite records zircon  $\epsilon\text{Hf}$  of -12.4 (Gardiner et al., 2016c). Triassic age granites from within the Inthanon Zone yielded zircon  $\epsilon\text{Hf}$  of -5.4 to -21.0 and  $\delta^{18}\text{O}$  between 6.5–9.9 ‰ (Wang et al., 2016). These samples all resolve to  $T_{\text{DM}^2}$  of ca. 1.6–1.9 Ga.

In summary, the Eastern Province comprises dominantly Triassic to Permian I-type magmatism, with evolved  $\epsilon\text{Hf}$  values (-10.9 to -6.4), whilst the Main Range Province hosts younger Triassic S-type magmatism (220–230 Ma), and also records highly evolved zircon  $\epsilon\text{Hf}$  (-13.5 to -8.8) and elevated zircon  $\delta^{18}\text{O}$  of 7–10 ‰. Evolved  $\epsilon\text{Hf}$  is typical of magmatism in continent-collision zones, where the reworking of existing crustal material predominates magmatic sources.

#### 4.1.2. *Neo–Tethyan Magmatic Belts*

The two late Mesozoic to Cenozoic magmatic belts outcropping within Myanmar (Figure 2A) are the Wuntho–Popa Arc and the Mogok–Mandalay–Mergui Belt, the latter is also known as the Western Belt (Cobbing et al., 1986) or Central Belt (Khin Zaw, 1990). These two belts have been linked to the closure and suturing of Neo-Tethys (Gardiner et al., 2015; Mitchell, 1993; Mitchell et al., 2012; Searle et al., 2017). The Wuntho–Popa Arc is a discontinuous magmatic arc that extends north-south for ~1100 km in western Myanmar (Figure 5), and comprises Mesozoic to Neogene intrusive and volcanic rocks. It is marked by three Pliocene to Quaternary calc-alkaline stratovolcanoes (Mounts Popa, Taung Thonlon and Loimye), although Mount Loimye was active in the Eocene (Chhibber, 1934). Prior to this recent magmatic activity, four major magmatic epochs have been recorded in the Wuntho–Popa Arc on the basis of zircon U-Pb ages: Mid–Late Cretaceous (105–95 Ma, and 70 Ma); Eocene (ca. 40 Ma); Miocene (ca. 19–16 Ma); and Neogene volcanism (Figure 4) (Barley et al., 2003; Gardiner et al., 2017a; Gardiner et al., 2016a; Lee et al., 2016; Maury et al., 2004; Mitchell et al., 2012). Wuntho–Popa Arc magmatism may also include the period 70–40 Ma on the evidence from recent U-Pb studies of both drill core samples, and of detrital zircons inferred to be derived from the Arc (Wang et al., 2014; Zhang et al., 2017).

Limited Hf and O isotope studies have been reported from the magmatic rocks of the Wuntho-Popa Arc. Gardiner et al. (2017a) undertook zircon Hf isotope analysis of four samples of Late Cretaceous (102–98 Ma) intrusive

rocks, reporting juvenile  $\epsilon\text{Hf}$  (positive) of between 13.3 to 6.4 (Figure 7), and which resolved to calculated Hf model ages ( $T_{\text{DM}^2}$ ) of 0.3–0.8 Ga. The Eocene diorite from the Shangalon mine site (MY145) also records zircon  $\epsilon\text{Hf}$  of 5.3 to 0.3 (Figure 7). These Hf values are similar to those analyzed in detrital zircons from the Chindwin Basin by Wang et al. (2014), who interpreted their origin to be the magmatic rocks of the Wuntho-Popa Arc (pink domain, Figure 7). The Chindwin detrital zircon samples record a span of U-Pb ages from the Late Cretaceous to the Eocene, and all have positive  $\epsilon\text{Hf}$  (0–15), with a  $T_{\text{DM}^2}$  of 0.1–1.2 Ga. Zircon Hf isotope values are in agreement with whole-rock Sm-Nd isotope data analyzed on Miocene samples from the Monywa and Mount Popa regions of the Wuntho-Popa Arc, with a reported  $\epsilon\text{Nd}$  of 1.6–3.6 (Lee et al., 2016; Mitchell et al., 2012). Zircon oxygen isotope data has also been measured in samples from the Wuntho-Popa Arc (Gardiner et al. (2017a), and this study), with a range in  $\delta^{18}\text{O}$  of 5.2–5.8 ‰, within error of mantle value (Figure 8).

In summary, zircon isotope analyses from Late Cretaceous, Palaeocene–Eocene, and Miocene Wuntho–Popa Arc magmatic rocks have juvenile Hf affinity and mantle-like O isotope values. These isotopic signatures, the I-type affinity of magmatic rocks, and the presence of Cu-Au type mineralization, are characteristic of the magmatic rocks being the product of subduction processes leading to an input of mafic crust (mantle) material into the source. The magmatism of the Wuntho–Popa Arc is driven by the eastwards subduction of Neo-Tethys under the Asian margin, as recorded by the Burma Seismic Zone (Stork et al., 2008). However, the apparent temporally

discontinuous nature of the magmatism implies phases of subduction, and the Hf isotopes of the Eocene (Shangalon) sample hints at a subtly different source to the Cretaceous rocks which volumetrically dominate the Wuntho massif.

The Mogok–Mandalay–Mergui Belt extends from Mogok in central Myanmar south towards Mergui and Phuket, along the Andaman Sea (Figure 2A). We discuss the Tin Province found in the southern part of the Belt separately from the Mogok Metamorphic Belt found in the north, on the basis of their distinctive magmatic and metamorphic histories recorded through zircon isotope data. The dominant country rock in the Tin Province, into which the granitoids intrude, are Late Palaeozoic low-grade meta-sedimentary rocks, which in Myanmar is termed the Slate Belt, or Mergui Series (Mitchell et al., 2004) (Figure 5). Zircon U-Pb geochronology studies show that Tin Province granites all have relatively similar magmatic ages ranging from 77–50 Ma (Late Cretaceous to Eocene; Figure 4) (Aung Zaw Myint et al., 2017; Gardiner et al., 2017a; Gardiner et al., 2016a; Jiang et al., 2017; Mitchell et al., 2012). However, Mi Paik (2017) reported magmatic ages of 121–107 Ma for three granite samples found in the Mawpalaw Taung area, north of the main Dawei tin district, which potentially stretch the magmatic history of the Tin Province back to the mid Cretaceous.

Reporting on Cretaceous to Paleocene aged granites which outcrop on the western margin of the Tin Province, Sanematsu et al. (2014) noticed the granitoids young towards the west, and with time trend towards more S-type affinity and become more reducing. These authors invoked an island arc

setting for their petrogenesis. Sanematsu et al. (2014) also proposed that the granites found outcropping near the Thai border to the east of the Tin Province are, in contrast to the granites on the western margin, geochemically distinct, being of dominantly S-type character and associated with significant Sn-W mineralization. Using isotope geochemistry, Jiang et al. (2017) interpreted both the Hermyingyi and Taungphila tin granites as being derived from Palaeoproterozoic (1922–1741 Ma) crust of tonalitic to granodioritic composition, with little mantle-derived magmatic contribution.

Zircon oxygen isotope data has been reported in samples from the Tin Province, with  $\delta^{18}\text{O}$  ranging from 5.6–8.3 ‰ (Gardiner et al., 2017a), trending from mantle value towards elevated values (Figure 8). It is clear from the isotope signatures (both zircon Hf and O) that the Tin Province granites, certainly those of Eocene age, are broadly derived from a magmatic source dominated by the recycling of existing crustal material. However, the geodynamic setting of their genesis is of some debate, with postulated settings including their being inboard of an Andean type margin (Gardiner et al., 2015; Mitchell, 1977), or within an extensional back-arc setting above a flat Neo-Tethyan subduction zone (Jiang et al., 2017; Sanematsu et al., 2014).

In summary, in contrast to samples analyzed from the Wuntho-Popa Arc, magmatic rocks of the Tin Province record evolved zircon Hf isotope values, ranging in  $\epsilon\text{Hf}$  from -1.2 to -15.2, equating to  $T_{\text{DM}^2}$  of 2.1–1.2 Ga (Figure 7) (Gardiner et al., 2017a; Jiang et al., 2017). These zircon Hf isotope values are

in agreement with published whole rock Nd isotope data ( $\epsilon_{\text{Nd}} -11$ ) from granites from the same region (Jiang et al., 2017).

The Mogok Metamorphic Belt is an amphibolite-grade sequence of meta-sedimentary and meta-igneous rocks intruded by granitoids of both I- and S-type affinity (Barley et al., 2003; Iyer, 1953; Mitchell et al., 2007; Searle et al., 2017; Searle et al., 2007). Evidenced by zircon geochronology, some of these granitoids exhibit a more complex magmatic history than those found within the Tin Province, with inherited zircon domains yielding multiple magmatic and/or metamorphic ages, and zircon cores recording ages as old as the Jurassic (ca. 170 Ma) (Barley et al., 2003, and this study; Crow and Khin Zaw, 2017) (Figure 4). This complex history may represent an overprinting of several arc-related phases of magmatism. Late Cretaceous (~120 Ma) ages are reported from granites with I-type affinity outcropping into the metasedimentary sequences in the vicinity of Mandalay (Barley et al., 2003, and this study), and Eocene and Miocene magmatic ages are also recorded (Barley et al., 2003, and this study; Gardiner et al., 2016a; Mitchell et al., 2012). Within the country rocks of the Mogok Metamorphic Belt, at least two phases of post-collisional Barrovian-type regional metamorphism up to sillimanite grade have been identified through zircon and monazite U-Pb geochronology: one pre- to Mid Palaeogene, and one Eocene–Oligocene (Barley et al., 2003; Searle et al., 2017; Searle et al., 2007), this latter age similar to that of Doi Inthanon in northern Thailand (Dunning et al., 1995; Gardiner et al., 2016b). Localized partial melting of the country rock also produced leucogranitic melts, with a tourmaline and garnet Himalayan-type

leucogranite dated at 24.5 Ma (Searle et al., 2007), and the Kabaing granite dated at 16.8 Ma (Gardiner et al., 2016a).

Zircon Hf isotopes analyzed from samples of granites which intrude the Mogok Metamorphic Belt record evolved  $\epsilon_{\text{Hf}}$  values. Zircons separated from granitoids intruding into the sillimanite-grade pelitic schists and gneisses which comprise the southern part of the Belt near Mandalay (MY1, MY4, MY9) record Hf isotope values ranging in  $\epsilon_{\text{Hf}}$  from -15 to -10. In contrast, the northern part of the belt near Mogok is comprised of high-grade marbles (Iyer, 1953; Searle et al., 2017). The aforementioned Kabaing Granite (sample MY106) has the least evolved Hf isotope signal recorded so far within the Mogok Metamorphic Belt ( $\epsilon_{\text{Hf}}$  -7.1). Zircon oxygen isotope data on samples of granites intruding the belt have elevated  $\delta^{18}\text{O}$ , ranging between 6.3 and 9.2 ‰.

In summary, the granites from the Mogok–Mandalay–Mergui Belt, both within the Tin Province and the Mogok Metamorphic Belt, have evolved zircon  $\epsilon_{\text{Hf}}$ , with elevated zircon  $\delta^{18}\text{O}$ . However, in terms of the data there remain complexities between the Tin Province and from the Mogok Metamorphic Belt, and additionally between the northern and southern parts of the Mogok Metamorphic Belt.

#### 4.1.3. *Tagaung-Myitkyina Belt*

The Tagaung-Myitkyina Belt, in northern Myanmar (Figure 5; Figure 6) is one of three parallel, major metamorphic belts found within Myanmar, the other two being the Mogok Metamorphic Belt and the Katha-Gangaw Ranges. The

Tagaung-Myitkyina Belt is poorly exposed and studied, and comprises several extents of ophiolitic material: in the Kyawbingyon region on the eastern bank of the Irrawaddy north of the Mogok Metamorphic Belt, and on its western bank north of Myitkyina (Figure 6B) (Searle et al., 2017). For a summary of the geology of both the Tagaung-Myitkyina Belt and the Katha-Gangaw Ranges please refer to Mitchell (2018).

Very little isotope data has been reported from rocks found outcropping within the Tagaung-Myitkyina Belt. The dacite sample MY182 we infer as being from the Tagaung-Myitkyina Belt, and it outcrops east of the Myitkyina ophiolite (Figure 6B). MY182 records a magmatic age of 171.9 Ma, a Middle Jurassic age comparable to that reported for the Myitkyina ophiolite itself of ca. 173 Ma (Liu et al., 2016). The zircon Hf isotope data from MY182 records a highly juvenile mean  $\epsilon_{\text{Hf}}$  of 15.1 (Figure 7). The locality of MY182 may represent a southerly exposure of an arcuate north–south perhaps I-type magmatic belt identified on Myanmar geological maps, and extending north towards Putao in northern Kachin State (Figure 5).

#### 4.2. Myanmar Crustal Evolution Trends

A Hf evolution diagram plots magmatic age (U-Pb) against  $\epsilon_{\text{Hf}}$ , measured within the same zircon grain (Figure 7). It allows interrogation of Hf isotope data within the context of Hf evolution arrays, whose trends in epsilon space with time are controlled by the production of radiogenic  $^{176}\text{Hf}$ , itself determined by source  $^{176}\text{Lu}/^{177}\text{Hf}$  (here 0.015). Evolution arrays are used to chart the Hf isotopic development of a package of crust, and allow determination of any external input into the magmatic system. If crust is reworked (remelted), then



addition of external material, either mantle-derived or existing exotic crust, may be interpreted where the isotopic composition of the daughter rock departs from the evolution array (Kemp et al., 2006; Kirkland et al., 2013). The evolution array may also be used to calculate Hf model ages, by projecting it back to intercept a modelled depleted mantle (DM). Figure 7 shows a Hf evolution plot for those data analyzed in the Myanmar samples (Table 1), and coloured by belt. Those samples from the two Palaeo-Tethyan belts, and from the Mogok-Mandalay-Mergui Belt, all plot with evolved, that is negative, zircon  $\epsilon_{\text{Hf}}$  values. Evolved  $\epsilon_{\text{Hf}}$  values may imply the rocks had their petrogenesis through a dominance of reworking of existing crustal material.

We characterize the Hf isotopic composition of eastern Sibumasu basement through anchoring an evolution array at the Hf data from the Eastern Province samples (Figure 7). Zircon Hf data from the Main Range Province plot within this evolution array, although they have slight differences in their Hf model ages which can be attributed to data scatter. Here, the implication is that the Hf isotopic composition of these samples can be attained purely through the reworking of the same source material as that of the Eastern Province. The geochemical similarity of Main Range and Eastern Belt granitoids has been noted in Malaysia (Wai-Pan Ng et al., 2015a), but the evolved Hf isotope data indicates that Eastern Belt magmatism is less I-type than previously thought, at least in Myanmar. If, alternatively, the Eastern Province represents magmatic rocks sourced from the Indochina terrane rather than from Sibumasu crust, then we infer little Hf isotopic difference between Indochina and Sibumasu. However, a common mid-crustal isotopic signature may be

expected if both Indochina and Sibumasu were autochthonous blocks derived from the same margin of Gondwana (Metcalf, 2011a).

If Sibumasu is a single contiguous crustal block, then its western margin is likely to have similar Hf isotopic characteristics as its eastern margin. Hf data from samples across the Mogok–Mandalay–Mergui Belt lie on or above the eastern Sibumasu evolution array (Figure 7), implying these are potentially sourced from, and intrude into, Sibumasu basement. Samples from the Tin Province generally plot above the array ( $\epsilon_{\text{Hf}}$  from -15 to -1), presenting an isotopic composition which may be attained through reworking of Sibumasu basement with an additional input of external juvenile material. Alternatively, the crustal source of the Tin Province granites may be different to those of eastern Sibumasu, with the implication that Sibumasu in its current definition may be a composite terrane, or at least a continental block hosting crustal domains of different ages and compositions.

In contrast to the Tin Province granites, samples from those Mogok Metamorphic Belt granites which intrude into sillimanite-grade schists and gneisses, identified as “Mogok South” in Figure 7, have a zircon Hf isotopic composition plotting close to the eastern Sibumasu evolution array. In particular, the earliest (Triassic) magmatic phase of MY9 records Hf isotope values which are isotopically identical to the Main Range Province. This may suggest a common crustal source for both sample MY9 and the Main Range Province magmatic rocks, implying Sibumasu contiguity from east to west. In contrast, the Kabaing Granite (MY106), intruding the Mogok high-grade marbles and identified on the diagram as “Mogok North”, records a less

evolved Hf isotope signal, plotting above the eastern Sibumasu evolution array (Figure 7). The Kabaing Granite is therefore likely to have a distinct crustal source to that of the Mogok South granitoids. Thus, from zircon Hf isotope evidence alone, it may be interpreted that the granitoids of Mogok South tapped a crustal source similar to that of eastern Sibumasu. However, both the Kabaing Granite, and those granites from the Tin Province, have distinct isotopic signatures to Mogok South, implying magmatic sources that either reflect the addition of juvenile material to existing Sibumasu basement, or the melting of a different crustal source.

Samples from the magmatic rocks of the Wuntho-Popa Arc record juvenile zircon  $\epsilon_{\text{Hf}}$  values (Figure 7). Also highlighted in Figure 7 (light red) is the range of U-Pb ages and  $\epsilon_{\text{Hf}}$  measured in detrital zircons interpreted to be sourced from the Wuntho-Popa Arc (Wang et al., 2014), and which record similar Hf isotopic values to the Cretaceous-aged Arc rocks. The detrital zircons were interpreted by Wang et al. (2014) to have a similar age and isotopic composition to the Kohistan-Ladakh-Gangdese belt within Tibet. These authors proposed that the Wuntho-Popa Arc represented an extension of the Gangdese belt along the Tethyan margin. Notably, the Eocene Shangalon sample (MY145) plots at less juvenile values, which implies it is tapping a subtly different source to the older, Cretaceous Arc magmatic rocks.

Oxygen isotopes measured in zircon complement Hf data in that they can further inform on the nature of source and are highly sensitive to any sedimentary contribution in the magmatic source, and reflected in heavier  $\delta^{18}\text{O}$  than a mantle value of 5.3 ‰. Zircon O isotope data from Myanmar has

mainly been reported in rocks from the two Neo-Tethyan magmatic belts, and plotting  $\epsilon_{\text{Hf}}$  versus  $\delta^{18}\text{O}$  (Figure 8) for samples from these belts shows that they are isotopically distinct. Wuntho–Popa Arc samples plot at juvenile  $\epsilon_{\text{Hf}}$  and mantle-like  $\delta^{18}\text{O}$ . In contrast, samples from both the Tin Province and Mogok Metamorphic Belt plot at evolved  $\epsilon_{\text{Hf}}$  with elevated  $\delta^{18}\text{O}$ . Further, there are discernable differences in the Hf–O arrays between the samples from the Tin Province and those from the Mogok Metamorphic Belt, notably in their  $\text{ox}^{\square\square\square\square\square\square\square\square\square\square}$  values. The Mogok samples are in general of elevated  $\delta^{18}\text{O}$ , plotting between ca. 6.3 and 9.2 ‰; Tin Province samples plot between 5.6 and 8.3 ‰. However, there is little difference in zircon oxygen isotope composition between the single sample from Mogok North and those reported from Mogok South. Any difference in oxygen isotope signature may reflect a difference in magmatic protolith between the granites of the Tin Province and Mogok Metamorphic Belt, and which is also implied by differences in their Hf isotope values.

The sample from the Tagaung-Myitkyina Belt in Kachin State plots at highly juvenile Hf isotope values, close to modelled DM (Figure 7), implying little to no existing continental crustal material was incorporated in its magmatic source.

## 5. Crustal Architecture, Blocks and Sutures

### 5.1. Contiguity of Sibumasu versus a Meso-Tethys Suture

Although the eastern boundary of Sibumasu is largely accepted as being delineated by the Palaeo–Tethys suture (Hutchison, 1975; Metcalfe, 1996;

Mitchell, 1977; Sone and Metcalfe, 2008), defining its western boundary has proved more contentious. The north–south Neogene–Recent Sagaing Fault provides one possible modern-day western boundary to Sibumasu (Figure 5). However, some workers have proposed a cryptic suture which may run along the Paung Laung–Mawchi Fault Zone located along the western edge of the Shan Scarps (Figure 1), thereby separating the Slate Belt sequences to the west from those on the Shan Plateau (Mitchell, 2018; Mitchell et al., 2012; Mitchell et al., 2015; Ridd, 2016). The model of Ridd (2016), in separating Sibumasu into two distinct blocks, represents one attempt to address whether a suture related to Meso-Tethys, an intermediate ocean basin lying between Palaeo- and Neo-Tethys, exists within Myanmar. In his model for a cryptic Meso-Tethys suture, Mitchell (2018) invoked a former west-dipping subduction zone which formed an island arc off the West Burma Block ca. 110–90 Ma.

Sutures related to the Meso-Tethys exist further north in Tibet and Yunnan, where they are collectively termed the Bangong–Nujiang Sutures (review in Burchfiel and Chen, 2012). The Nujiang Suture is proposed to separate the Tengchong and Baoshan Blocks, of which a key difference is the nature of Carboniferous to Early Permian glacio-marine sediments. These sediments reach thicknesses of kilometres on the Tengchong block, but are much less well-developed on the Baoshan block, only reaching 10–100's of metres in thickness. These differences in stratigraphic thickness may be explained either by their being separated by an ocean basin, or through variations on a single continental block having developed through rifting (Ridd, 2009).

The stratigraphic arguments for defining separate Tengchong and Baoshan blocks, and the cryptic nature of the suture zone (as reviewed by Burchfiel and Chen (2012)), are very similar to those proposed to be present along the Paung Laung Fault in Myanmar, the Three Pagodas and Khlong Marui faults in Thailand, and the Straits of Malacca between Malaysia and Sumatra (Mitchell et al., 2015; Ridd, 2015). The so-called *Medial Suture Zone* in Myanmar (Mitchell et al., 2015) (Figure 9B), would in effect separate Sibumasu into two separate blocks (Ridd, 2016), with Ridd (2015) using the terms “*Irrawaddy Block*” and “*Sibuma*” to refer to the western and eastern areas respectively (Figure 9C), the correlatives of the Tengchong and Baoshan blocks. Ridd (2017) however accepted the term “*Karen–Tenasserim Unit*” for the Irrawaddy Block, recognizing the primacy of Bender (1983) who first postulated the existence of a separate terrane west of the Paung Laung Fault. However, structural and tectonic evidence for such a suture, especially along the Paung Laung Fault, is not strong, although this may have been obscured by later over-thrusting and strike-slip faulting (Ridd, 2015). In their models, the Meso-Tethys ocean basin closed in the Late Jurassic to Early Cretaceous (Mitchell et al., 2015; Ridd, 2016). However, this period is one of tectonic quiescence in western Thailand, with no radiometric ages from gneisses that lie close to the proposed suture and which may indicate metamorphism during, and following on from, the proposed collision time (Kanjapayont et al., 2012; Kawakami et al., 2014; Nantasiri et al., 2012).

Separation of Sibumasu from Australia did not occur until the Early Permian (e.g., Metcalfe, 2013), hence the Carboniferous–Permian stratigraphic differences occurred too early in the rifting process to be explained by an

oceanic rift. This problem is recognized by Ridd (2016) who presents an unscaled palaeogeographic solution by placing eastern Sibumasu outboard of the Lhasa Block, leaving his Irrawaddy Block free to the east to transition into oceanic crust. However, when this reconstruction is done to scale it requires a 2000 km-long margin connected to the ocean. Due to the length of the other blocks that must be present (see reconstructions shown in Metcalfe (2013)), there is insufficient room on the northwestern Australian margin for this reconstruction to be viable.

Ridd (2017) argues (a) that the protolith of the eastern Irrawaddy Block metamorphics (i.e. the Mogok South metamorphic rocks) includes sediments up to Permian age (following Mitchell (1993); (Mitchell, 2018), Mitchell et al. (2012)), whereas (b) the protolith of the metamorphic rocks found within the Mogok area itself in the north – Mogok North; marbles and rare meta-pelitic material – is Precambrian in age, presumably due to the age of the overlying Chaung Magyi Group. However, there is clear evidence that metamorphic rocks around Mogok are not Precambrian. Peak metamorphism in the Mogok Metamorphic Belt is of Cenozoic age (Searle et al., 2007; Win et al., 2016; Yonemura et al., 2016). The marbles and rubies in the Mogok area are interpreted as resulting from metamorphism of a limestone sequence containing evaporites (e.g., Brunnschweiler, 1970; Garnier et al., 2008), and limited to the northern Shan Plateau area. Those marbles in the Mogok area may have as their protolith the “Plateau Limestone” units of Middle–Upper Permian age found within the Shan Plateau (Searle et al., 2017), whilst marble sequences found further south of Mogok have reported relict Ordovician, Silurian and mid-Permian fossils (Mitchell et al., 2012).

The Myanmar Median or Meso-Tethys suture models of Mitchell et al. (2015) and Ridd (2015, 2017) would suggest that there is a significant difference between Sibumasu lying east of the suture, and a terrane that includes the southern Mogok metamorphic rocks (the Irrawaddy Block of Ridd (2017)) to the west. However, at least on the basis of the zircon isotope data we see little evidence for this division. Instead, we find strong similarities between the Hf isotopes measured in zircons sourced from magmatic rocks in both the Mogok South area, and in Eastern Sibumasu (Figure 7).

Barley et al. (2003) reported zircon U-Pb ages of ca. 170 Ma from both an (I-type) biotite orthogneiss from the Kyanigan Hills, and a hornblende-bearing syenite from Mandalay Hill. Zircon U-Pb ages of 181–183 Ma have been reported from a biotite granite and a leucogranite from Monbinzon on the western margin of the Shan Plateau (Crow and Khin Zaw, 2017). These Jurassic ages may represent relics of an Andean-type margin for which other geological evidence has been lost. Rocks attributed to a similar period of subduction activity can be found elsewhere in Myanmar. Liu et al. (2016) reported a middle Jurassic magmatic age for the Myitkyina ophiolite, part of the Eastern Belt ophiolites in Kachin State, which they interpreted as marking an extension of the Nujiang Suture. These Jurassic ages may potentially be related to the closure of a Meso-Tethys ocean, however the location of the Myitkyina ophiolite is about 170 km west of the identified boundary between the Tengchong and Baoshan blocks in Yunnan (i.e. the southern extent of the Nujiang Suture). Hence it is difficult to place the Nujiang suture – as relating to the closure of Meso-Tethys – in Kachin State, unless it is simply a remnant of a large over-thrust sheet of ophiolites, displaced westwards from the suture



zone as suggested by Mitchell et al. (2015). Alternatively (a) the Myitkyina ophiolite does not equate with the Nuijiang Suture, and is perhaps a separate branch of the Meso-Tethys, or (b) the documented Jurassic ages were driven through the subduction of Neo-Tethys, thereby extending the period of magmatism in Myanmar relating to Neo-Tethys back to the Mid-Mesozoic (Khin Zaw, 2017). Our magmatic age for the dacite (MY182) outcropping immediately to the east of the Myitkyina ophiolite is also Mid-Jurassic (172 Ma). If this sample within the Tagaung-Myitkyina Belt represents the existence of I-type magmatism of this era within northern Myanmar, and related to the subduction of Meso-Tethys, its geographical siting east of the Myitkyina ophiolite would suggest east-wards directed subduction.

## 5.2. Isotopic differences between the Mogok Metamorphic Belt and the Tin Province

There are clear isotopic differences between that measured in zircons from granitoids outcropping within the Mogok Metamorphic Belt, and from those intruding the Tin Province. Zircon U-Pb magmatic ages imply different phases of magmatism; Tin Province granites record a main period of magmatic activity ca. 85–45 Ma, which overlaps with a period of magmatism recorded in the granitoids intruding into the Mogok Metamorphic Belt, although both older and younger phases are recorded (Figure 4). In terms of their zircon Hf isotopes, Tin Province granites are in general less evolved than the Mogok South granites (Figure 7). There are also contrasts between the two regions in the country rock into which the granites are emplaced. Tin Province granitoids intrude the low-grade metasediments of the Slate Belt, in contrast to the high–

grade pelitic and marble country rocks which dominate the Mogok Metamorphic Belt. Specifically, the Tin Province lacks any evidence for the Cenozoic high-grade metamorphic events recorded within the Barrovian-style rocks of the southern part of the Mogok Metamorphic Belt (Searle et al., 2017; Searle et al., 2007).

One significant stratigraphic difference between the Mogok Metamorphic Belt and the Tin Province is that the Permo-Carboniferous glacio-marine sediments (termed the Kaeng Krachan Group in Thailand, and the Slate Belt/Mergui Group in Myanmar; Figure 5) thicken from north to south. Although the basement is not well exposed in Peninsular Myanmar or in the adjacent areas of Thailand, Watkinson et al. (2011) describe sheared migmatites containing stretched pebbles of quartz and granite, along the Ranong and Khlong Marui Faults in Peninsular Thailand. These pebbles suggest the protolith to the migmatites are the pebbly mudstones of the Kaeng Krachan Group (Watkinson et al., 2011). Hence, at least part of the source of the granitic melts found within the Tin Province are these thick Permo–Carboniferous clastic sediments. These clastics represent a different magmatic source from the granites of the Mogok Metamorphic Belt, which may help explain the isotopic differences observed between the two regions. Possibly, there are further differences in the underlying Palaeozoic rocks between the two regions, but much of the isotopic differences may be due to the presence of the thick Kaeng Krachan and Mergui Group sediments that mask the deeper section within the Tin Province.

### 5.3. The Shan Plateau

The northern Shan Plateau of Myanmar, and the Baoshan Block in Yunnan, are both characterized by a sequence of weakly metamorphosed siliciclastic and carbonate rocks, which pass upwards into intercalated volcanic rocks. In Yunnan these are called the Gongyanghe Group. Metabasalts have U-Pb ages of around 499 Ma (Yang et al., 2012), while granitic magmatism lasted from about 500 Ma to 450 Ma (Li et al., 2016). The sequence is interpreted as an Andean-type belt on the northern active margin of Gondwana (Li et al., 2016; Zhu et al., 2012). In Myanmar's northern Shan Plateau, the Chaung Maygi Group is the equivalent to the Gongyanghe Group (Figure 5). The famous Pb–Zn–Ag Bawdwin Mine sited in the northern Shan States is located within the Late Precambrian–Cambrian shales, slates and greywackes of the Chaung Maygi Group (Hopwood, 1985) (Figure 5). These sequences are unconformably overlain by the Cambrian–Ordovician volcanoclastic agglomerates and tuffs of the Bawdwin Volcanic Formation, and the clastic sediments of the Pangyun Formation (BGR, 1976; Brinckmann and Hinze, 1981; Hopwood, 1985). The Bawdwin Mine has been interpreted as a volcanogenic massive sulphide-type deposit that may have formed on an Andean-type margin during the Cambrian to Ordovician (Gardiner et al., 2017b).

Additional evidence for lower Palaeozoic magmatism in the northern Shan Plateau comes from analysis of the Sedawgyi biotite gneiss which lies 35 km north of Mandalay on the eastern margin of the Mogok metamorphic belt. This gneiss has been dated through zircon U-Pb at  $491 \pm 4$  Ma, with the age

interpreted as that of the granite protolith (Mitchell et al., 2012). The same authors reported highly-evolved whole-rock  $\epsilon\text{Nd}$  of -10.3 for the gneiss. The magmatic age of the Sedawgyi gneiss thus has an equivalence in the granites of the Baoshan block in Yunnan. Broad evidence therefore exists for early Palaeozoic magmatic and volcanic activity within the broad region of the northern Shan Plateau extending into the Baoshan Block.

The Andean type setting invoked for the northern Shan Plateau contrasts with the Cambrian quartzite and Ordovician limestone deposits of Sibumasu further south in Thailand and much of the Shan Plateau in Myanmar (Bunopas, 1981). These extensive Cambrian to Ordovician sequences indicate a very different source area to that of the northern Shan Plateau. However, there is evidence for Cambro–Ordovician igneous activity on the eastern margin of Sibumasu from tuffaceous beds interbedded with sandstones and siltstone from Tarutao Island in Southern Thailand, and orthogneisses of Cambrian age south of Hua Hin in Peninsular Thailand at Khanom, and from a possible collided arc sequence near Chonburi (Kawakami et al., 2014; Ridd, 2011). The simplest solution is for the Andean margin in present-day Myanmar and Yunnan to run across the northern end of Sibumasu, following an ENE-WSW trend then down the eastern margin (as indicated by the red dashed line, Figure 5). Such a difference in stratigraphy and inferred geodynamic setting between north and south Sibumasu has inevitable implications for the Mogok Metamorphic Belt in particular. Ridd (2016); Ridd (2017) seeks to find differences between the Mogok Metamorphic Belt around Mogok, and the rest of the Mogok Metamorphic Belt further south, as is necessary for his model, where the Luxi–Nujiang

Suture/Shweli Fault separates the two. From an isotopic perspective (U-Pb and Hf), a terrane boundary in the Northern Shan states may help explain the subtle differences we find between the magmatic rocks of the Mogok South and Mogok North areas (Figure 7).

#### 5.4. The West Burma Terrane

The major active fault within Myanmar is the north-south trending Neogene-era dextral Sagaing Fault (Figure 5). This fault has been interpreted as a major structural boundary, separating western Myanmar, which hosts the Wuntho-Popa Arc, from central and eastern Myanmar, i.e. that currently assigned to the Sibumasu block, thereby defining the West Burma Terrane or West Burma Block (e.g., Figure 9A). However, the question remains whether the Sagaing Fault is a recent artifact dividing a previously contiguous terrane, or whether it is a remobilized lithospheric boundary, and thus western Myanmar represents a separate accreted terrane. The extensive cover of Cenozoic sediments over western Myanmar (Figure 5) is one of the contributing factors to the profusion and variety of tectonic models proposed for its Mesozoic development. These models have been reviewed extensively by Sevastjanova et al. (2016), Ridd (2017), Morley and Searle (2017), and by Barber et al. (2017b). Hence we more selectively discuss some of the models in this study, and provide Table 6, which summarizes the current range of models invoked to explain western Myanmar.

In seeking to identify additional suture zones, at least two ophiolite belts are found within Myanmar (Figure 1). The *Western Belt* predominantly outcrops within the Indo-Burman Ranges, while the *Eastern Belt* is found in central

Myanmar (Archarya, 2007; Searle et al., 2017). The Western Belt – including the Naga, Chin Hills and Andaman Island ophiolites – is thrust oceanic crust within an accretionary prism setting, which has been interpreted as representing the eastern suture of the Indian Plate, part of the Neo-Tethys suture (Archarya, 2007; Rangin et al., 2013). The Eastern Belt ophiolites are poorly exposed, and in this definition comprise the Jade Mines Belt in Kachin State, as well as potential outcrops within central Myanmar. Eastern Belt ophiolites are unconformably overlain by Albian carbonates (Mitchell, 1993), and have been interpreted as either representing the Palaeo-Tethys suture (Archarya, 2007; Rangin et al., 2013), or an extension of the Nujiang Suture (Meso-Tethys) based on the Mid-Jurassic age for the Myitkyina ophiolite (Liu et al., 2016). These latter authors also reported an Early Cretaceous age (ca. 127 Ma) from the Kalaymyo ophiolite, part of the Western Belt, which they correlated with the Yarlung-Tsangpo suture in Tibet, thereby interpreting it as representing a fragment of the Neo-Tethys ocean basin. For a complete review of models invoked to explain the Myanmar ophiolites see Searle et al. (2017).

In the “*Greater Sibumasu*” model of Morley and Searle (2017), Sibumasu as a crustal entity includes west Burma, with its western boundary defined by the Western Ophiolite Belt (Figure 1). The Greater Sibumasu model assumes the Slate Belt/Mergui Series metasedimentary sequences to represent either the passive margin of Sibumasu during its rifting from the Gondwanan margin, or a rifted trough within Sibumasu. The Greater Sibumasu model also has an advantage in that it accommodates the detrital zircon conclusions of Sevastjanova et al. (2016). These authors, in investigating the heavy mineral

assemblages of the Triassic Pane Chaung Group from the Mount Victoria area, reported an abundance of Permian to Triassic-aged zircons. Sevastjanova et al. (2016) took this evidence as indicating the zircons were derived from the Palaeo-Tethyan magmatic belts, thereby indicating that West Burma had docked onto Southeast Asia by the Triassic (their “West Burma Model A”). However, since the Greater Sibumasu model does not accommodate the existence of any suture zone splitting Sibumasu into two or more blocks, the Eastern Belt ophiolites are not satisfactorily explained. Further, the isotopic trends observed in both zircon Hf and O isotopes from magmatic rocks of the Wuntho–Popa Arc (Figs. 7 & 8) are not conclusive in discriminating between the crust comprising West Burma and that of Sibumasu. These data record a significant input of juvenile material into the magmatic source of the Wuntho–Popa Arc, which disturbs any potential evolution trend.

The “*West Burma Block B*” model of Barber and Crow (2009) implies a Triassic joining of a West Burma Block with Sibumasu, which accommodates the Permian–Triassic detrital zircon age spectra of Sevastjanova et al. (2016). However, the West Burma Block B model requires a Cathaysian origin for the West Burma Block, implying a more outboard position on the Gondwana (Australian) margin than for Sibumasu, which contradicts the findings of Sevastjanova et al. (2016) who determined a more inboard position on the Gondwana margin, similar to Sibumasu. The West Burma Block B model also does not accommodate any southerly extension of the Jurassic Nuijiang Suture due to the docking of West Burma in the Triassic.

Both the “*Mogok Foreland*” (Figure 9B) and the “*Irrawaddy Block*” (Figure 9C) models solve the issue of a “hanging” Nujiang Suture terminating at the northern Shan Plateau, however they are unable to accommodate the requirement of the detrital zircon spectra for assembly on or before the Triassic. Further, these models separate eastern Sibumasu either entirely from the Mogok Metamorphics (Mogok Foreland model) or from Mogok South (Irrawaddy model). Placing Mogok South on a different terrane to Eastern Sibumasu may make it difficult to explain the Hf isotope evidence suggesting the Mogok South and Eastern Sibumasu magmatic rocks have a common magmatic source, unless both blocks were close by on the Gondwana margin. These models also struggle to explain the apparent identical magmatic age of sample MY9 in South Mogok to that of the Main Range Province granites.

#### 5.5. The Greater Sibumasu–Tengchong Model

Here, we lean towards a hybrid model involving a Greater Sibumasu. This model assumes that significant stratigraphic, radiometric ages, metamorphic, igneous and geochemical variations can be explained as variations within a ribbon continent, rather than requiring separate blocks. In particular, the isotopic variations we observe where Mogok North is less similar to the Shan Plateau region than Mogok South, is the opposite of what would be expected from the Irrawaddy model of Ridd (2015), which we attribute either to compositional variations within a single Sibumasu, or to Mogok North lying within a discrete northern Shan domain of Palaeozoic-era basement.

Further, to deal with the “hanging” Nujiang Suture we accept the presence of a separate Tengchong Block within Myanmar, and one which provides for a



southerly termination of this suture immediately north of the Mogok area. Such a “*Greater Sibumasu–Tengchong Model*” is outlined in Figure 10. In this definition, the Tengchong Block hosts both the Tagaung–Myitkyina and the Katha–Gangaw Belts (Figure 5), this latter being comprised of high-grade Barrovian-style metamorphic rocks of unknown age (Searle et al., 2017), and which has no obvious analogue further south. The Tagaung–Myitkyina Belt comprises ophiolitic material found outcropping on the eastern bank of the Irrawaddy. These rocks are reportedly typical Tethyan ophiolitic mantle rocks (serpentinized harzburgites) (Searle et al., 2017), and in places are mineralized, hosting the Tagaung Taung nickel laterite mine (Schellmann, 1989). The Tagaung–Myitkyina Belt may be part of the Eastern Belt of ophiolites, typified by the Jurassic age of the Myitkyina ophiolite (Liu et al., 2016), given by their regional association with Late Jurassic radiolarian cherts and Albian-Cenomanian limestones (Mitchell et al., 2012).

We assume the Baoshan Block and Greater Sibumasu were assembled on or before the Triassic, the assembly of which may be marked by an Andean margin lying east-west across the Northern Shan Plateau (Figure 5), as postulated earlier. Alternatively the Baoshan Block and Sibumasu are simply the same terrane, with different names across a political, not a geological boundary. We also assume a contiguous Sibumasu/Baoshan Block sutured onto the Sukothai Arc/Indochina Block margin in the Late Permian to Early Triassic following the subduction of Palaeo-Tethys (Figure 10A).

Any tectonic model needs to explain the Triassic to Mid–Jurassic magmatic ages recorded within I-type granitoids in the southern part of the Mogok

Metamorphic Belt (Figure 4). Cobbing et al. (1992) described an evolutionary series of granites in the Mogok-Mandalay-Mergui Belt (their Western Belt) from an I-type hornblende and/or biotite granite, through leucocratic main phase granites, to S-type Sn-bearing composite batholiths of K-feldspar and biotite-bearing granites. The implication of this is that this magmatic belt has witnessed earlier Late Triassic to Jurassic subduction-related I-type magmatism, trending towards S-type crustal melt magmatism in the Late Cretaceous to Palaeogene. Searle et al. (2012) reported a  $214.4 \pm 2.4$  Ma Late Triassic age from an I-type granitoid on Phuket Island, Thailand, the southern extension of the belt, and a similar age to the early phase of MY9. These authors explained the similar magmatic age to that of the Main Range Province as resulting from two subduction zones operating simultaneously. It may be that this discontinuous arc of Late Triassic to Jurassic magmatic ages in Myanmar, and perhaps as far south as Phuket, represents the relics of a separate Andean-type margin sited above a subducting Meso-Tethys, for which other geological evidence has been lost. Thus, In our model, we propose this latter period of magmatism represents subduction of Meso-Tethys between the Tengchong Block and Sibumasu (Figure 10C). The Tengchong Block we then interpret as suturing onto Greater Sibumasu before the Late Cretaceous (Figure 10D), after which subduction of Neo-Tethys drove the magmatism found in the Wuntho–Popa Arc and ultimately that of the Tin Province (Figure 10E). Our model requires the Wuntho–Popa Arc to be offset from the Tin Province by the Sagaing Fault, which may require some ~400 km of displacement (Figure 10F). This would then result in a crustal architecture as outlined in Figure 11.

The Greater Sibumasu–Tengchong Model does not explain all the geological evidence observed within Myanmar. It may not explain the Late Triassic magmatism found within the vicinity of Mandalay, e.g. MY9. It fails to explain the location and origin of the Myitkyina ophiolite, and perhaps the associated arc-related rocks within the Tagaung-Myitkyina Belt. These may best explained as either (a) westwards-thrusted remnants 10's to 100's kms from the suture, thereby not actually defining a suture zone; or (b) perhaps a separate branch of the Meso-Tethys.

## **6. Metallogenic Implications of Myanmar's tectonic history**

The Tethys margin in central and eastern Asia is endowed with a significant diversity of mineral deposits (Khin Zaw et al., 2014; Searle et al., 2016). Myanmar, at the heart of this region, is highly prospective, however it remains a poorly explored minerals jurisdiction (Chhibber, 1934; Gardiner et al., 2014; Khin Zaw, 2017; Soe Win and Malar Myo Myint, 1998). The Tethys-related orogenies and concomitant magmatism are the major drivers for ore formation within this region. We briefly review the main ore deposit types that have their genesis directly linked to Myanmar's magmatic history; recent work has made significant progress in providing a geologic and tectonic framework for better understanding the richness and diversity of Myanmar's mineral provinces, and for more detail we refer readers to Mitchell (2018) and Barber et al. (2017a) which cover this topic in depth. We then briefly discuss the tectonic framework of Myanmar and surrounding region, and summarize the related metallogenic patterns and zonation.

An orogenic system, such as the subduction of an ocean basins and collision of continental fragments, provides a dynamic framework for the development of large-scale discrete Earth processes, which also finds expression in the genesis of diverse mineral deposits (Groves and Bierlein, 2007; Kerrich et al., 2005). Orogenic belts evolve, and geologic processes develop that lead to characteristic mineral deposit types through the lifecycle of a belt. Gardiner et al. (2016a) presented a model that linked the genesis of mineral deposit styles found within Myanmar to the subduction and suturing of Neo-Tethys. These authors defined four major orogenic stages (Figure 13): (a) accretionary stage (100–50 Ma); (b) collisional stage (50–40 Ma); (c) late collisional stage (40–15 Ma); and (d) oblique collisional stage (15–0 Ma). Within these stages were placed the genesis of different types of mineral deposits found within Myanmar; some deposit types found within Myanmar have robust geochronological constraints (e.g., Sn-W and Cu-Au porphyry), however for other types with poor age constraints, a potential age of formation was interpreted with respect to the orogenic cycle. During the Accretionary Stage, Gardiner et al. (2016a) proposed that magmatism associated with Sn-W mineralization intruded into the Tin Province, while I-type magmatism formed the Wuntho–Popa Arc. The Collisional Stage marked the suturing of the Neo-Tethys ocean basin, and the transition to a continent-continent collision setting. Before, or during, this event, emplacement of ophiolitic material related to the Neo-Tethys basin was responsible for the formation of several ultramafic-associated ore deposits, such as the Ni laterite deposits at Tagaung Taung and the Jade Belts. During the Collisional Stage, ongoing orogeny drove metamorphism, and possibly resulted in the orogenic Au now

found within central Myanmar (Figure 13B), although this remains subjective due to poor age constraints. The Late Collisional Stage (Figure 13C) resulted in the development of the Cu mineralization at Monywa, and in Pb-Zn-Cu skarn deposits associated with late-stage magmatism within the Mogok Metamorphic Belt. Finally, the Oblique Collisional Stage was responsible for the development of epithermal-type Au mineralization, such as the Kyaukpahto deposit in central Myanmar, which developed in small pull-apart basins close to the Sagaing Fault (Ye Myint Swe et al., 2004).

Khin Zaw (2017) presented a tectonic-metallogenic model for Myanmar, documenting tectonic events as far back as the Palaeozoic. In particular, he considered that Neo-Tethys related orogeny and magmatism extended back to at least the Jurassic. He assigned the Slate Belt hosted orogenic Au deposits found within central Myanmar, for example at Modi Taung, as having their genesis during the Late Mesozoic. Further, Khin Zaw (2017) highlighted that Cu-(Au) deposits documented within central Myanmar within or east of the Mogok Metamorphic Belt, such as at Monbinzon on the western margin of the Shan Plateau, are related to I-type Jurassic magmatism, and their genesis assigned to Neo-Tethys related subduction processes.

#### 6.1. Myanmar's Magmatic-Hydrothermal Mineralization

Mineralization associated with the arcs of Myanmar is largely magmatic-hydrothermal in character, although significant styles of mineralization classed as orogenic (Au) and magmatic (Ni) also occur. The granites found within the Tin Province have long been known for their association with extensive deposits of vein and pegmatite-type Sn-W mineralization (Chhibber, 1934;

Hutchison and Taylor, 1978), and Myanmar's principal Sn-W districts are found in the vicinity of Dawei, further south near Mergui, and also the Mawchi W-Sn mine district ~250 km northeast of Yangon (Coggin Brown and Heron, 1923; Garson et al., 1975; Hutchison, 1989; Khin Zaw and Khin Myo Thet, 1983). Sn-W mineralization in the Tin Province is found as cassiterite and/or wolframite-bearing pegmatites and greisen-bordered quartz veins. These are hosted both by the granites, and also by the Slate Belt country rock. For the most part, Sn-W mineralization is associated with Palaeogene S-type granites (Than Htun et al., 2017), and the mineralization is assumed to be of that age.

Porphyry style Cu mineralization, found with associated Mo and Au, is known to occur at Shangalon in the northern Wuntho region of the Wuntho-Popa Arc, southwest of the town of Kawlin (Mitchell et al., 2011). The Shangalon prospect is centred on a suite of ca. 40 Ma (Oligocene) granodiorite to dioritic plutons (e.g., Gardiner et al., 2016a) that intrude the ca. 105–95 Ma granodiorites of the Kanzachaung–Wuntho batholith, in addition to a well-exposed sequence of andesitic volcanics termed the Mawgyi Volcanics. The Mawgyi Volcanics are intruded by the Kanzachaung–Wuntho batholith but extrusive activity continued until at least late Cretaceous times (ca. 70 Ma). At Shangalon, mineralization is dominated by copper sulphides (chalcopyrite and minor bornite) in quartz veins that also contain occasional Mo and sporadic Au (Figure 12). Well-defined potassic and phyllic alteration systems are not evident in the main Shangalon area, although exploration in the broader region has identified other zones of mineralization and more extensive alteration. Likewise, more extensive indication of Au mineralization in the

region suggests that epithermal styles of Cu-Au ore formation may also be present.

In the Monywa district of the Wuntho-Popa Arc, at least two world-class high-sulphidation epithermal Cu deposits occur at Kyisintaung-Sabetaung and Letpadaung. These deposits are hosted by porphyritic andesite dykes, sandstones, and pyroclastics. Miocene sandstones and shales underlie the pyroclastics, and the sequences are underlain and intruded by andesite porphyry that yielded a mid-Miocene U-Pb zircon age of 13.6 Ma (Mitchell et al., 2011). In both deposits the andesitic porphyry bodies intrude a stratified volcaniclastic unit, which is the principal ore-bearing host rock. Hydrothermal alteration is pervasive in all rock types, comprising an outer chlorite (epidote) zone surrounding widespread quartz-sericite-pyrophyllite, occasional hematite, and quartz-pyrite-alunite. Copper sulphides are predominantly digenite-chalcocite, lesser covellite and enargite, and rare chalcopyrite and bornite. Mineralization is structurally-controlled, occurring in planar and stockwork veins, and in breccia dykes with a sulphide matrix. Gold is insignificant in both deposits. A prominent, up to 50m thick, oxidized zone is present at the surface comprising a leached cap and associated underlying zone of supergene enrichment.

## 6.2. Southeast Asia's paired magmatic belts and metallogenic implications

Collectively, the four granite belts of southeast Asia (Figure 14C) represent one of the great metallogenic belts of the World – their metallogenic endowment is dominated by Sn-W (predominantly in the Main Range of Malaysia and the Mogoke-Mandalay-Mergui Belt of Myanmar), with significant Cu-Au-Mo

porphyry-epithermal mineralization being a feature of the Wuntho–Popa Arc. The relationships between tectonic evolution, the timing of granitoid magmatism, and the formation of magmatic-hydrothermal mineral deposits in the region is a topic that has long attracted the interest of researchers.

To the east of Myanmar, the Main Range and Eastern Province form belts of granite that extend from Yunnan in China, through Thailand and into the Malaysian peninsula (Figure 14A, B). The Main Range Province is dominated by S-type granites that host substantial Sn mineralization, such as the prolific Kinta Valley deposits, that is both primary and alluvial/eluvial in character. The Eastern Province, also containing Sn mineralization, such as at Sungai Lembing and Kuantan, has traditionally been described as of predominantly I-type in character, although this classification has more recently been questioned (Wai-Pan Ng et al., 2015a, and here), with the implication that a breakdown of granites in Southeast Asia into S- and I-types does not accord with either their petrogenetic or metallogenic characteristics.

In contrast to the paired Thai-Malaysian granite belts, the spine of Myanmar is constructed by two near-parallel, broadly coeval, magmatic belts that are markedly different from one another in terms of metallogenic endowment (Figure 14A). The westerly Wuntho-Popa Arc comprises I-type granites with prominent Cu-Au mineralization. The easterly Mogok-Mandalay-Mergui Belt – here subdivided into a northerly Mogok Metamorphic Belt and a southerly Tin Province – comprising mainly S-type granites together with lesser I-type granites, and characterized by significant Sn-W mineralization, although some workers have classified these as A-types (Aung Zaw Myint et al., 2017; Jiang



et al., 2017). These two belts are coeval, forming between the early Cretaceous and mid-Miocene, and linked to Himalayan orogenesis and the closure of Neo-Tethys (Figure 4). Their spatial juxtaposition and their respective metallogenic endowments bear strong similarities to the metallogenic belts of the South American Cordillera (Gardiner et al., 2015).

Destruction of the Tethyan ocean in Southeast Asia commenced in the Permian as Palaeo-Tethys was subducted beneath the Asian plate; magmatism commenced at around 280 Ma in the southeast of Malaysia (Figure 14B), and attained its maximum volumetric output in the early Triassic (250–240 Ma) forming the Eastern Province granites prior to, or perhaps during, collision of Sibumasu with the Asian plate along the Bentong-Raub suture (Figure 14B). Crustal thickening and collision-related magmatism reached its nexus in the mid-to-late Triassic (230–210 Ma) to form the voluminous and highly stanniferous Main Range batholiths. Zircon isotope data from the Eastern and Main Range Provinces define the commencement of the Eastern Sibumasu Hf-isotope evolution trend marked on the  $\epsilon_{\text{Hf}}$  evolution plot (Figure 7). Eastern Province zircon U-Pb ages are older and have slightly less evolved  $\epsilon_{\text{Hf}}$  than the Main Range Province, consistent with a crustal signature for both, but with a more prolific tin endowment for the more evolved suite. Palaeo-Tethys is suggested to have been consumed fairly rapidly with maximum production of granite magma in the Triassic period and culminating in accretion of Sibumasu onto Asia by 230 Ma (Figure 4).

The subsequent evolution of the Neo-Tethyan related paired magmatic belts in Myanmar is slightly different to that of the Palaeo-Tethyan belts in Malaysia,

despite the fact that many parallels exist. Destruction of Neo-Tethys commenced at ca. 120 Ma (Figure 4) as oceanic crust was subducted beneath the western margin of Sibumasu. The oldest granites in the Wuntho-Popa Arc are I-type granites formed at 105–94 Ma (here, and Crow and Khin Zaw, 2017), accompanied by outpouring of the dominantly calc-alkaline Mawgyi Volcanics at around the same time and extending down to ca. 70 Ma. Subsequent pulses of granitoid magmatism occurred in the Palaeocene to Eocene at 60–40 Ma, and again in the mid-Miocene at 20–10 Ma. Mineralization is associated with both these events. The diorite and granodiorite-hosting porphyry style Cu-Mo-Au mineralization at Shangalon have been dated at 53 Ma and 38 Ma (Crow and Khin Zaw, 2017; Gardiner et al., 2016a), and the high sulphidation epithermal Cu mineralization at Monywa has been interpreted as forming at 13 Ma (Mitchell et al., 2011). The absence of reported mineralization in Late Cretaceous Wuntho–Popa magmatic suites contrasts with these mineralized younger suites. The zircon Hf isotope data imply that the Shangalon porphyry diorite may be sourced in part from the older granodiorite material, their more evolved  $\epsilon_{\text{Hf}}$  lying on a crustal evolution trend (Figure 7). Thus, it may be the Cu-Au endowment of the younger Cenozoic magmatic suites is related partly to processes of crustal reworking.

Collision of the Indian plate with Asia occurred at 50 Ma in the western and central Himalaya (e.g., Green et al., 2008), but subduction of Neo-Tethys continued through the Palaeogene period to the east and also along the western margins of Sibumasu. Construction of the Mogok-Mandalay-Mergui Belt was broadly coeval with the Wuntho–Popa Arc (Figure 4). Here, the oldest granites formed in the range 130–120 Ma, with the major pulse of

magmatism occurring in the Palaeocene to Eocene at 60–40 Ma. The host granite and associated W-Sn mineralization at the Mawchi Mine has been dated at 43 Ma (Aung Zaw Myint et al., 2017). It is pertinent to emphasize that mineralization in the Mogok-Mandalay-Mergui Belt is characterized by significant concentrations of tungsten in addition to, and often superseding, tin. As in the Wuntho–Popa Arc, late stage magmatism in the Mogok-Mandalay-Mergui Belt also occurred in mid-Miocene times, such as the 17 Ma Kabaing granite which is spatially associated with Cu-Au mineralization in the Mogok Metamorphic Belt.

Unlike the Eastern Province and Main Range Province granite belts in Malaysia that formed sequentially and largely within the Triassic period, the paired magmatic belts in Myanmar are coeval and formed over a more extended time period that ranged from Early Cretaceous to mid-Miocene. Collision did not herald the onset of crustal melting and magmatism in Myanmar but rather, as in the Andes, I- and S-type magmatism occurred contemporaneously, with differences in granite melt compositions reflecting differing protoliths as well as increasing distances from the trench and progressive enhancement of crustal input. This pattern is evident in the zircon Hf and O isotope trends of Figure 8. The Wuntho–Popa Arc is characterized by zircons with mantle  $\delta^{18}\text{O}$  signatures, whereas zircons from the Mogok-Mandalay-Mergui Belt are variably contaminated with crustal material. In terms of  $\epsilon\text{Hf}$  trends, Wuntho–Popa Arc isotopes define a mantle-like trend that evolves towards the chondritic (CHUR) value over time (Figure 7). Parts of the Mogok Metamorphic Belt fall on the Eastern Sibumasu  $\epsilon\text{Hf}$  evolution trend, however the Tin Province, as well as the northerly portion of the Mogok zone,

reflecting crustal sources that are less evolved than would be expected if Sibumasu basement were present as, or dominated, the protolith. Interestingly, it is this protolith (i.e. the so-called 'Slate Belt' lithologies or Mergui Group) that appear to have been responsible for the *Sn plus W* endowment of the Tin Province – this is in contrast to the *Sn only* endowment provided by the Eastern Sibumasu basement in Malaysia. These data suggest that the crustal source material that was melted to form the S-type, stanniferous granites of Southeast Asia differed as a function of geography and the secular tectonic evolution of the region.

These data are relevant to suggestions that the gap between Palaeo-Tethyan suturing at 230 Ma, and the onset of Neo-Tethyan subduction at ca. 130 Ma, an interval of relative magmatic quiescence (Figure 4), is one which may have witnessed the docking of a Tengchong Block onto northern Sibumasu during the closure of Meso-Tethys (Figure 10). This model finds support from the age of the Myitkyina ophiolite at 173 Ma (Liu et al., 2016), and our dating of a dacite at 172 Ma that defines the possible existence of a magmatic arc referred to here as part of the Tagaung-Myitkyina Belt. This latter belt on the basis of age determination alone cannot be part of the Wuntho–Popa Arc, but rather we suggest reflects subduction of a Meso-Tethys ocean beneath the northern (Baoshan) portion of Sibumasu (Figure 10). We interpret the Tagaung-Myitkyina Belt to be presently sited within the Tengchong Block, thus invoking a scenario whereby this belt is overthrust (westwards) onto the Tengchong Block during final suturing. The presence of such an arc could have implications for the prospectively of (poorly-explored) northern Myanmar,

since it is likely to be similar in its metallogenic signature to the Wuntho-Popa Arc.

### 6.3. The Zircon Geochemical Response to Myanmar's Metallogeny

In the Tin Province and the Wuntho–Popa Arc, Myanmar hosts two magmatic belts which have developed contrasting metallogeny: vein-and-pegmatite Sn-W versus porphyry Cu-Au and epithermal Cu styles. Their geographic location only a few 100 km's apart, the fact that they record near-contemporary magmatism (Figure 4) potentially driven through the same geodynamic event, means they present a natural laboratory for constraining the petrogenetic development of magmatic-hydrothermal mineralization. Accordingly, Gardiner et al. (2017a) undertook a zircon-based trace element and isotope study to constrain how zircon geochemistry may inform on the different characteristics leading to the contrasting types of metallogeny. In focusing on the role of source, redox and fractionation, these authors showed how the two belts may be broadly distinguished through zircon trace elements. A plot of U/Yb versus Hf highlights a greater crustal contribution in the source of the Tin Province (Figure 15A). Magmatic source is also distinguished through zircon Hf and O isotopes, as discussed for these two belts earlier (Figure 8).

Sn-W mineralization is associated with reducing, more fractionated magmatic systems, and Cu-Au with oxidizing, less fractionated magmatic systems (Blevin and Chappell, 1995; Ishihara, 2004). The Ce and Eu anomalies in zircon ( $Ce/Ce^*$  and  $Eu/Eu^*$ ) may be sensitive to redox and magma fractionation respectively (Gardiner et al., 2017a; Trail et al., 2012). When zircon  $Ce/Ce^*$  versus zircon  $Eu/Eu^*$  are plotted for the samples from both the

Myanmar belts (Figure 15B), the zircon analyses from Wuntho–Popa Arc granites are seen to have elevated Ce/Ce\* and higher Eu/Eu\*, whilst those from the Tin Province samples have lower Ce/Ce\*, and lower Eu/Eu\* (Gardiner et al., 2017a). These differences in Ce and Eu anomalies reflect the differences in redox and fractionation expected for Cu-Au and Sn-W bearing granites (Blevin and Chappell, 1995). Significantly, those Tin Province samples with elevated whole-rock Sn contents were shown to have significantly lower Eu/Eu\*, implying significant fractionation and concentration Sn.

#### 6.4. Southeast Asian Metallotects: Summary

The metallogenic character of granite belts in Myanmar and Malaysia reflects the crustal architecture of the region and can be used to constrain the secular tectonic evolution of Indosinian and Himalayan orogenesis, as well as in identifying zones of mineralization and the nature of granite melt protoliths and magma fertility. The region is remarkable for its prolific endowment of granite-hosted Sn-W mineralization in two quite distinct granite belts related to sequential Indosinian and Himalayan orogenesis. The Wuntho-Popa Arc is an unadulterated calc-alkaline, I-type magmatic belt whose magma isotopic and geochemical compositions reflect a strong mantle-like protolith, and whose metallogenic endowment is dominated by porphyry and epithermal style Cu-Au(-Mo) mineralization. It formed in response to Neo-Tethyan subduction over an extended period from the early Cretaceous to mid-Miocene. An older, mid-Jurassic, version of this arc may be present in the Tagaung-Myitkyina Belt of northern Myanmar, if it can be demonstrated that a (Tengchong) crustal block

docked onto northern Sibumasu in Meso-Tethyan times, i.e. the mid-Jurassic, and which may also find some expression in the older magmatism of the Mogok Metamorphic Belt.

The Mogok-Mandalay-Mergui Belt and Main Range Province of Malaysia, which together extend over a strike length of some 2500 km and represent the pre-eminent Sn-W metallotect on the planet, had a convoluted origin that involved successive periods of Palaeo- and Neo-Tethyan subduction/collision and the generation of crustally-dominated granite melts derived from different protoliths and/or continental blocks. These differences may explain the different Sn and Sn-W endowments evident in the Main Range (Malaysia) and Mogok-Mandalay-Mergui (Myanmar) Belts respectively. An evolved crustal signature is clearly a pre-requisite for Sn-W fertility in granite-hosted magmatic-hydrothermal styles of mineralization, although this study raises questions regarding the causes of repeated Large Ion Lithophile (LILE) endowment in granites that formed at different times and from different crustal sources. The degree of LILE fertility in granite magmas also appears to be related to magma generation and source constraints, as suggested in the differing extents to which the Main Range and Eastern Province granite belts are mineralized for tin.

## **7. Postscript**

Zircon-based geochronology and isotope studies provide a foundation both for constraining lithospheric architecture and tectonic history, but also for understanding the source of magma, which ultimately develops magmatic-

hydrothermal mineralization. In presenting zircon U-Pb, Lu-Hf and O isotope data from magmatic rocks across Myanmar, we attempt to isotopically characterize Myanmar's magmatic belts. The results can then be interpreted to further inform on the nature of crustal architecture and tectonic assembly, and to understand the metallogenic character of the major magmatic belts. In proposing a tectonic model for the assembly of Myanmar we acknowledge that neither our model nor the existing models accommodate all the available geological evidence. There remains work to be done.

### **Acknowledgments**

We thank M. Santosh for extending the invite to author this contribution. We acknowledge the Oxford University Fell Fund (Ref. DGD07260), Dark Capital Ltd, Highland Metals Pte Ltd, and Six Degrees Investor Relations Pty Ltd for financial support of the Oxford Burma Project, and Curtin University for financial support of NJG. Analytical support at NIGL was funded through NIGFSC grant IP-1554-0515. Andrew Mitchell is thanked for the use of Figure 6. We acknowledge logistical assistance from U Kyi Htun, U Tin Aung Myint, Daw Than Than Nu, U Win Zaw and U Aung Tin. U Nyunt Htay is thanked for the Yadanabon Mine sample. Brad McDonald is thanked for technical support at Curtin. We thank Tony Barber and Mike Crow for their helpful reviews, and M Santosh for editorial handling. The NordSIMS facility is operated under an agreement between the research funding agencies of Denmark, Iceland, Norway and Sweden, the Geological Survey of Finland and the Swedish Museum of Natural History, and we are indebted to Kerstin Lindén and Lev



Ilyinsky for technical support whilst at NordSIMS. This is NordSIMS publication 549.

## References

Ahrendt, H., Hansen, B.T., Lumjuan, A., Mickein, A., Wemmer, K., 1997. Tectonometamorphic evolution of NW-Thailand deduced from U/Pb-, Rb/Sr-, Sm/Nd- and K/Ar-isotope investigations, The International Conference on Stratigraphy and Tectonic Evolution of Southeast Asia and the South Pacific, Bangkok.

Archaryya, S.K., 2007. Collisional emplacement history of the Naga-Andaman ophiolites and the position of the eastern Indian suture. *Journal of Asian Earth Sciences* 29, 229-242.

Audley-Charles, M.G., 1988. Evolution of the southern margin of Tethys (North Australian region) from Early Permian to Late Cretaceous, In: Audley-Charles, M.G., Hallam, A. (Eds.), *Gondwana and Tethys*. The Geological Society, London, pp. 79-100.

Aung Zaw Myint, Khin Zaw, Ye Myint Swe, Yonezu, K., Cai, Y., Manaka, T., Watanabe, K., 2017. Geochemistry and geochronology of granites hosting the Mawchi Sn-W deposit, Myanmar: Implications for tectonic setting and granite emplacement, In: Barber, A.J., Khin Zaw, Crow, M.J. (Eds.), *Myanmar: Geology, Resources and Tectonics*. The Geological Society, Memoir 48, London, pp. 387-402.

Barber, A., Crow, M., 2009. Structure of Sumatra and its implications for the tectonic assembly of Southeast Asia and the destruction of Paleotethys. *Island Arc* 18, 3-20.

Barber, A., Khin Zaw, Crow, M., 2017a. Myanmar: Geology, Resources and Tectonics, Memoirs. The Geological Society, Memoir 48.

Barber, A., Khin Zaw, Crow, M., 2017b. The pre-Cenozoic tectonic evolution of Myanmar, In: Barber, A., Khin Zaw, Crow, M. (Eds.), *Myanmar: Geology, Resources and Tectonics*. The Geological Society, Memoir 48, London, pp. 689-714.

Barber, A., Ridd, M.F., Crow, M., 2011. The origin, movement and assembly of the pre-Tertiary tectonic units of Thailand, In: Ridd, M.F., Barber, A., Crow, M. (Eds.), *The Geology of Thailand*. The Geological Society, London, pp. 507-537.

Barley, M.E., Pickard, A.L., Khin Zaw, Rak, P., Doyle, M.G., 2003. Jurassic to Miocene magmatism and metamorphism in the Mogok metamorphic belt and the India-Eurasia collision in Myanmar. *Tectonics* 22, n/a-n/a.

Barr, S.M., Macdonald, A.S., 1991. Toward a late Paleozoic–early Mesozoic tectonic model for Thailand. *Thailand Journal of Geosciences* 1, 11-22.

Barr, S.M., MacDonald, A.S., Dunning, G.R., Ounchanum, P., Yaowanoyothin, W., 2000. Petrochemistry, U–Pb (zircon) age, and paleotectonic setting of the Lampang volcanic belt, northern Thailand. *Journal of the Geological Society* 157, 553-563.

Barr, S.M., Macdonald, A.S., Ounchanum, P., Hamilton, M.A., 2006. Age, tectonic setting and regional implications of the Chiang Khong volcanic suite, northern Thailand. *Journal of the Geological Society* 163, 1037-1046.

Belousova, E.A., Kostitsyn, Y.A., Griffin, W.L., Begg, G.C., O'Reilly, S.Y., Pearson, N.J., 2010. The growth of the continental crust: Constraints from zircon Hf-isotope data. *Lithos* 119, 457-466.

Bender, F., 1983. *Geology of Burma*. Gebruder Borntraeger, Berlin.

Bertrand, G., Rangin, C., Maluski, H., Bellon, H., 2001. Diachronous cooling along the Mogok Metamorphic Belt (Shan scarp, Myanmar); the trace of the northward migration of the Indian syntaxis. *Journal of Asian Earth Sciences* 19, 649-659.

BGR, 1976. *Concluding Report on Lead/Silver/Zinc Ore Exploration in the Vicinity of the Bawdwin Mine, Shan State (North East Burma)*. Bundesanstalt für Geowissenschaften und Rohstoffe, Hanover.

Blevin, P.L., Chappell, B.W., 1995. Chemistry Origin, and Evolution of Mineralized Granites in the Lachlan Fold Belt, Australia: The Metallogeny of I- and S-Type Granites. *Economic Geology* 90, 1604-1619.

Brinckmann, J., Hinze, C., 1981. On the geology of the Bawdwin lead–zinc mine, Northern Shan State, Burma. *Geologisches Jahrbuch* D43, 7-45.

Brunnschweiler, R.O., 1970. Contribution to the post-Silurian geology of Burma (Northern Shan States and Karen State). *Journal of the Geological Society of Australia* 17, 59-79.

Bunopas, S., 1981. *Paleogeographic History of Western Thailand and Adjacent Parts of South-east Asia*. Victoria University of Wellington, Wellington.

Burchfiel, B.C., Chen, Z., 2012. *Tectonics of the Southeastern Tibetan Plateau and Its Adjacent Foreland*. Geological Society of America, Boulder.

Chhibber, H.L., 1934. *The mineral resources of Burma*. Macmillan and Co, London.

Cobbing, E.J., 2005. Granites, In: Barber, A., Crow, M., Milsom, J.S. (Eds.), *Sumatra: Geology, Resources and Tectonic Evolution*. Geological Society, London, pp. 54-62.

Cobbing, E.J., Mallick, D.I.J., Pitfield, P.E.J., Teoh, L.H., 1986. The granites of the Southeast Asian Tin Belt. *Journal of the Geological Society* 143, 537-550.

Cobbing, E.J., Pitfield, P.E.J., Darbyshire, D., Mallick, D.I.J., 1992. The granites of the Southeast Asian Tin Belt. *British Geological Survey, Overseas Memoirs* 10.

Coggin Brown, J., Heron, A., 1923. *The Geology and Ore Deposits of the Tavoy District*. Geological Survey of India, Calcutta.

Crow, M., Khin Zaw, 2017. Geochronology in Myanmar, In: Barber, A., Khin Zaw, Crow, M. (Eds.), *Myanmar: Geology, Resources and Tectonics*. The Geological Society, Memoir 48, London, pp. 713-759.

Dhuime, B., Hawkesworth, C., Cawood, P.A., Storey, C.D., 2012. A Change in the Geodynamics of Continental Growth 3 Billion Years Ago. *Science* 335, 1334-1336.

Dong, G., Mo, X., Zhao, Z., Zhu, D., Goodman, R.C., Kong, H., Wang, S., 2013. Zircon U–Pb dating and the petrological and geochemical constraints on Lincang granite in Western Yunnan, China: Implications for the closure of the Paleo-Tethys Ocean. *Journal of Asian Earth Sciences* 62, 282-294.

Dunning, G.R., Macdonald, A.S., Barr, S.M., 1995. Zircon and monazite U-Pb dating of the Doi Inthanon core complex, northern Thailand: implications for extension within the Indosinian Orogen. *Tectonophysics* 251, 197-213.

Gardiner, N.J., Hawkesworth, C.J., Robb, L.J., Whitehouse, M.J., Roberts, N.M., Kirkland, C.L., Evans, N.J., 2017a. Contrasting Granite Metallogeny through the Zircon Record: A Case Study from Myanmar. *Scientific Reports* 7, 748.

Gardiner, N.J., Robb, L.J., Morley, C.K., Searle, M.P., Cawood, P.A., Whitehouse, M.J., Kirkland, C.L., Roberts, N.M.W., Tin Aung Myint, 2016a. The tectonic and metallogenic framework of Myanmar: A Tethyan mineral system. *Ore Geology Reviews* 79, 26-45.

Gardiner, N.J., Robb, L.J., Searle, M.P., 2014. The metallogenic provinces of Myanmar. *Applied Earth Science* 123, 25-38.

Gardiner, N.J., Robb, L.J., Searle, M.P., Kyi Htun, Khin Zaw, 2017b. The Bawdwin Mine, Myanmar: a review of its geological setting and genesis, In: Barber, A., Khin Zaw, Crow, M. (Eds.), *Myanmar: Geology, Resources and Tectonics*. The Geological Society, Memoir 48, London, pp. 671-188.

Gardiner, N.J., Roberts, N.M.W., Morley, C.K., Searle, M.P., Whitehouse, M.J., 2016b. Did Oligocene crustal thickening precede basin development in

northern Thailand? A geochronological reassessment of Doi Inthanon and Doi Suthep. *Lithos* 240-243, 69-83.

Gardiner, N.J., Searle, M.P., Morley, C.K., Whitehouse, M.P., Spencer, C.J., Robb, L.J., 2016c. The closure of Palaeo-Tethys in Eastern Myanmar and Northern Thailand: New insights from zircon U–Pb and Hf isotope data. *Gondwana Research* 39, 401-422.

Gardiner, N.J., Searle, M.P., Robb, L.J., Morley, C.K., 2015. Neo-Tethyan magmatism and metallogeny in Myanmar – An Andean analogue? *Journal of Asian Earth Sciences* 106, 197-215.

Garnier, V., Giuliani, G., Ohnenstetter, D., Fallick, A.E., Dubessy, J., Banks, D., Vinh, H.Q., Lhomme, T., Maluski, H., Pêcher, A., Bakhsh, K.A., Long, P.V., Trinh, P.T., Schwarz, D., 2008. Marble-hosted ruby deposits from Central and Southeast Asia: Towards a new genetic model. *Ore Geology Reviews* 34, 169-191.

Garson, M.S., Young, B., Mitchell, A.H.G., Tarr, B.A.R., 1975. The geology of the tin belt on Peninsula Thailand around Phuket, Phang-Nga and Takua Pa. Institute of Geological Sciences, London.

Gatinsky, Y.G., Hutchison, C.S., 1987. Cathaysia, Gondwanaland and the Palaeotethys in the evolution of continental Southeast Asia. *Geological Society of Malaysia Bulletin* 20, 179-199.

Green, O.R., Searle, M.P., Corfield, R.I., Corfield, R.M., 2008. Cretaceous-Tertiary Carbonate Platform Evolution and the Age of the India-Asia Collision along the Ladakh Himalaya (Northwest India). *The Journal of Geology* 116, 331-353.

Grimes, C.B., Wooden, J.L., Cheadle, M.J., John, B.E., 2015. "Fingerprinting" tectono-magmatic provenance using trace elements in igneous zircon. *Contributions to Mineralogy and Petrology* 170.

Groves, D.I., Bierlein, F.P., 2007. Geodynamic settings of mineral deposit systems. *Journal of the Geological Society* 164, 19-30.

Hall, R., 2012. Late Jurassic–Cenozoic reconstructions of the Indonesian region and the Indian Ocean. *Tectonophysics* 570-571, 1-41.

Hall, R., 2014. The origin of Sundaland, In: Basuki, N.I., Dahlius, A.Z. (Eds.), MGEI Annual Convention, Proceedings of Sundaland Resources, Palembang, South Sumatra, Indonesia, pp. 1-25.

Hall, R., Clements, B., Smyth, H.R., 2009. Sundaland: basement character, structure and plate tectonic development, Proceedings Indonesian Petroleum Association. Thirty- Third Annual Convention and Exhibition (IPA09-G134), pp. 131-176.

Hawkesworth, C.J., Kemp, A.I.S., 2006. Using hafnium and oxygen isotopes in zircons to unravel the record of crustal evolution. *Chemical Geology* 226, 144-162.

Hennig, D., Lehmann, B., Frei, D., Belyatsky, B., Zhao, X.F., Cabral, A.R., Zeng, P.S., Zhou, M.F., Schmidt, K., 2009. Early Permian seafloor to continental arc magmatism in the eastern Paleo-Tethys: U–Pb age and Nd–Sr isotope data from the southern Lancangjiang Zone, Yunnan, China. *Lithos* 113, 408-422.

Hodges, K.V., 2000. Tectonics of the Himalaya and southern Tibet from two perspectives. *Geological Society of America Bulletin* 112, 324-350.

Hopwood, T., 1985. Exploration Potential of the Bawdwin Silver–Lead Mine, Northern Shan States, Burma, TH Report No. 85. Australian Mineral Development Laboratories, Adelaide.

Hutchison, C.S., 1975. Ophiolite in Southeast Asia. *Geological Society of America Bulletin* 86, 797-806.

Hutchison, C.S., 1989. *Geological Evolution of South-East Asia*. Clarendon Press, Oxford.

Hutchison, C.S., Taylor, D., 1978. Metallogensis in SE Asia. *Journal of the Geological Society* 135, 407-428.

Ishihara, S., 2004. The redox state of granitoids relative to tectonic setting and earth history: The magnetite–ilmenite series 30 years later. *Transactions of the Royal Society of Edinburgh: Earth Sciences* 95, 23-33.

Iyer, L.A.N., 1953. The geology and gemstones of the Mogok Stone Tract, Burma. *Memoirs of the Geological Survey of India* 82, 100.

Jackson, S.E., Pearson, N.J., Griffin, W.L., Belousova, E.A., 2004. The application of laser ablation-inductively coupled plasma-mass spectrometry to in situ U–Pb zircon geochronology. *Chemical Geology* 211, 47-69.

Jiang, H., Li, W.-Q., Jiang, S.-Y., Wang, H., Wei, X.-P., 2017. Geochronological, geochemical and Sr-Nd-Hf isotopic constraints on the petrogenesis of Late Cretaceous A-type granites from the Sibumasu Block, Southern Myanmar, SE Asia. *Lithos* 268-271, 32-47.

Kanjanapayont, P., Klotz, U., Thoni, M., Grasemann, B., Edwards, M., 2012. Rb-Sr, Sm-Nd and U-Pb geochronology of the rocks within the Khlong Marui shear zone, southern Thailand. *Journal of Asian Earth Sciences* 56, 263-275.

Kawakami, T., Nakano, N., Higashino, F., Hokada, T., Osanai, Y., Yuhara, M., Charusiri, P., Kamikubo, H., Yonemura, K., Hirata, T., 2014. U-Pb zircon and CHIME monazite dating of granitoids and high-grade metamorphic rocks from the Eastern and Peninsular Thailand — A new report of Early Paleozoic granite. *Lithos* 200-201, 64-79.

Kemp, A.I., Hawkesworth, C.J., Foster, G.L., Paterson, B.A., Woodhead, J.D., Hergt, J.M., Gray, C.M., Whitehouse, M.J., 2007. Magmatic and crustal differentiation history of granitic rocks from Hf-O isotopes in zircon. *Science* 315, 980-983.

Kemp, A.I., Hawkesworth, C.J., Paterson, B.A., Kinny, P.D., 2006. Episodic growth of the Gondwana supercontinent from hafnium and oxygen isotopes in zircon. *Nature* 439, 580-583.

Kerrick, R., Goldfarb, R.J., Richards, J.P., 2005. Metallogenic provinces in an evolving geodynamic framework. *Economic Geology 100th Anniversary Volume*, 1097-1136.

Khin Zaw, 1990. Geological, petrological and geochemical characteristics of granitoid rocks in Burma: with special reference to the associated W-Sn mineralization and their tectonic setting. *Journal of Southeast Asian Earth Sciences* 4, 293-335.

Khin Zaw, 2017. Overview of mineralization styles and tectonic-metallogenic setting in Myanmar, In: Barber, A., Khin Zaw, Crow, M. (Eds.), *Myanmar: Geology, Resources and Tectonics*. The Geological Society, Memoir 48, London, pp. 533-557.

Khin Zaw, Khin Myo Thet, 1983. A note on a fluid inclusion study of tin-tungsten mineralization at Mawchi Mine, Kayah State, Burma. *Economic Geology* 78, 530-534.

Khin Zaw, Meffre, S., Lai, C.-K., Burrett, C., Santosh, M., Graham, I., Manaka, T., Salam, A., Kamvong, T., Cromie, P., 2014. Tectonics and metallogeny of mainland Southeast Asia — A review and contribution. *Gondwana Research* 26, 5-30.

Kirkland, C.L., Smithies, R.H., Woodhouse, A.J., Howard, H.M., Wingate, M.T.D., Belousova, E.A., Cliff, J.B., Murphy, R.C., Spaggiari, C.V., 2013. Constraints and deception in the isotopic record; the crustal evolution of the west Musgrave Province, central Australia. *Gondwana Research* 23, 759-781.

Lee, H.-Y., Chung, S.-L., Yang, H.-M., 2016. Late Cenozoic volcanism in central Myanmar: Geochemical characteristics and geodynamic significance. *Lithos* 245, 174-190.

Li, G.J., Wang, Q.F., Huang, Y.H., Gao, L., Yu, L., 2016. Petrogenesis of middle Ordovician peraluminous granites in the Baoshan block: Implications for the early Paleozoic tectonic evolution along East Gondwana. *Lithos* 245, 76-92.

Liu, C.-Z., Chung, S.-L., Wu, F.-Y., Zhang, C., Xu, Y., Wang, J.-G., Chen, Y., Guo, S., 2016. Tethyan suturing in Southeast Asia: Zircon U-Pb and Hf-O isotopic constraints from Myanmar ophiolites. *Geology* 44, 311-314.

Ludwig, K.R., 2004. User's manual for Isoplot, 3.16: A Geochronological Toolkit for Microsoft Excel, Berkeley Geochronology Center Special Publication, Ridge Road, Berkeley CA, USA.

Macdonald, A.S., Barr, S.M., Dunning, G.A., Yaowanoyothin, W., 1993a. The Doi Inthanon metamorphic core complex in NW Thailand: age and tectonic significance. *Journal of Southeast Asian Earth Sciences* 8, 117-125.

Macdonald, A.S., Barr, S.M., Dunning, G.R., Yaowanoyothin, W., 1993b. The Doi Inthanon metamorphic core complex in NW Thailand: age and tectonic significance. *Journal of Southeast Asian Earth Sciences* 8, 117-125.

Maury, R.C., Pubellier, M., Rangin, C., Wulput, L., Cotton, J., Socquet, A., Bellon, H., Guillaud, J.P., Hla Myo Htun, 2004. Quaternary calc-alkaline and alkaline volcanism in an hyper-oblique

convergence setting, central Myanmar and western Yunnan. *Bulletin de la Societe Geologique de France* 175, 461-472.

Metcalfe, I., 1990. Allochthonous terrane processes in Southeast Asia. *Philosophical Transactions, Royal Society of London A331*, 625-640.

Metcalfe, I., 1996. Pre-Cretaceous evolution of SE Asian terranes. *Geological Society, London, Special Publications* 106, 97-122.

Metcalfe, I., 2000. The Bentong-Raub Suture Zone. *Journal of Asian Earth Sciences* 18, 691-712.

Metcalfe, I., 2011a. Palaeozoic–Mesozoic history of SE Asia. *Geological Society, London, Special Publications* 355, 7-35.

Metcalfe, I., 2011b. Tectonic framework and Phanerozoic evolution of Sundaland. *Gondwana Research* 19, 3-21.

Metcalfe, I., 2013. Gondwana dispersion and Asian accretion: Tectonic and palaeogeographic evolution of eastern Tethys. *Journal of Asian Earth Sciences* 66, 1-33.

Mi Paik, 2017. Geochemistry and geochronology of granitoid rocks in the Mawpalaw, Taung area, Thanbyuzayat Township, southern Myanmar: their petrogenesis and tectonic setting, In: Barber, A., Khin Zaw, Crow, M. (Eds.), Myanmar: Geology, Resources and Tectonics. The Geological Society, Memoir 48, London, pp. 403-414.

Mitchell, A.H.G., 1977. Tectonic settings for emplacement of Southeast Asian tin granites. *Bulletin of the Geological Society of Malaysia* 9, 123-140.

Mitchell, A.H.G., 1993. Cretaceous-Cenozoic tectonic events in the western Myanmar (Burma)-Assam region. *Journal of the Geological Society* 150, 1089-1102.

Mitchell, A.H.G., 2018. Geological Belts, Plate Boundaries, and Mineral Deposits in Myanmar. Elsevier.

Mitchell, A.H.G., AUSA, C.A., Deiparine, L., Tin Hlaing, Nuant Htay, Khine, A., 2004. The Modi Taung–Nankwe gold district, Slate belt, central Myanmar: mesothermal veins in a Mesozoic orogen. *Journal of Asian Earth Sciences* 23, 321-341.

Mitchell, A.H.G., Chung, S.-L., Thura Oo, Lin, T.-H., Hung, C.-H., 2012. Zircon U–Pb ages in Myanmar: Magmatic–metamorphic events and the closure of a neo-Tethys ocean? *Journal of Asian Earth Sciences* 56, 1-23.

Mitchell, A.H.G., Myint Thein Htay, Kyaw Min Htun, 2015. The Medial Myanmar Suture Zone and the Western Myanmar- Mogok foreland. *Journal of the Myanmar Geosciences Society* 6, 73-88.

Mitchell, A.H.G., Myint Thein Htay, Kyaw Min Htun, Myint Naing Win, Thura Oo, Tin Hlaing, 2007. Rock relationships in the Mogok metamorphic belt, Tatkon to Mandalay, central Myanmar. *Journal of Asian Earth Sciences* 29, 891-910.

Mitchell, A.H.G., Win Myint, Kyi Lynn, Myint Thein Htay, Maw Oo, Thein Zaw, 2011. Geology of the High Sulfidation Copper Deposits, Monywa Mine, Myanmar. *Resource Geology* 61, 1-29.

Morley, C.K., 2012. Late Cretaceous–Early Palaeogene tectonic development of SE Asia. *Earth-Science Reviews* 115, 37-75.

Morley, C.K., Searle, M., 2017. Chapter 5 Regional tectonics, structure and evolution of the Andaman–Nicobar Islands from ophiolite formation and obduction to collision and back-arc spreading. Geological Society, London, *Memoirs* 47, 51-74.

Myanmar Geosciences Society, 2014. Geological Map of Myanmar, 1:2,250,000. Myanmar Geosciences Society, Yangon.

Nantasini, P., Hauzenberger, C., Liu, X., Krenn, K., Dong, Y., Thoni, M., Wathanakul, P., 2012. Occurrence of high grade Thabsila metamorphic complex within the low grade Three Pagodas shear zone, Kanchanaburi Province, western Thailand, petrology and geochronology. *Journal of Asian Earth Sciences* 60, 68-87.

Nowell, G., Parrish, R.R., 2001. Simultaneous acquisition of isotope compositions and parent/daughter ratios by non-isotope dilution-mode Plasma Ionisation Multi-collector Mass Spectrometry (PIMMS). *Special Publication Royal Society of Chemistry* 267, 298-310.

Palin, R.M., Searle, M.P., Morley, C.K., Charusiri, P., Horstwood, M.S.A., Roberts, N.M.W., 2013. Timing of metamorphism of the Lansang gneiss and implications for left-lateral motion along the Mae Ping (Wang Chao) strike-slip fault, Thailand. *Journal of Asian Earth Sciences* 76, 120-136.



- Paton, C., Hellstrom, J., Paul, B., Woodhead, J.D., Hergt, J.M., 2011. Iolite: Freeware for the visualisation and processing of mass spectrometric data. *Journal of Analytical Atomic Spectrometry* 26, 2508-2518.
- Peng, T., Wang, Y., Zhao, G., Fan, W., Peng, B., 2008. Arc-like volcanic rocks from the southern Lancangjiang zone, SW China: geochronological and geochemical constraints on their petrogenesis and tectonic implications. *Lithos* 102, 358-373.
- Peng, T., Wilde, S.A., Wang, Y., Fan, W., Peng, B., 2013. Mid-Triassic felsic igneous rocks from the southern Lancangjiang Zone, SW China: petrogenesis and implications for the evolution of Paleo-Tethys. *Lithos* 168, 15-32.
- Rangin, C., Maurin, T., Masson, F., 2013. Combined effects of Eurasia/Sunda oblique convergence and East-Tibetan crustal flow on the active tectonics of Burma. *Journal of Asian Earth Sciences* 76, 185-194.
- Replumaz, A., Tapponnier, P., 2003. Reconstruction of the deformed collision zone Between India and Asia by backward motion of lithospheric blocks. *Journal of Geophysical Research* 108, 2285.
- Ridd, M.F., 2009. The Phuket Terrane: A Late Palaeozoic rift at the margin of Sibumasu. *Journal of Asian Earth Sciences* 36, 238-251.
- Ridd, M.F., 2011. Lower Palaeozoic, In: Ridd, M.F., Barber, A., Crow, M. (Eds.), *The Geology of Thailand*. The Geological Society, London, pp. 33-51.
- Ridd, M.F., 2015. East flank of the Sibumasu block in NW Thailand and Myanmar and its possible northward continuation into Yunnan: a review and suggested tectono-stratigraphic interpretation. *Journal of Asian Earth Sciences* 104, 160-174.
- Ridd, M.F., 2016. Should Sibumasu be renamed Sibuma? The case for a discrete Gondwana-derived block embracing western Myanmar, upper Peninsular Thailand and NE Sumatra. *Journal of the Geological Society* 173, 249-264.
- Ridd, M.F., 2017. Karen-Tenasserim unit, In: Barber, A., Khin Zaw, Crow, M. (Eds.), *Myanmar: Geology, Resources and Tectonics*. The Geological Society, Memoir 48, London.
- Roberts, N.M.W., Spencer, C.J., 2015. The zircon archive of continent formation through time. Geological Society, London, Special Publications 389, 197-225.
- Sanematsu, K., Manaka, T., Khin Zaw, 2014. Geochemical and Geochronological Characteristics of Granites and Sn-W-REE Mineralization in the Thanintharyi Region, Southern Myanmar, GEOSEA XIII - GeoMyanmar 2014, Yangon, pp. 19-20.

- Schellmann, W., 1989. Composition and origin of lateritic nickel ore at Tagaung Taung, Burma. *Mineralium Deposita* 24, 161-168.
- Scherer, E.E., Munker, C., Mezger, K., 2001. Calibration of the Lutetium-Hafnium Clock. *Science* 293, 683-686.
- Scherer, E.E., Whitehouse, M., Munker, C., 2007. Zircon as a Monitor of Crustal Growth. *Elements* 3, 19-24.
- Searle, M.P., Elliott, J.R., Phillips, R.J., Chung, S.L., 2011. Crustal-lithospheric structure and continental extrusion of Tibet. *Journal of the Geological Society* 168, 633-672.
- Searle, M.P., Morley, C.K., 2011. Tectonic and thermal evolution of Thailand in the regional context of SE Asia, In: Ridd, M.F., Barber, A., Crow, M. (Eds.), *The Geology of Thailand*. The Geological Society, London, pp. 539-572.
- Searle, M.P., Morley, C.K., Waters, D.J., Gardiner, N.J., Kyi Htun, Than Than Nu, Robb, L.J., 2017. Tectonic and metamorphic evolution of the Mogok Metamorphic and Jade Mines belts and ophiolitic terranes of Burma (Myanmar), In: Barber, A., Khin Zaw, Crow, M. (Eds.), *Myanmar: Geology, Resources and Tectonics*, 48 ed. The Geological Society, Memoir 48, London, pp. 261-293.
- Searle, M.P., Noble, S.R., Cottle, J.M., Waters, D.J., Mitchell, A.H.G., Tin Hlaing, Horstwood, M.S.A., 2007. Tectonic evolution of the Mogok metamorphic belt, Burma (Myanmar) constrained by U-Th-Pb dating of metamorphic and magmatic rocks. *Tectonics* 26, n/a-n/a.
- Searle, M.P., Robb, L.J., Gardiner, N.J., 2016. Tectonic Processes and Metallogeny along the Tethyan Mountain Ranges of the Middle East and South Asia (Oman, Himalaya, Karakoram, Tibet, Myanmar, Thailand, Malaysia). *Economic Geology Special Publication* 19, 301-327.
- Searle, M.P., Whitehouse, M.J., Robb, L.J., Ghani, A.A., Hutchison, C.S., Sone, M., Ng, S.W.P., Roselee, M.H., Chung, S.L., Oliver, G.J.H., 2012. Tectonic evolution of the Sibumasu-Indochina terrane collision zone in Thailand and Malaysia: constraints from new U-Pb zircon chronology of SE Asian tin granitoids. *Journal of the Geological Society* 169, 489-500.
- Sengor, A.M.C., 1987. Tectonics of the Tethysides: orogenic collage development in a collisional setting. *Annual Review of Earth and Planetary Sciences* 15, 213-244.
- Sevastjanova, I., Hall, R., Rittner, M., Saw Mu Tha Lay Paw, Tin Tin Naing, Alderton, D.H., Comfort, G., 2016. Myanmar and Asia united, Australia left behind long ago. *Gondwana Research* 32, 24-40.
- Sláma, J., Košler, J., Condon, D.J., Crowley, J.L., Gerdes, A., Hanchar, J.M., Horstwood, M.S.A., Morris, G.A., Nasdala, L., Norberg, N., Schaltegger, U., Schoene, B., Tubrett, M.N., Whitehouse, M.J., 2008. Plešovice zircon — A

new natural reference material for U–Pb and Hf isotopic microanalysis. *Chemical Geology* 249, 1-35.

Soe Win, Malar Myo Myint, 1998. Mineral Potential of Myanmar. *Resource Geology* 48, 209-218.

Sone, M., Metcalfe, I., 2008. Parallel Tethyan sutures in mainland Southeast Asia: New insights for Palaeo-Tethys closure and implications for the Indosinian orogeny. *Comptes Rendus Geoscience* 340, 166-179.

Spencer, C.J., Cawood, P.A., Hawkesworth, C.J., Prave, A.R., Roberts, N.M.W., Horstwood, M.S.A., Whitehouse, M.J., 2015. Generation and preservation of continental crust in the Grenville Orogeny. *Geoscience Frontiers* 6, 357-372.

Stacey, J.S., Kramers, J.D., 1975. Approximation of terrestrial lead isotope evolution by a two-stage model. *Earth and Planetary Science Letters* 26, 207-221.

Stork, A.L., Selby, N.D., Heyburn, R., Searle, M.P., 2008. Accurate Relative Earthquake Hypocenters Reveal Structure of the Burma Subduction Zone. *Bulletin of the Seismological Society of America* 98, 2815-2827.

Than Htun, Than Htay, Khin Zaw, 2017. Tin-tungsten deposits of Myanmar, In: Barber, A., Khin Zaw, Crow, M. (Eds.), *Myanmar: Geology, Resources and Tectonics*. The Geological Society, Memoir 48, London, pp. 627-629.

Trail, D., Bruce Watson, E., Tailby, N.D., 2012. Ce and Eu anomalies in zircon as proxies for the oxidation state of magmas. *Geochimica et Cosmochimica Acta* 97, 70-87.

Valley, J., 2003. Oxygen Isotopes in Zircon. *Reviews in Mineralogy and Geochemistry* 53, 343-385.

Veevers, J.J., 1988. Morphotectonics of Australia's northwestern margin — a review, In: Purcell, P.G., Purcell, R.R. (Eds.), *Shelf Proceedings of Petroleum Exploration Society of Australia Symposium*, Perth, pp. 19-27.

Wai-Pan Ng, S., Chung, S.-L., Robb, L.J., Searle, M.P., Ghani, A.A., Whitehouse, M.J., Oliver, G.J.H., Sone, M., Gardiner, N.J., Roselee, M.H., 2015a. Petrogenesis of Malaysian granitoids in the Southeast Asian tin belt: Part 1. Geochemical and Sr-Nd isotopic characteristics. *Geological Society of America Bulletin* 127, 1209-1237.

Wai-Pan Ng, S., Whitehouse, M.J., Roselee, M.H., Teschner, C., Murtadha, S., Oliver, G.J.H., Ghani, A.A., Chang, S.-C., 2017. Late Triassic granites from Bangka, Indonesia: A continuation of the Main Range granite province of the South-East Asian Tin Belt. *Journal of Asian Earth Sciences* 138, 548-561.

Wai-Pan Ng, S., Whitehouse, M.J., Searle, M.P., Robb, L.J., Ghani, A.A., Chung, S.-L., Oliver, G.J.H., Sone, M., Gardiner, N.J., Roselee, M.H., 2015b.

Petrogenesis of Malaysian granitoids in the Southeast Asian tin belt: Part 2. U-Pb zircon geochronology and tectonic model. *Geological Society of America Bulletin* 127, 1238-1258.

Wang, J.-G., Wu, F.-Y., Tan, X.-C., Liu, C.-Z., 2014. Magmatic evolution of the Western Myanmar Arc documented by U-Pb and Hf isotopes in detrital zircon. *Tectonophysics* 612-613, 97-105.

Wang, Y., He, H., Cawood, P.A., Srithai, B., Feng, Q., Fan, W., Zhang, Y., Qian, X., 2016. Geochronological, elemental and Sr-Nd-Hf-O isotopic constraints on the petrogenesis of the Triassic post-collisional granitic rocks in NW Thailand and its Paleotethyan implications. *Lithos* 266-267, 264-286.

Watkinson, I., Elders, C., Batt, G., Jourdan, F., Hall, R., McNaughton, N.J., 2011. The timing of strike-slip shear along the Ranong and Khlong Marui faults, Thailand. *Journal of Geophysical Research* 116.

Whitehouse, M.J., Kamber, B.S., 2005. Assigning Dates to Thin Gneissic Veins in High-Grade Metamorphic Terranes: A Cautionary Tale from Akilia, Southwest Greenland. *Journal of Petrology* 46, 291-318.

Whitehouse, M.J., Kamber, B.S., Moorbath, S., 1999. Age significance of U-Th-Pb zircon data from early Archaean rocks of west Greenland—a reassessment based on combined ion-microprobe and imaging studies. *Chemical Geology* 160, 201-224.

Whitehouse, M.J., Nemchin, A., 2009. High precision, high accuracy measurement of oxygen isotopes in a large lunar zircon by SIMS. *Chemical Geology* 261, 32-42.

Wiedenbeck, M., Hanchar, J.M., Peck, W.H., Sylvester, P., Valley, J., Whitehouse, M., Kronz, A., Morishita, Y., Nasdala, L., Fiebig, J., Franchi, I., Girard, J.-P., Greenwood, R.C., Hinton, R., Kita, N., Mason, P.R.D., Norman, M., Ogasawara, M., Piccoli, P.M., Rhede, D., Satoh, H., Schulz-Dobrick, B., Skår, O., Spicuzza, M., Terada, K., Tindle, A., Togashi, S., Vennemann, T., Xie, Q., Zheng, Y.-F., 2004. Further characterisation of the 91500 zircon crystal. *Geostandards and Geoanalytical Research* 28, 9-39.

Win, M.M., Masaki, E., Takenori, K., 2016. Metamorphic conditions and CHIME monazite ages of Late Eocene to Late Oligocene high-temperature Mogok metamorphic rocks in central Myanmar. *Journal of Asian Earth Sciences* 117, 304-316.

Woodhead, J.D., Hergt, J.M., 2005. A preliminary appraisal of seven natural zircon reference materials for in situ Hf isotope determination. *Geostandards and Geoanalytical Research* 29, 183-195.

Yang, X.C., Jia, C.L., Xiong, X.Z., Bai, B.X., Huang, G., Luo, C.B., 2012. LA-ICP-MS zircon U-Pb age of metamorphic basic volcanic rock in Gongyanghe Group of southern Gaoligong Mountain, western Yunnan Province, and its geological significance. *Geological Bulletin of China* 31, 264-276.

Ye Myint Swe, Lee, I., Than Htay, Min Aung, 2004. Gold Mineralization at the Kyaukpahto Mine Area, Northern Myanmar. *Resource Geology* 54, 197-204.

Yonemura, K., Osanai, Y., Nakano, N., Adachi, T., Charusiri, P., Zaw, T.N., 2016. U-Th-Pb monazite dating of metamorphic rocks from the Mogok metamorphic belt, central Myanmar. *Journal of Mineralogical and Petrological Sciences* 108, 184-188.

Zhang, P., Mei, L., Hu, X., Li, R., Wu, L., Zhou, Z., Qiu, H., 2017. Structures, uplift, and magmatism of the Western Myanmar Arc: Constraints to mid-Cretaceous-Paleogene tectonic evolution of the western Myanmar continental margin. *Gondwana Research* 52, 18-38.

Zhu, D.C., Zhao, Z.D., Niu, Y., Dilek, Y., Wang, Q., Ji, W.H., Dong, G.C., Sui, Q.L., Liu, Y.S., Yuan, H.L., Mo, X.X., 2012. Cambrian bimodal volcanism in the Lhasa Terrane, southern Tibet: Record of an early Paleozoic Andean-type magmatic arc in the Australian proto-Tethyan margin. *Chemical Geology* 328, 290-308.

Zi, J.-W., Cawood, P.A., Fan, W.-M., Wang, Y.-J., Tohver, E., McCuaig, T.C., Peng, T.-P., 2012. Triassic collision in the Paleo-Tethys Ocean constrained by volcanic activity in SW China. *Lithos* 144-145, 145-160.

## Figure Captions

Figure 1. Geological terrane map of the Eastern Himalaya, southeast Tibet, Myanmar, Yunnan and Thailand. See legend and: ITPS – Indus-Tsangpo suture zone; SH – Shillong plateau; SFZ – Sagaing fault zone; TPFZ – Three Pagodas Fault zone; MPFZ – Mae Ping Fault Zone; PFZ – Panlaung Fault Zone; ST – Sibumasu; ASRR – Ailao Shan – Red River shear zone. Of note are the two ophiolite belts: WB – Western Belt; EB – Eastern Belt .

Figure 2. A: Schematic map of the main magmatic belts discussed in the text, both within Myanmar and extending into Northern Thailand. B: Sample locality map; orange circles represent those samples from which new data are presented here, grey circles are those samples with existing published data.

Figure 3. Terra-Wasserburg Concordia diagrams for all analyzed samples, showing common Pb-corrected zircon U-Pb analyses (red circles) selected for calculation of Concordia ages (black circle). Error ellipses are 2 sigma.

Figure 4. Timechart showing reported zircon U-Pb age data from granitoids across the major belts discussed in this paper. Also annotated are ages of detrital zircons, timing of metamorphic events, and reported ages of ophiolite belts. The horizontal lines show our assumed ages of the final suturing of Neo-Tethys and Palaeo-Tethys respectively. Data from this paper, and Ahrendt et al. (1997); Barley et al. (2003); Barr et al. (2000); Barr et al. (2006); Dong et al. (2013); Dunning et al. (1995); Gardiner et al. (2016a); Gardiner et al. (2016b); Gardiner et al. (2016c); Hennig et al. (2009); Liu et al. (2016); Mitchell et al. (2012); Palin et al. (2013); Peng et al. (2008); Peng et al.

(2013); Searle et al. (2007); Searle et al. (2012); Wai-Pan Ng et al. (2015b); Wang et al. (2014); Watkinson et al. (2011). Inferred suturing ages from Green et al. (2008) and Gardiner et al. (2016c). Epoch ages based on the International Chronostratigraphic Chart v 2014/02.

Figure 5. Geological map of Myanmar. TMB = Tagaung-Myitkyina Belt. The locations of the Shangalon mining district and the Bawdwin mine are identified. After Myanmar Geosciences Society (2014).

Figure 6. Maps of the Tagaung-Myitkyina Belt and the Katha-Gangaw Range. A: geographical, and B: geological, after Mitchell (2018), and Myanmar Geosciences Society (2014). The approximate location of sample MY182 is identified.

Figure 7. Hf evolution diagram plotting zircon magmatic age versus zircon Hf isotope data from the major granite belts in Myanmar. Also shown in light red is a domain defined by detrital zircon Hf data from the Chindwin basin of Wang et al. (2014), interpreted as of Wuntho-Popa Arc provenance.

Figure 8. Plot of zircon  $\epsilon\text{Hf}$  versus  $\delta^{18}\text{O}$  for samples from the Wuntho-Popa Arc, the Mogok Metamorphic Belt, and the Tin Province.

Figure 9. Tectonic models. A. Map of the major terranes in Southeast Asia modified from Sone and Metcalfe (2008), Metcalfe (2011b) and Barber et al. (2011). This map shows separate West Burma and Sibumasu terranes. B. The medial suture zone, the Western Myanmar Mogok Foreland model after Mitchell (2018). C. The Irrawaddy Block model: modification to Sibumasu as

proposed by Ridd (2015), where this terrane is split into western (Irrawaddy) and eastern (Sibuma) blocks. A and C taken from Morley and Searle (2017).

Figure 10. Schematic tectonic development of the Greater Sibumasu–Tengchong tectonic model for the assembly of present-day Myanmar. See text for discussion.

Figure 11. Tectonic subdivision of Southeast Asia, detailing a Greater Sibumasu cut by movement on the north-south Sagaing Fault. Modified after Metcalfe (2011a). Also shows is the Tengchong (T'chong) Block, and a postulated suture between Sibumasu and the Baoshan block running east-west across the northern Shan Plateau.

Figure 12. A. Surface workings at the discovery site of the Shangalon mineralized system - showing sheeted and stockwork vein sets in oxidized granodiorite (part of the Kanzachaung batholith); B and C. Core samples from drilling carried out at Shangalon – B. granodiorite and diorite rocks similar to those that host vein-related Cu-Mo mineralization; C. Dacite porphyry samples considered to intrude rocks of the Kanzachaung batholith.

Figure 13. Schematic tectonic evolution of Myanmar, detailing interpreted metallogenesis related to each major stage and location of major mines. A. Accretionary Stage (100–50 Ma): An Andean-type accretionary setting on the margins of Neo-Tethys, with extensive magmatism driving Cu-Au mineralization in the Wuntho-Popa Arc and Sn-W in the Tin Province respectively. B. Collisional Stage (50-40 Ma): Suturing of Neo-Tethys marks the onset of continent collision. Tethys ophiolite fragments hosts deposits of



platinum, chromite, jade and nickel. C. Late Collisional Stage (40-15 Ma): Ongoing orogeny and enhanced crustal thickening results in amphibolite-grade metamorphism in the Mogok Metamorphic Belt. D. Oblique Collisional Stage (15-0 Ma): Ongoing clockwise rotation during Oligocene-Miocene times initiated movement on the strike-slip Sagaing Fault and the development of dominantly oblique convergence and faulting, resulting in sandstone-hosted hydrothermal Au mineralization, such as at the Kyaukpahto Au deposit (Ye Myint Swe et al., 2004).

Figure 14. Distribution of exposed granite intrusions, and their ages, in A: Myanmar (ages from Aung Zaw Myint et al., 2017; Gardiner et al., 2017a; Gardiner et al., 2016c); B: on the Malaysian peninsula (ages from Wai-Pan Ng et al., 2017; Wai-Pan Ng et al., 2015b); C: Simplified map showing the granite belts of Southeast Asia with location of maps A and B. After Cobbing et al. (1986).

Figure 15. Paired metallogenic belts study. A. Zircon isotope and trace element plot of U/Yb versus Hf (*sensu* Grimes et al., 2015) highlighting source, plotted by sample and suite. Samples MY71, MY75 and MY76 have a high (>15 ppm) whole-rock Sn content (white crosses). B. Plot of median zircon Eu/Eu\* versus Ce/Ce\* for the Cu-Au and Sn-W granites. The grey curves represent the modelled isothermal covariance of Ce/Ce\* with Eu/Eu\* as a function of log  $fO_2$  (values annotated) for different temperatures. Both plots from Gardiner et al. (2017a).

## Table Captions

**Table 1:** Summary table of all samples discussed by magmatic belt, with location, description, assigned U-Pb magmatic age, and mean Lu-Hf and O isotope data. Some data previously reported in <sup>†</sup>Gardiner et al. (2016a); <sup>‡</sup>Gardiner et al. (2017a); \*Gardiner et al. (2016c).

**Table 2:** Compilation of new SIMS and LA-ICP-MS (MY182) zircon U-Pb age data. Errors quoted are 1 $\sigma$ . <sup>207</sup>Pb-corrected ages calculated as per Ludwig (2004). f<sub>207</sub> %: % of common <sup>207</sup>Pb estimated from measured <sup>204</sup>Pb. <sup>‡</sup>Disc. %: discordance of the centrepoint of data error ellipse regardless of uncertainty.

**Table 3:** Compilation of new zircon Lu-Hf isotope data from the Myanmar samples. A <sup>176</sup>Lu/<sup>177</sup>Hf of 0.015 was used for the calculation of two-stage Hf model ages (T<sub>DM</sub><sup>2</sup>).

**Table 4:** Analytical details for SIMS zircon O isotope analysis.

**Table 5:** Summary of isotope characteristics of the major magmatic belts within Myanmar and Northern Thailand, discriminated on the basis of age. Data from this study, and Gardiner et al. (2017a); Gardiner et al. (2016a); Gardiner et al. (2016c); Jiang et al. (2017); Lee et al. (2016); Mitchell et al. (2012).

**Table 6:** Summary of the major tectonic models invoked for Mesozoic–Cenozoic Myanmar. See text for discussion.

TABLE 1

SAMPLE	Description	Locality	N/E	U-Pb age (2 $\sigma$ )	$\epsilon_{\text{Hf}}$ (2 $\sigma$ )	$\delta^{18}\text{O}$ (2 $\sigma$ )
<b>Tin Province</b>						
MYAD	granite	Yadanabon	11°17'45"N/ 99°16'10"E	50.3 $\pm$ 0.6 <sup>†</sup>	-10.3 $\pm$ 0.8	
MY37	granite	Dawei	14°19'85"N/ 98°11'55"E	69.5 $\pm$ 1.0 <sup>†</sup>	-11.8 $\pm$ 1.9	
MY34	granite	Dawei	14°10'79"N/ 98°21'46"E	62.3 $\pm$ 0.6 <sup>†</sup>	-11.4 $\pm$ 0.5	
MY71	bt + pl + kfs granite	Dawei	14°16'32"N/ 98°15'37"E	75.6 $\pm$ 8.8 <sup>‡</sup>	-10.4 $\pm$ 1.1 <sup>‡</sup>	6.3 $\pm$ 0.3 <sup>‡</sup>
MY72	bt + pl + kfs granite	Dawei	14°08'15"N/ 98°07'06"E	64.1 $\pm$ 1.6 <sup>‡</sup>	-7.0 $\pm$ 1.0 <sup>‡</sup>	6.6 $\pm$ 0.3 <sup>‡</sup>
MY73	bt + pl + kfs granite		13°40'12"N/ 98°23'00"E	58.5 $\pm$ 0.5 <sup>‡</sup>	-13 $\pm$ 1.2 <sup>‡</sup>	7.1 $\pm$ 0.3 <sup>‡</sup>
MY74	bt + pl + kfs granite		13°34'05"N/ 98°25'13"E	58.7 $\pm$ 0.6 <sup>‡</sup>	-9.4 $\pm$ 1.1 <sup>‡</sup>	7.2 $\pm$ 0.3 <sup>‡</sup>
MY75	bt + pl + kfs granite	Myeik	12°41'31"N/ 98°44'12"E	72.1 $\pm$ 1.3 <sup>‡</sup>	-10.3 $\pm$ 1.4 <sup>‡</sup>	7.7 $\pm$ 0.3 <sup>‡</sup>
MY76	bt + pl + kfs granite	Myeik	12°29'36"N/ 98°41'55"E	75.3 $\pm$ 7.7 <sup>†</sup>	-10.2 $\pm$ 3.4	6.2 $\pm$ 0.3
<b>Mogok Metamorphic Belt</b>						
MY-9	Ms granite	Payangazu	20°44'28"N/ 96°13'29"E	71.9 $\pm$ 1.1	-15.0 $\pm$ 1.3	
				123.4 $\pm$ 2.0	-9.7 $\pm$ 0.4	
				218.9 $\pm$ 2.5	-13.4 $\pm$ 1.3	
MY-4	Bt granite	Nattanng	20°16'41"N/ 96°15'35"E	71.1 $\pm$ 0.6	-15.9 $\pm$ 0.9	8.9 $\pm$ 0.3
MY-1	Bt-Kfs granite	Byinge	20°03'29"N/ 96°15'33"E	55.1 $\pm$ 0.5	-13.3 $\pm$ 2.4	7.3 $\pm$ 0.3
MY106	granite	Kabaing	22°55'19"N/ 96°20'79"E	16.8 $\pm$ 0.5 <sup>†</sup>	-7.3 $\pm$ 1.2	8.5 $\pm$ 0.3
<b>Wuntho-Popa Arc</b>						
MY109	granodiorite	Banmauk	24°24'46"N/ 95°45'35"E	102.1 $\pm$ 0.95 <sup>‡</sup>	11.5 $\pm$ 1.2 <sup>‡</sup>	5.2 $\pm$ 0.2 <sup>‡</sup>
MY145	granodiorite	Shangalon	23°42'03"N/ 95°31'28"E	40.0 $\pm$ 0.2 <sup>†</sup>	1.9 $\pm$ 1.5 <sup>‡</sup>	5.5 $\pm$ 0.4 <sup>‡</sup>
MY149	granodiorite	Wuntho	24°00'12"N/ 95°27'56"E	98.1 $\pm$ 0.47 <sup>‡</sup>	7.6 $\pm$ 0.9 <sup>‡</sup>	5.4 $\pm$ 0.3 <sup>‡</sup>
MY150	granodiorite	Monywa	22°10'30"N/ 94°58'05"E	99.8 $\pm$ 1.3 <sup>‡</sup>	7.3 $\pm$ 1.4 <sup>‡</sup>	5.4 $\pm$ 0.4 <sup>‡</sup>
MY151	diorite	Salyingyi	21°56'49"N/ 95°05'32"E	98.3 $\pm$ 1.0 <sup>‡</sup>	7.4 $\pm$ 1.7 <sup>‡</sup>	5.5 $\pm$ 0.4 <sup>‡</sup>
<b>Tagaung-Myitkyina Belt</b>						
MY182	dacite	Myitkyina	25°25'48"N/ 97°25'58"E	171.9 $\pm$ 0.7	15.3 $\pm$ 2.1	
<b>Main Range Province</b>						
MY55	granite	Kyaing Tong	21°23'63"N/ 99°62'17"E	219.3 $\pm$ 1.3 <sup>*</sup>	-10.5 $\pm$ 1.0 <sup>*</sup>	
MY56	granite	Kyaing Tong	21°29'22"N/ 99°57'41"E	220.1 $\pm$ 1.1 <sup>*</sup>	-12.4 $\pm$ 0.9 <sup>*</sup>	
<b>Eastern Province</b>						
MY53	granodiorite	Tachileik	20°56'14"N/ 99°97'72"E	265.8 $\pm$ 2.1 <sup>*</sup>	-9.6 $\pm$ 1.2 <sup>*</sup>	

Table 2

Sam ple/ spot #							207- corrected ratios					Ag e Ma		Ag e Ma		207- corr	
	[U]	[Th]	[Pb]	Th /U mea s	<sup>206</sup> Pb / <sup>204</sup> Pb mea s	f <sub>206</sub> %	<sup>238</sup> U	±σ	<sup>207</sup> Pb	±σ	Dis c. %	<sup>207</sup> Pb	±σ	<sup>206</sup> Pb	±σ	207- corr	±σ
	pp m	pp m	pp m				<sup>206</sup> Pb	%	<sup>206</sup> Pb	%	con v.	<sup>206</sup> Pb		<sup>238</sup> U		age (Ma)	
<b>MY1</b>																	
n511	525	16		0.			128.2	1.5	51	.8	80.	246	29	50.	0.		0.
4-11	.2	3.6	4.8	31	451	4.15	151	0	1	0	0	.6	1	1	7	49.8	9
n511	773	23		0.	1164	{0.1	118.5	0.8	47	1.		58.	33	54.	0.		0.
4-08	.1	4.0	7.5	30	8	6}	310	9	1	40	-8.0	9	.0	2	5	54.2	5
n511	414	14		0.	8455	{0.0	118.3	0.9	48	1.	57.	127	43	54.	0.		0.
4-01	.1	3.6	4.1	35	9	2}	614	7	5	89	8	.7	.8	2	5	54.1	5
n511	463	30		0.	1630	{0.1	118.2	1.0	47	1.	14.	63.	42	54.	0.		0.
4-12	.7	5.4	4.9	66	8	1}	110	0	2	81	5	4	.7	3	5	54.3	5
n511	284	20		0.	3701	{0.0	117.3	0.9	48	2.	56.	125	53	54.	0.		0.
4-06	.9	2.4	3.1	71	9	5}	760	6	5	32	6	.3	.6	7	5	54.6	5
n511	216	12		0.	1651	{0.1	117.2	1.0	48	2.	62.	143	60	54.	0.		0.
4-02	.3	9.7	2.3	60	6	1}	255	8	9	62	0	.1	.5	8	6	54.6	6
n511	126	68	13.	0.	2345	{0.0	115.1	0.8	47	1.	44.	99.	44	55.	0.		0.
4-10	9.5	0.2	4	54	3	8}	895	4	9	91	0	1	.5	7	5	55.7	5
n511	190	19.	23.	1.	2641		114.6	0.8	46	0.	109	26.	22	56.	0.		0.
4-07	5.8	2	0	11	2	0.07	028	0	5	95	.7	8	.7	0	4	56.0	4
n511	344	37		1.		{0.0	114.2	1.4	46	2.	59.	35.	49	56.	0.		0.
4-09	.5	1.9	4.2	08	>1e6	0}	663	0	7	08	4	3	.1	2	8	56.2	8
n511	21.	93.	16	0.		{0.0	101.4	1.0	47	0.	21.	80.	8.	63.	0.		0.
4-03	0	6	2.9	10	>1e6	0}	252	5	6	35	4	3	4	2	7	63.2	7
n511	183	61.	23.	0.	3240		101.2	4.2	46	1.	0		33	63.	2.		2.
4-05	3.2	4	5	91	1	0.06	462	9	1	10	.4	0.0	.2	4	7	63.4	7
n511	377	29	41.	0.			98.64	1.3	49	8.	63.	176	4.	65.	0.		1.
4-14	5.8	3.6	4	08	873	2.14	20	5	6	35	5	.5	0	0	9	64.8	0
<b>MY4</b>																	
n511	615	23		0.			93.22	0.8	47	2.	26.	93.	48	68.	0.		0.
2-06	.8	4.5	7.3	38	4886	0.38	11	3	8	08	4	3	.6	8	6	68.7	6
n511	629	26		0.		{0.0	91.50	0.9	47	1.		70.	32	70.	0.		0.
2-09	.2	0.2	8.1	41	>1e6	0}	32	1	4	37	-0.1	1	.4	1	6	70.1	6
n511	761	27		0.	1287		91.49	0.8	46	1.	161	26.	34	70.	0.		0.
2-12	.4	1.2	9.6	36	9	0.15	89	4	5	46	.3	9	.6	1	6	70.1	6
n511	937	20	11.	0.	4755	{0.0	91.16	0.9	46	1.	61.	43.	26	70.	0.		0.
2-08	.1	5.8	5	22	9	4}	31	0	8	13	0	8	.8	3	6	70.4	6
n511	909	31	11.	0.	2562	{0.0	90.95	1.5	48	1.	32.	103	24	70.	1.		1.
2-03	.7	6.1	6	35	6	7}	36	3	0	04	1	.5	.4	5	1	70.4	1
n511	741	15		0.	2921	{0.0	90.20	0.8	48	1.	28.	99.	28	71.	0.		0.
2-13	.4	5.3	9.1	21	2	6}	05	7	0	23	8	7	.9	1	6	71.0	6
n511	936	13	11.	0.	1555		89.97	0.9	46	1.	50.	47.	31	71.	0.		0.
2-10	.2	0.1	3	14	6	0.12	50	3	9	34	5	4	.8	3	7	71.3	7
n511	137	16	16.	0.	2419	{0.0	89.60	0.8	47	1.	19.	89.	23	71.	0.		0.
2-04	6.5	1.2	7	12	35	1}	84	6	7	01	8	1	.8	5	6	71.5	6

n511	676	13		0.				89.01	1.8	46	1.	>10			54	72.	1.		1.
2-01	.9	7.2	8.5	20	9660	0.19		44	5	2	80	0		0.0	.8	0	3	72.1	3
n511	894	24	11.	0.	1187			88.83	0.8	46	1.	>10			43	72.	0.		0.
2-05	.8	4.5	4	27	6	0.16		68	1	1	51	0		0.0	.8	2	6	72.3	6
n511	110	24	14.	0.	7435	{0.0		88.39	0.9	47	1.			79.	23	72.	0.		0.
2-11	7.2	7.1	0	22	0	3}		71	9	5	01	-8.3		0	.7	5	7	72.5	7
n511	132	25.	67.	4.				84.91	2.3	41	2.	130		253	55	75.	1.		1.
2-07	7.7	7	6	61	1397	1.34		48	0	5	23	.5		.5	.6	5	7	76.0	8
n511	103	68	10	0.		{0.0		12.94	0.9	56	0.			490	11	479	4.	479.	4.
2-14	8.7	9.9	1.1	66	>1e6	0}		03	4	9	53	-2.2		.2	.7	.9	4	7	4
MY9																			
n510	191	91	18.	0.				119.0	1.1	39	2.	115		-	67	53.	0.		0.
4-13	5.7	7.7	9	48	1706	1.10		510	2	7	66	.1		.2	.7	9	6	54.4	6
n510																			
4-	374	75.		0.	1521	{0.1		92.80	0.9	48	1.	40.		116	34	69.	0.		0.
09x	.0	2	4.5	20	6	2}		05	2	3	50	9		.5	.9	1	6	69.0	6
n510																			
4-	607	14		0.	2369	{0.0		91.54	0.9	47	1.	15.		60.	35	70.	0.		0.
08x	.2	8.1	7.5	24	0	8}		36	7	2	52	5		7	.7	0	7	70.1	7
n510	801	14		0.	2174	{0.0		91.29	1.3	48	1.	31.		101	27	70.	0.		0.
4-08	.6	8.9	9.7	19	0	9}		15	2	0	17	0		.5	.5	2	9	70.2	9
n510	561	12		0.	2553	{0.0		89.85	1.1	47	1.	23.		57.	33	71.	0.		0.
4-09	.9	2.1	7.0	22	0	7}		14	9	1	40	6		8	.0	3	8	71.4	9
n510																			
4-	136	48.	20.	0.				87.92	0.7	47	2.			79.	62	72.	0.		0.
03x	4.4	5	1	77	2921	0.64		31	7	6	68	-8.8		9	.4	9	6	72.9	6
n510	157	45	20.	0.				87.36	1.1	47	1.	16.		63.	46	73.	0.		0.
4-03	4.9	8.0	7	29	4261	0.44		13	0	2	99	4		1	.8	4	8	73.4	8
n510	677	66	15.	0.				85.48	2.0	43	5.	155		137	2.	75.	1.		1.
4-20	.8	8.0	6	99	744	2.51		59	4	5	55	.6		.1	0	0	5	75.3	6
n510	232	62.	40.	1.	3671			79.48	2.6	47	0.			77.	19	80.	2.		2.
4-31	6.8	9	9	23	1	0.05		57	1	5	81	4.6		1	.1	6	1	80.6	1
n510	512	85	15.	1.	2806			52.86	0.8	48	1.	12.		137	24	120	1.	120.	1.
4-21	.6	3.8	6	67	4	0.07		92	6	7	04	2		.5	.1	.8	0	7	0
n510	153	22		1.	2523	{0.0		51.44	0.9	46	1.	194		42.	42	124	1.	124.	1.
4-27	.3	9.3	4.6	50	3	7}		75	8	8	80	.8		4	.6	.1	2	4	2
n510																			
4-	264	25		0.	3714	{0.0		51.30	0.8	47	1.	55.		80.	32	124	1.	124.	1.
01x	.1	1.0	7.0	95	5	5}		40	3	6	37	8		1	.3	.4	0	6	0
n510	335	31		0.	3828	{0.0		51.05	1.1	48	1.	14.		146	31	125	1.	125.	1.
4-01	.2	6.4	8.9	94	8	5}		83	5	9	37	7		.4	.8	.0	4	0	4
n510	03.	45.	59	0.				34.41	2.5	49	0.			174	6.	184	4.	184.	4.
4-04	0	3	7.8	41	8201	0.23		48	6	5	28	6.2		.0	4	.6	7	7	7
n510	191	44.	66.	0.	4897			30.51	1.3	49	0.			190	10	207	2.	207.	2.
4-02	3.1	8	2	02	3	0.04		87	2	8	47	9.4		.2	.9	.8	7	9	7
n510	277	12	96.	0.				30.50	1.6	49	1.			190	24	208	3.	208.	3.
4-24	4.0	7.6	6	05	9891	0.19		11	8	9	05	9.3		.5	.3	.0	4	1	5
n510	150	12		0.				30.38	1.0	50	2.			201	51	208	2.	208.	2.
4-39	.9	2.6	6.5	81	5625	0.33		06	9	1	27	3.5		.8	.8	.8	2	8	3
n510	302	19	12.	0.		{0.0		30.00	1.2	50	1.			212	27	211	2.	211.	2.
4-07	.1	4.6	7	64	>1e6	0}		59	9	3	19	-0.5		.4	.3	.3	7	3	7
n510	511	48	23.	0.				29.85	0.8	50	1.			222	30	212	1.	212.	1.
4-30	.3	4.7	2	95	3919	0.48		10	1	6	34	-4.7		.8	.7	.4	7	4	7
n510	825	47	34.	0.	1771	0.11		29.68	0.8	0.0	0.	13.		188	14	213	1.	213.	1.

4-34	.8	0.3	1	57	1		55	2	49	64	8	.0	.8	.6	7	7	7
									8								
									0.0								
n510	41.	61.		1.		{0.0	29.66	1.0	49	2.	29.	166	58	213	2.	214.	2.
4-22	2	0	2.1	48	>1e6	0}	53	5	3	56	2	.1	.8	.7	2	0	2
									0.0								
n510	784	93.	28.	0.	3036	{0.0	29.49	0.8	50	0.		229	15	214	1.	214.	1.
4-32	.7	4	9	12	09	1}	87	2	7	68	-6.4	.5	.6	.9	7	8	8
									0.0								
n510	895	87.	33.	0.	8045	{0.0	29.23	1.1	50	0.		202	13	216	2.	216.	2.
4-05	.1	6	2	10	5	2}	59	9	1	58	7.4	.2	.4	.8	5	9	5
									0.0								
n510	959	63	41.	0.			29.06	1.2	49	0.	20.	180	17	218	2.	218.	2.
4-16	.4	7.1	4	66	9693	0.19	35	2	6	73	9	.8	.0	.1	6	3	6
									0.0								
n510	519	60	25.	1.	4327	{0.0	29.00	1.0	49	1.	16.	188	24	218	2.	218.	2.
4-10	.6	9.0	5	17	1	4}	02	6	8	06	5	.0	.5	.5	3	7	3
									0.0								
n510	67.	25.		0.	5009	{0.0	28.94	0.9	49	2.	30.	169	60	219	2.	219.	2.
4-25	1	0	2.7	37	8	4}	30	7	4	65	0	.2	.7	.0	1	3	1
									0.0								
n510	120	34	48.	0.	3912		28.38	1.0	50	0.		224	11	223	2.	223.	2.
4-33	9.0	4.9	8	29	9	0.05	43	1	6	51	-0.7	.8	.7	.2	2	2	2
									0.0								
n510	724	43	31.	0.	1361	{0.0	28.33	1.5	49	0.	15.	194	20	223	3.	223.	3.
4-19	.2	3.7	5	60	74	1}	67	7	9	88	1	.7	.3	.6	5	7	5
									0.0								
n510	463	23	20.	0.	5048	{0.0	27.76	1.7	50	0.	11.	205	22	228	3.	228.	3.
4-06	.6	0.8	0	50	8	4}	02	3	2	99	2	.5	.8	.1	9	3	9
									0.0								
n510	393	24.	16	0.	5749		25.18	0.9	49	0.	31.	192	7.	251	2.	251.	2.
4-29	0.2	2	4.1	01	9	0.03	21	9	9	31	1	.3	2	.0	4	4	5
									0.0								
n510	568	17	56.	0.	4167	{0.0	11.82	1.6	60	0.	14.	609	8.	523	8.	521.	8.
4-36	.4	2.0	2	30	88	0}	86	4	1	39	7	.4	4	.2	2	6	3
n510									0.0								
4-02x	787	31	86.	0.	1912	{0.0	11.60	1.5	66	0.	37.	826	6.	532	7.	527.	8.
	.6	2.9	9	40	02	1}	57	5	6	33	0	.8	8	.8	9	0	0
									0.0								
n510	145	62	24	0.	8550		7.331	2.9	95	0.	49.	152	7.	824	3.	794.	3.
4-15	1.8	9.9	6.7	43	7	0.02	1	7	0	41	0	8.7	7	.3	0	7	3
									0.0								
n510	108	62	25	0.	6344	{0.0	5.249	1.1	76	0.		109	3.	112	2.	112	2.
4-40	6.5	1.4	8.0	57	21	0}	5	8	0	17	2.8	6.1	4	4.1	2	5.6	9
									0.1								
n510	682	44	25	0.	4845	{0.0	3.418	1.2	00	0.		162	3.	165	8.	>12	
4-14	.0	4.0	7.7	65	14	0}	3	5	1	19	1.8	7.8	6	4.2	2	00	
									0.2								
n510	131	65	12.	0.			1.637	0.7	45	0.		315	1.	307	9.	>12	
4-37	8.3	8.1	6	50	>1e6	0.00	7	8	0	10	-3.2	3.1	5	2.4	1	00	
MY1																	
82																	
									0.0								
1	71.	26.		0.	260		37.45	0.9	48	0.	55.	109	88	169	2.	170.	4.
	2	0	2.3	37	2200	0.00	32	3	2	00	7	.1	.2	.9	0	1	1
									0.0								
2	99.	39.		0.	720		37.67	0.8	48	0.	31.	128	82	168	1.	169.	3.
	5	8	3.3	40	5400	0.00	90	5	6	00	3	.6	.8	.9	8	0	8
									0.0								
3	62.	19.		0.	340		37.45	0.8	47	0.	245	49.	1.	169	1.	170.	4.
	9	6	1.6	31	2700	0.00	32	8	0	00	.1	2	5	.9	9	4	0
									0.0								
4	64.	19.		0.	480		36.71	0.8	43	0.	219	144	6.	173	1.	174.	4.
	2	4	1.5	30	2300	0.00	07	5	4	01	.8	.6	6	.3	9	6	0
									0.0								
6	68.	18.		0.	540		37.11	0.8	49	0.		162	8.	171	1.	171.	3.
	3	0	1.4	26	2800	0.00	95	4	3	01	-5.7	.1	9	.4	9	4	8
									0.0								
7	72.	18.		0.	560		36.77	0.8	49	0.		166	0.	172	1.	173.	3.
	1	4	1.6	26	4900	0.00	82	4	4	01	-3.6	.9	4	.9	9	0	9
									0.0								
9	93.	37.		0.	560		37.35	0.8	46	0.	620	23.	7.	170	1.	170.	3.
	5	1	3.0	40	3000	0.00	53	5	5	00	.9	6	6	.3	9	9	8
	86.	31.		0.	440		36.94	0.9	0.0	0.	104	-	87	172	2.	173.	4.
10	8	6	2.8	36	4100	0.00	13	0	45	00	6.8	18.	.8	.2	0	0	1

								7		2							
						110		0.0									
	114	50.		0.	1500	00.0	36.96	0.8	51	0.	33.	258	68	172	2.	171.	4.
11	.1	7	3.9	44	0	0	86	9	4	00	5	.8	.5	.1	0	7	1
									0.0		-						
	105	33.		0.		490	37.52	0.8	49	0.	14.	147	73	169	1.	169.	3.
12	.4	9	2.7	32	1900	0.00	35	2	0	00	7	.8	.2	.5	8	6	6
									0.0								
	102	36.		0.		660	33.27	0.7	50	0.	19.	236	71	190	2.	190.	4.
13	.0	5	3.6	36	900	0.00	79	5	9	00	2	.3	.5	.9	1	6	3
									0.0		-						
	58.	17.		0.	-	550	36.03	0.8	48	0.	61.	109	96	176	2.	176.	4.
14	3	9	1.6	31	2600	0.00	60	7	2	00	7	.1	.9	.5	1	8	2
									0.0								
	62.	20.		0.		290	36.61	0.7	50	0.	16.	208	1.	173	1.	173.	3.
16	6	5	1.7	33	2500	0.00	66	2	3	00	8	.9	.7	.7	7	5	4
									0.0								
	203	35.		0.	1800	00.0	37.66	0.8	53	0.	54.	366	54	168	1.	168.	3.
17	.3	3	3.6	17	0	0	48	4	9	00	0	.9	.6	.9	8	0	7
									0.0		-						
	69.	24.		0.		570	35.91	0.8	45	0.	548	39.	5.	177	2.	178.	4.
18	7	4	2.0	35	3300	0.00	95	9	3	00	.2	5	5	.0	1	0	3
									0.0								
	102	39.		0.		600	38.68	1.2	52	0.	47.	315	68	164	2.	163.	5.
19	.7	5	3.0	38	5200	0.00	47	3	7	00	9	.9	.2	.5	5	8	2
									0.0								
	56.	10.		0.		430	37.10	0.9	57	0.	65.	503	94	171	2.	169.	4.
20	1	9	0.8	19	600	0.00	58	4	3	01	9	.1	.1	.4	1	8	3
									0.0								
	54.	14.		0.	1500	00.0	36.48	0.9	52	0.	38.	285	0.	174	2.	173.	4.
22	6	8	1.2	27	0	0	30	8	0	01	9	.4	8	.3	3	8	6
									0.0								
	62.	15.		0.	-	570	33.90	1.0	50	0.		204	99	187	2.	187.	5.
23	9	3	1.5	24	2800	0.00	98	0	2	00	8.3	.3	.9	.4	6	3	4
									0.0		-						
	53.			0.		480	36.44	1.0	48	0.	26.	138	8.	174	2.	174.	4.
24	3	9.5	0.8	18	600	0.00	32	1	8	01	2	.2	8	.5	3	7	8
									0.0								
	65.	20.		0.		800	36.84	0.8	51	0.	33.	258	82	172	1.	172.	4.
25	7	6	1.8	31	3000	0.00	60	6	4	00	3	.8	.8	.6	9	2	0

**Table 3**

Analysis No.	Age (Ma)	1s	$^{176}\text{Hf}/^{177}\text{Hf}$	1 se	$^{176}\text{Lu}/^{177}\text{Hf}$	$^{176}\text{Yb}/^{177}\text{Hf}$	$^{176}\text{Hf}/^{177}\text{Hf}$ initial	$\epsilon\text{Hf}$	1 $\sigma$	$T_{\text{DM}}$ (Ga)	$T_{\text{DM}}^2$ crustal (Ga)
<b>MY37</b>											
MY37_3	69.5	1	0.28247 1	0.0074 34	0.00183 1	0.0690	0.28246 8	-9.2	0. 7	1.1 3	1.72
MY37_11	69.5	1	0.28233 3	0.0037 19	0.00190 0	0.0711	0.28233 0	14. 1	0. 4	1.3 3	2.03
MY37_13	69.5	1	0.28242 6	0.0053 11	0.00169 8	0.0638	0.28242 3	10. 8	0. 5	1.1 9	1.82
MY37_14	69.5	1	0.28241 8	0.0049 57	0.00152 9	0.0559	0.28241 6	11. 1	0. 5	1.1 9	1.84
MY37_15	69.5	1	0.28240 0	0.0081 44	0.00179 1	0.0667	0.28239 7	11. 7	0. 8	1.2 3	1.88
MY37_18	69.5	1	0.28233 5	0.0074 38	0.00081 8	0.0281	0.28233 3	14. 0	0. 7	1.2 8	2.02
<b>MY34</b>											
MY-34_1	62.3	0.6	0.28240 8	0.0037 18	0.00251 0	0.0900	0.28240 5	11. 6	0. 4	1.2 4	1.87
MY-34_3	62.3	0.6	0.28242 1	0.0049 57	0.00085 3	0.0261	0.28242 0	11. 1	0. 5	1.1 7	1.83
MY-34_4	62.3	0.6	0.28241 5	0.0049 57	0.00162 1	0.0495	0.28241 3	11. 3	0. 5	1.2 0	1.85
MY-34_5	62.3	0.6	0.28239 2	0.0037 18	0.00513 0	0.1670	0.28238 6	12. 3	0. 4	1.3 6	1.91
MY-34_6	62.3	0.6	0.28241 4	0.0054 88	0.00093 5	0.0318	0.28241 2	11. 3	0. 5	1.1 8	1.85
MY-34_7	62.3	0.6	0.28243 5	0.0046 03	0.00211 5	0.0662	0.28243 2	10. 6	0. 5	1.1 9	1.81
MY-34_9	62.3	0.6	0.28239 8	0.0054 89	0.00096 2	0.0297	0.28239 6	11. 9	0. 5	1.2 0	1.89
MY-34_10	62.3	0.6	0.28242 2	0.0044 26	0.00160 3	0.0466	0.28242 0	11. 1	0. 4	1.1 9	1.83
MY-34_11	62.3	0.6	0.28240 3	0.0047 80	0.00163 3	0.0466	0.28240 1	11. 8	0. 5	1.2 2	1.88
MY-34_12	62.3	0.6	0.28243 1	0.0053 11	0.00089 1	0.0241	0.28242 9	10. 7	0. 5	1.1 5	1.81
MY-34_13	62.3	0.6	0.28240 6	0.0051 34	0.00140 0	0.0384	0.28240 4	11. 6	0. 5	1.2 0	1.87
MY-34_14	62.3	0.6	0.28239 1	0.0037 18	0.00152 0	0.0401	0.28238 9	12. 2	0. 4	1.2 3	1.90
MY-34_15	62.3	0.6	0.28240 9	0.0033 64	0.00189 9	0.0550	0.28240 6	11. 6	0. 3	1.2 2	1.86
MY-34_16	62.3	0.6	0.28240 9	0.0037 18	0.00259 6	0.0719	0.28240 5	11. 6	0. 4	1.2 4	1.87
MY-34_21	62.3	0.6	0.28242 4	0.0047 80	0.00147 4	0.0390	0.28242 2	11. 0	0. 5	1.1 8	1.83
<b>MYAD</b>											
MY-YAD_1	50.3	0.6	0.28243 3	0.0054 88	0.00111 6	0.0269	0.28243 1	10. 9	0. 5	1.1 6	1.81



MY-YAD_6	50.3	0.6	0.28247 6	0.0042 48	0.00113 8	0.0282	0.28247 4	-9.4	0. 4	1.1 0	1.72
MY-YAD_7	50.3	0.6	0.28245 3	0.0042 48	0.00160 6	0.0402	0.28245 1	10. 2	0. 4	1.1 4	1.77
MY-YAD_8	50.3	0.6	0.28242 9	0.0047 80	0.00159 8	0.0393	0.28242 7	11. 1	0. 5	1.1 8	1.86
MY-YAD_9	50.3	0.6	0.28242 1	0.0049 57	0.00089 0	0.0218	0.28242 0	11. 3	0. 5	1.1 7	1.84
MY-YAD_10	50.3	0.6	0.28245 4	0.0038 94	0.00085 6	0.0208	0.28245 3	10. 2	0. 4	1.1 2	1.77
MY-YAD_11	50.3	0.6	0.28242 2	0.0033 64	0.00322 0	0.0754	0.28241 8	11. 4	0. 3	1.2 4	1.84
MY-YAD_12	50.3	0.6	0.28247 6	0.0044 25	0.00087 9	0.0195	0.28247 5	-9.4	0. 4	1.0 9	1.72
MY-YAD_13	50.3	0.6	0.28245 1	0.0040 72	0.00160 3	0.0406	0.28244 9	10. 3	0. 4	1.1 5	1.78
MY-YAD_15	50.3	0.6	0.28248 0	0.0069 03	0.00126 0	0.0335	0.28247 8	-9.3	0. 7	1.1 0	1.71
MY-YAD_16	50.3	0.6	0.28245 1	0.0044 26	0.00054 9	0.0148	0.28245 0	10. 3	0. 4	1.1 2	1.77
<b>MY1</b>											
MY1_1	55.0 2	0.5 3	0.28243 8	0.0072 58	0.00080 4	0.0270	0.28243 7	10. 6	0. 7	1.1 4	1.80
MY1_2	55.0 2	0.5 3	0.28230 6	0.0040 74	0.00064 5	0.0199	0.28230 5	15. 3	0. 4	1.3 2	2.09
MY1_6	55.0 2	0.5 3	0.28232 2	0.0030 11	0.00059 7	0.0184	0.28232 1	14. 7	0. 3	1.3 0	2.06
MY1_7	55.0 2	0.5 3	0.28246 7	0.0038 94	0.00267 0	0.0865	0.28246 4	-9.7	0. 4	1.1 6	1.74
MY1_8	55.0 2	0.5 3	0.28242 2	0.0035 41	0.00122 7	0.0378	0.28242 0	11. 2	0. 4	1.1 8	1.84
MY1_9	55.0 2	0.5 3	0.28231 6	0.0031 88	0.00097 0	0.0311	0.28231 5	15. 0	0. 3	1.3 2	2.07
MY1_10	55.0 2	0.5 3	0.28231 2	0.0035 42	0.00100 6	0.0318	0.28231 0	15. 1	0. 4	1.3 2	2.08
MY1_12	55.0 2	0.5 3	0.28231 9	0.0058 44	0.00093 0	0.0314	0.28231 8	14. 9	0. 6	1.3 1	2.06
<b>MY4</b>											
MY4_1	71.1 2	0.5 5	0.28229 2	0.0058 45	0.00186 7	0.0602	0.28228 9	15. 5	0. 6	1.3 8	2.12
MY4_3	71.1 2	0.5 5	0.28223 3	0.0024 80	0.00120 1	0.0425	0.28223 1	17. 6	0. 2	1.4 4	2.25
MY4_4	71.1 2	0.5 5	0.28231 2	0.0040 74	0.00178 4	0.0632	0.28230 9	14. 8	0. 4	1.3 5	2.07
MY4_5	71.1 2	0.5 5	0.28230 1	0.0037 19	0.00150 3	0.0521	0.28229 9	15. 2	0. 4	1.3 6	2.10
MY4_8	71.1 2	0.5 5	0.28227 6	0.0040 74	0.00132 4	0.0461	0.28227 4	16. 0	0. 4	1.3 9	2.15
MY4_9	71.1 2	0.5 5	0.28228 1	0.0056 68	0.00117 1	0.0415	0.28227 9	15. 9	0. 6	1.3 7	2.14
MY4_10	71.1 2	0.5 5	0.28225 0	0.0047 83	0.00129 8	0.0456	0.28224 8	17. 0	0. 5	1.4 2	2.21

MY4_11	71.1 2	0.5 5	0.28226 9	0.0037 20	0.00145 2	0.0528	0.28226 7	16. 3	0. 4	1.4 0	2.17
MY4_12	71.1 2	0.5 5	0.28228 5	0.0042 51	0.00102 4	0.0371	0.28228 3	15. 7	0. 4	1.3 6	2.13
MY4_13	71.1 2	0.5 5	0.28230 1	0.0042 51	0.00179 9	0.0624	0.28229 8	15. 2	0. 4	1.3 7	2.10
<b>MY9</b>											
MY-9_3	71.9	0.6	0.28236 2	0.0049 58	0.00212 8	0.0573	0.28235 9	13. 0	0. 5	1.2 9	1.96
MY-9_8	71.9	0.6	0.28229 0	0.0044 28	0.00142 8	0.0393	0.28228 8	15. 5	0. 4	1.3 7	2.12
MY-9_9	71.9	0.6	0.28228 1	0.0042 51	0.00154 9	0.0434	0.28227 8	15. 9	0. 4	1.3 9	2.14
MY-9_20	71.9	0.6	0.28228 7	0.0056 68	0.00091 2	0.0230	0.28228 5	15. 6	0. 6	1.3 5	2.13
MY-9_1	123	1	0.28242 6	0.0047 80	0.00122 5	0.0323	0.28242 3	0. -9.6	1.1 5	1.79	1.79
MY-9_21	123	1	0.28243 8	0.0042 49	0.00222 7	0.0546	0.28243 2	0. -9.3	1.1 4	1.78	1.78
MY-9_27	123	1	0.28241 4	0.0040 72	0.00219 9	0.0538	0.28240 8	10. 1	0. 4	1.2 2	1.82
MY-9_5	218. 9	1.3	0.28225 9	0.0044 29	0.00065 6	0.0176	0.28225 6	13. 4	0. 4	1.3 8	2.10
MY-9_7	218. 9	1.3	0.28226 5	0.0044 28	0.00103 9	0.0278	0.28226 0	13. 3	0. 4	1.3 9	2.09
MY-9_10	218. 9	1.3	0.28228 3	0.0061 99	0.00143 0	0.0351	0.28227 7	12. 7	0. 6	1.3 8	2.06
MY-9_15	218. 9	1.3	0.28216 1	0.0044 30	0.00232 8	0.0537	0.28215 1	17. 1	0. 4	1.5 9	2.34
MY-9_16	218. 9	1.3	0.28229 3	0.0053 14	0.00079 8	0.0196	0.28228 9	12. 3	0. 5	1.3 4	2.03
MY-9_22	218. 9	1.3	0.28228 8	0.0056 68	0.00141 7	0.0383	0.28228 2	12. 5	0. 6	1.3 7	2.05
MY-9_30	218. 9	1.3	0.28223 9	0.0042 52	0.00099 8	0.0231	0.28223 4	14. 2	0. 4	1.4 3	2.15
MY-9_32	218. 9	1.3	0.28227 4	0.0046 05	0.00080 4	0.0196	0.28227 0	12. 9	0. 5	1.3 7	2.07
MY-9_34	218. 9	1.3	0.28226 2	0.0035 43	0.00105 6	0.0256	0.28225 7	13. 4	0. 4	1.4 0	2.10
MY-9_38	218. 9	1.3	0.28227 1	0.0040 74	0.00077 2	0.0186	0.28226 7	13. 0	0. 4	1.3 7	2.08
MY-9_39	218. 9	1.3	0.28227 6	0.0047 83	0.00099 9	0.0272	0.28227 1	12. 9	0. 5	1.3 7	2.07
<b>MY106</b>											
MY106_01	16.8	0.5	0.28260 1	0.0148 62	0.00059 6	0.0192	0.28260 0	-5.7	0. 4	0.9 1	1.46
MY106_02	16.8	0.5	0.28253 6	0.0069 02	0.00052 8	0.0203	0.28253 5	-8.0	0. 7	1.0 0	1.60
MY106_03	16.8	0.5	0.28256 2	0.0074 32	0.00069 1	0.0257	0.28256 1	-7.1	0. 7	0.9 6	1.55
MY106_04	16.8	0.5	0.28259 2	0.0079 62	0.00130 0	0.0555	0.28259 1	-6.0	2. 1	0.9 4	1.48
MY106_05	16.8	0.5	0.28256 3	0.0051 32	0.00080 6	0.0308	0.28256 2	-7.0	1. 4	0.9 7	1.54

MY106_06	16.8	0.5	0.28253 1	0.0053 09	0.00051 4	0.0195	0.28253 0	0. -8.2	1.0 2	0 0	1.62
MY106_07	16.8	0.5	0.28253 5	0.0070 79	0.00078 3	0.0271	0.28253 4	0. -8.0	1.0 7	0 0	1.61
MY106_08	16.8	0.5	0.28254 2	0.0053 09	0.00070 6	0.0273	0.28254 1	1. -7.8	0.9 0	0 9	1.59
MY106_09	16.8	0.5	0.28253 1	0.0054 86	0.00018 2	0.0068	0.28253 0	0. -8.2	0.9 5	0 9	1.62
MY106_10	16.8	0.5	0.28250 0	0.0058 41	0.00021 3	0.0083	0.28249 9	1. -9.3	1.0 3	0 4	1.68
MY106_11	16.8	0.5	0.28256 9	0.0054 85	0.00065 0	0.0245	0.28256 8	0. -6.8	0.9 4	0 5	1.53
MY106_12	16.8	0.5	0.28254 0	0.0063 71	0.00075 2	0.0281	0.28253 9	0. -7.8	1.0 8	0 0	1.59
MY106_13	16.8	0.5	0.28254 4	0.0056 63	0.00072 4	0.0249	0.28254 3	0. -7.7	0.9 5	0 9	1.59
MY106_14	16.8	0.5	0.28251 8	0.0084 95	0.00103 6	0.0392	0.28251 7	0. -8.6	1.0 7	0 4	1.64
MY106_15	16.8	0.5	0.28257 4	0.0063 70	0.00081 6	0.0320	0.28257 3	0. -6.6	0.9 8	0 5	1.51
MY106_16	16.8	0.5	0.28263 3	0.0171 60	0.00109 0	0.0423	0.28263 2	2. -4.6	0.8 3	0 7	1.38
<b>MY145</b>											
MY145_01	40	0.2	0.28280 6	0.0159 12	0.00348 4	0.1400	0.28280 3	1. 2.0	0.6 7	0 7	0.99
MY145_02	40	0.2	0.28279 2	0.0038 90	0.00144 9	0.0507	0.28279 0	0. 1.5	0.6 9	0 6	1.01
MY145_04	40	0.2	0.28280 3	0.0058 34	0.00204 6	0.0724	0.28280 1	1. 1.9	0.6 4	0 5	0.99
MY145_05	40	0.2	0.28278 9	0.0067 19	0.00194 0	0.0696	0.28278 7	3. 1.4	0.6 0	0 7	1.02
MY145_06	40	0.2	0.28277 5	0.0088 41	0.00201 0	0.0710	0.28277 3	3. 0.9	0.6 9	0 9	1.05
MY145_07	40	0.2	0.28275 6	0.0074 27	0.00190 5	0.0674	0.28275 4	1. 0.3	0.7 3	0 2	1.10
MY145_08	40	0.2	0.28280 0	0.0067 19	0.00186 0	0.0660	0.28279 8	2. 1.8	0.6 3	0 5	1.00
MY145_10	40	0.2	0.28282 5	0.0084 86	0.00288 0	0.1020	0.28282 2	5. 2.7	0.6 1	0 3	0.94
MY145_11	40	0.2	0.28274 7	0.0067 20	0.00084 3	0.0292	0.28274 6	0. -0.0	0.7 3	0 1	1.11
MY145_12	40	0.2	0.28278 3	0.0104 32	0.00154 0	0.0523	0.28278 1	1. 1.2	0.6 8	0 7	1.03
MY145_13	40	0.2	0.28277 7	0.0076 03	0.00160 1	0.0565	0.28277 5	1. 1.0	0.6 6	0 8	1.05
MY145_14	40	0.2	0.28283 2	0.0077 78	0.00287 0	0.0988	0.28282 9	3. 2.9	0.6 7	0 2	0.93
<b>MY182</b>											
MY182 - 1	172	0.7	0.28317 1	0.0000 89	0.00633 0	0.0834	0.28315 0	17. 2	2. 4	0.1 3	0.11
MY182 - 2	172	0.7	0.28304 6	0.0000 88	0.00792 2	0.1226	0.28302 0	12. 6	2. 2	0.3 5	0.41
MY182 - 3	172	0.7	0.28310 0	0.0001 00	0.00452 0	0.0643	0.28308 5	14. 9	3. 0	0.2 3	0.26
MY182 - 4	172	0.7	0.28319 0	0.0001 10	0.00437 8	0.0643	0.28317 5	18. 1	3. 4	0.0 9	0.06
MY182 - 6	172	0.7	0.28318 0	0.0001 00	0.00340 1	0.0511	0.28316 9	17. 8	3. 2	0.1 0	0.07
MY182 - 7	172	0.7	0.28307 6	0.0000 84	0.00321 0	0.0501	0.28306 5	14. 2	2. 6	0.2 6	0.31
MY182 - 8	172	0.7	0.28305 0	0.0001 00	0.00296 6	0.0498	0.28304 0	13. 3	3. 2	0.3 0	0.37
MY182 - 9	172	0.7	0.28304 0	0.0001 40	0.00560 2	0.1133	0.28302 2	12. 6	4. 3	0.3 4	0.41
MY182 - 10	172	0.7	0.28307 0	0.0001 00	0.00524 7	0.1036	0.28305 3	13. 7	2. 9	0.2 9	0.34
MY182 - 11	172	0.7	0.28313 8	0.0000 87	0.00455 0	0.0820	0.28312 3	16. 2	2. 6	0.1 7	0.18
MY182 - 12	172	0.7	0.28317 0	0.0000 87	0.00467 0	0.1056	0.28315 4	17. 3	2. 5	0.1 2	0.10
MY182 - 16	172	0.7	0.28315 0	0.0000 84	0.00316 6	0.0714	0.28313 9	16. 8	2. 6	0.1 5	0.14
MY182 - 17	172	0.7	0.28309 4	0.0000 85	0.00247 2	0.0546	0.28308 6	14. 9	2. 7	0.2 3	0.26

MY182	-		0.28311	0.0000	0.00401		0.28309	15.	3.	0.2	
18		172 0.7	2	99	0	0.1035	9	3	0	1	0.23
MY182	-		0.28315	0.0001	0.00130		0.28314	16.	5.	0.1	
21		172 0.7	0	60	5	0.0284	5	9	5	4	0.13
MY182	-		0.28312	0.0000	0.00230		0.28311	16.	1.	0.1	
22		172 0.7	5	60	8	0.0493	7	0	9	8	0.19
MY182	-		0.28314	0.0000	0.00242		0.28314	16.	2.	0.1	
23		172 0.7	8	82	0	0.0591	0	8	6	5	0.14
MY182	-		0.28298	0.0001	0.00256		0.28297	10.	3.	0.4	
24		172 0.7	0	00	0	0.0550	1	8	2	0	0.52

**Table 4**

Sample	Seq. in	$^{18}\text{O}/^{16}\text{O}$	Samples	Standards	Stage Position		Field	
							Aperture	
ID	run	drift corrected	$\delta^{18}\text{O}$ (‰)	$\delta^{18}\text{O}$ (‰)			Centring	
					x	y	X	Y
<b>MY4</b>								
915ox_mt1428_@1	1	0.00201976 $\pm$ 13		9.76 $\pm$ 0.13	-5560	701	-13	-4
915ox_mt1428_@2	2	0.00201996 $\pm$ 13		9.86 $\pm$ 0.13	-5620	701	-13	-5
915ox_mt1428_@3	3	0.00201981 $\pm$ 19		9.78 $\pm$ 0.15	-5680	701	-14	-5
Tem2ox_mt1428_@1	4	0.00201609 $\pm$ 17		7.92 $\pm$ 0.14	-4965	3691	-8	-2
n5334ox_@1	5	0.00201808 $\pm$ 25	8.92 $\pm$ 0.17		-928	-3097	0	-8
n5334ox_@2	6	0.00201819 $\pm$ 21	8.97 $\pm$ 0.15		-886	-2973	0	-7
n5334ox_@3	7	0.00201795 $\pm$ 13	8.85 $\pm$ 0.13		-852	-2937	1	-7
n5334ox_@4	8	0.00201796 $\pm$ 17	8.86 $\pm$ 0.14		-684	-2388	4	-6
n5334ox_@5	9	0.00201822 $\pm$ 19	8.99 $\pm$ 0.15		-725	-2830	2	-7
n5334ox_@6	10	0.00201800 $\pm$ 23	8.88 $\pm$ 0.16		-465	-3149	3	-8
915ox_mt1428_@4	11	0.00201992 $\pm$ 30		9.84 $\pm$ 0.19	-5560	641	-15	-5
915ox_mt1428_@5	12	0.00202027 $\pm$ 23		10.01 $\pm$ 0.16	-5620	641	-15	-6
n5334ox_@7	13	0.00201788 $\pm$ 17	8.81 $\pm$ 0.14		-316	-3578	3	-9
n5334ox_@8	14	0.00201829 $\pm$ 27	9.02 $\pm$ 0.17		-313	-3629	2	-9
n5334ox_@9	15	0.00201843 $\pm$ 23	9.09 $\pm$ 0.16		-226	-3635	3	-9
n5334ox_@10	16	0.00201843 $\pm$ 24	9.09 $\pm$ 0.16		-693	-3789	-1	-9
n5334ox_@11	17	0.00201765 $\pm$ 27	8.70 $\pm$ 0.18		-717	-3694	-1	-9

							-
n5334ox_@12	18	0.00201809 ± 18	8.92 ± 0.14		-875	-4254	-4 10
915ox_mt1428_@6	19	0.00201973 ± 17	9.74 ± 0.14	-5680	641	-16	-6
915ox_mt1428_@7	20	0.00202021 ± 19	9.98 ± 0.15	-5740	641	-16	-6
Tem2ox_mt1428_@2	21	0.00201573 ± 21	7.74 ± 0.15	-4640	4032	-5	-2
							-
n5334ox_@13	22	0.00201830 ± 13	9.02 ± 0.13	-841	-4725	-5	11
<b>MY1</b>							
n5333ox_@1	23	0.00201544 ± 19	7.60 ± 0.15	2504	-4411	25	-9
							-
n5333ox_@2	24	0.00201601 ± 16	7.88 ± 0.14	2462	-4417	23	10
n5333ox_@3	25	0.00201462 ± 16	7.19 ± 0.14	2393	-4211	23	-9
n5333ox_@4	26	0.00201427 ± 23	7.01 ± 0.16	2591	-4296	26	-8
n5333ox_@5	27	0.00201551 ± 22	7.63 ± 0.16	2862	-4108	27	-9
915ox_mt1428_@8	28	0.00202029 ± 17	10.02 ± 0.14	-5800	641	-17	-5
915ox_mt1428_@9	29	0.00202012 ± 29	9.94 ± 0.18	-5560	581	-17	-5
n5333ox_@6	30	0.00201501 ± 21	7.38 ± 0.15	2827	-3824	28	-7
n5333ox_@7	31	0.00201291 ± 26	6.33 ± 0.17	2599	-3566	26	-7
n5333ox_@8	32	0.00201558 ± 18	7.67 ± 0.14	2641	-3286	26	-7
n5333ox_@9	33	0.00201543 ± 20	7.59 ± 0.15	2613	-2840	27	-7
n5333ox_@10	34	0.00201452 ± 27	7.13 ± 0.18	2392	-2895	25	-7
n5333ox_@11	35	0.00201252 ± 20	6.14 ± 0.15	2552	-2466	28	-6
915ox_mt1428_@10	36	0.00202035 ± 24	10.05 ± 0.17	-5620	581	-17	-5
915ox_mt1428_@11	37	0.00201956 ± 20	9.65 ± 0.15	-5680	581	-17	-6

Tem2ox_mt1428_@3	38	0.00201628 ± 18		8.02 ± 0.14	-4468	3498	-7	-1
n5333ox_@12	39	0.00201178 ± 23	5.77 ± 0.16		2745	-2310	30	-6
n5333ox_@13	40	0.00201631 ± 14	8.03 ± 0.13		2809	-2003	31	-6
n5333ox_@14	41	0.00201354 ± 15	6.65 ± 0.14		2461	-1883	28	-6
915ox_mt1428_@12	46	0.00201967 ± 21		9.71 ± 0.15	-5740	581	-17	-6
915ox_mt1428_@13	47	0.00201989 ± 16		9.82 ± 0.14	-5800	581	-17	-5
<b>MY145</b>								
n5329ox_@1	32	0.00201362 ± 33	5.79 ± 0.21		-1440	-655	3	3
n5329ox_@02	33	0.00201281 ± 19	5.38 ± 0.17		-1109	-670	5	3
n5329ox_@03	34	0.00201360 ± 18	5.78 ± 0.16		-1157	-693	4	2
915ox_mt1432_@10	35	0.00202144 ± 29		9.70 ± 0.20	-3739	1776	0	3
915ox_mt1432_@11	36	0.00202216 ± 16		10.05 ± 0.16	-3831	1435	-3	3
n5329ox_@04	37	0.00201326 ± 24	5.61 ± 0.18		-1494	-1284	0	2
n5329ox_@05	38	0.00201293 ± 25	5.44 ± 0.19		-1215	-1044	3	1
n5329ox_@06	39	0.00201293 ± 14	5.45 ± 0.15		-670	-1090	6	1
n5329ox_@07	40	0.00201286 ± 25	5.41 ± 0.18		-629	-1804	4	2
n5329ox_@08	41	0.00201309 ± 20	5.52 ± 0.17		-463	-2008	4	0
n5329ox_@09	42	0.00201310 ± 14	5.53 ± 0.15		-442	-2088	4	0
915ox_mt1432_@12	43	0.00202167 ± 25		9.81 ± 0.18	-3847	1360	-2	3
915ox_mt1432_@13	44	0.00202187 ± 24		9.91 ± 0.18	-3840	1288	-3	2
n5329ox_@10	45	0.00201278 ± 28	5.37 ± 0.19		-846	-2195	1	-1
n5329ox_@11	46	0.00201311 ± 16	5.54 ± 0.16		-1234	-2411	-2	-1

n5329ox_@12	47	0.00201276 ± 21	5.36 ± 0.17		-903	-2716	-1	-1
n5329ox_@13	48	0.00201266 ± 18	5.31 ± 0.16		-580	-2969	0	-1
n5329ox_@14	49	0.00201291 ± 23	5.43 ± 0.18		-280	-2948	3	-1
n5329ox_@15	50	0.00201266 ± 32	5.31 ± 0.21		-206	-2952	3	-2
915ox_mt1432_@14	51	0.00202080 ± 35			-3919	1452	-2	2
915ox_mt1432_@15	52	0.00202130 ± 14		9.63 ± 0.16	-3924	1389	-2	2
n5329ox_@16	53	0.00201279 ± 15	5.37 ± 0.16		-1282	-3505	-7	-2
<b>MY106</b>								
915ox_mt1433_@1	1	0.00202383 ± 18		9.89 ± 0.13	-5207	-116	-34	7
915ox_mt1433_@2	2	0.00202371 ± 19		9.83 ± 0.13	-5234	-178	-36	7
915ox_mt1433_@3	3	0.00202356 ± 12		9.75 ± 0.11	-5301	-161	-35	7
Tem2ox_mt1433_@1	4	0.00201975 ± 34		7.85 ± 0.19	-4667	-4968	-106	11
n5326ox_@1	5	0.00202015 ± 16	8.05 ± 0.12		-198	-1620	-25	7
n5326ox_@02	6	0.00202141 ± 22	8.68 ± 0.14		-103	-1658	-26	6
n5326ox_@03	7	0.00202162 ± 19	8.78 ± 0.13		-56	-1259	-18	7
n5326ox_@04	8	0.00202209 ± 20	9.02 ± 0.14		-56	-1132	-17	7
n5326ox_@05	9	0.00202119 ± 13	8.57 ± 0.11		430	-1259	-15	7
n5326ox_@06	10	0.00202149 ± 12	8.72 ± 0.11		-582	-1414	-24	7
915ox_mt1433_@4	11	0.00202390 ± 15		9.92 ± 0.12	-5301	-85	-31	7
915ox_mt1433_@5	12	0.00202406 ± 21		10.00 ± 0.14	-5316	-14	-30	7
Tem2ox_mt1433_@2	13	0.00202034 ± 21		8.14 ± 0.14	-4707	-4935	-103	10
n5326ox_@07	14	0.00202198 ± 19	8.96 ± 0.13		-813	-1420	-24	6



n5326ox_@08	15	0.00202105 ± 27	8.50 ± 0.16	-1163	-1406	-27	6
n5326ox_@09	16	0.00202016 ± 22	8.06 ± 0.14	-1184	-897	-20	6
n5326ox_@10	17	0.00201966 ± 16	7.81 ± 0.12	-1091	-890	-20	6
n5326ox_@11	18	0.00202049 ± 20	8.22 ± 0.13	-532	-1036	-17	7
n5326ox_@12	19	0.00202032 ± 18	8.13 ± 0.13	-398	-1414	-22	7
915ox_mt1433_@6	20	0.00202394 ± 17	9.94 ± 0.13	-5311	58	-28	7
915ox_mt1433_@7	21	0.00202371 ± 18	9.83 ± 0.13	-5606	16	-29	6
Tem2ox_mt1433_@3	22	0.00202019 ± 12	8.07 ± 0.11	-4721	-4973	-102	8

---

**TABLE 5**

<b>Belt</b>	<b>Age (Ma)</b>	<b><math>\epsilon_{\text{Hf}}</math></b>	<b><math>\delta^{18}\text{O}</math> ‰</b>	<b>□□□□□□</b>	<b>Notes</b>
Eastern Province	266	-10.9 – -6.4		Pre to Post Collisional/ Arc	Palaeo-Tethys
Main Range Province	220 (80–70)	-13.5 – -8.8		Post Collisional	Palaeo-Tethys
Tagaung-Myitkyina Belt	172	18.1 – 10.8		?Pre-Collisional Arc	Meso-Tethys?
Mogok-Mandalay-Mergui Belt (Tin Province)	77–50	-1.2 – -15.2	5.6–8.3	Pre to Post Collisional or back-arc	Neo-Tethys
Mogok-Mandalay-Mergui Belt (Mogok Belt)	219; 123; 71–55; 17	-4.6 – -17.6	6.3–9.2	Post Collisional	Neo-Tethys
Wuntho-Popa Arc	102–98; 40 (16)	13.3 – 0.3	5.2–5.8	Pre and Post Collisional Arc	Neo-Tethys

TABLE 6

	Advantages	Requirements	Problems
<b>1) Greater Sibumasu</b> (Morley and Searle, 2017)	1) Is a good size for a ribbon continent, Lord Howe Rise is a good analogue. 2) Simplest model. 3) Compatible with detrital zircon data of Sevastjanova et al. (2016)	1) Pre Middle Cretaceous ophiolite (s) emplaced from west. 2) Gondwana origin for block. 3) Rifting can explain the stratigraphic variations in the Carboniferous-Permian section.	1) What to do with SW to southern extension of Luxi-Nujiang suture? 2) How to explain Carboniferous-Permian Cathaysian fauna in NE Central Myanmar Basin?
<b>2) West Burma Block A</b> (Gatinsky and Hutchison, 1987; Hall, 2012, 2014; Hall et al., 2009; Hutchison, 1989; Metcalfe, 2011b; Mitchell, 1993; Morley, 2012; Sevastjanova et al., 2016)	1) Evidence for location, and timing of collision (in Triassic) from detrital zircon data (Sevastjanova et al., 2016)	1) Gondwana origin for block. 2) Early collision or amalgamation with Sibumasu (Triassic). 3) Pre Middle Cretaceous ophiolite (s) emplaced from west. 4) Rifting can explain the stratigraphic variations in the Carboniferous-Permian section.	1) What to do with SW to southern extension of Luxi-Nujiang suture? 2) How to explain Carboniferous-Permian Cathaysian fauna in NE Central Myanmar Basin?
<b>3) West Burma Block B.</b> (Barber and Crow, 2009; Metcalfe, 2013)	1) Possibly Mt Victoria area represents a Gondwana fragment outboard of the Cathaysian Block. 2) Is consistent with the origin of terranes in Sumatra.	1) Cathaysian origin for block. 2) Collision in Triassic, then long-distance strike-slip motion to put in position adjacent to Sibumasu. 3) Pre Middle Cretaceous ophiolite (s) emplaced from west.	1) Evidence for Indosinian age strike-slip fault on eastern margin has yet to be established. 2) What to do with SW to southern extension of Luxi-Nujiang suture? 3) Does not directly address stratigraphic variations (particularly those in the Carboniferous-Permian) across Sibumasu
<b>4) West Burma Block C</b> (Audley-Charles, 1988; Metcalfe, 1990; Sengor, 1987; Veevers, 1988)		1) Separated from Western Australia in Jurassic. 2) Accreted to SE Asia in Cretaceous.	1) Timing of separation from Western Australia is incompatible in plate reconstructions with Cretaceous collision with Myanmar (Hall, 2012, 2014). 2) Scenario incompatible with findings from Detrital zircon study of Sevastjanova et al. (2016)
<b>5) Irrawaddy Block</b> (Ridd, 2016; Ridd, 2017)	1) Permits emplacement of pre-Mid Cretaceous ophiolites from the east. 2) Explains the projection of the Luxi-Nujiang suture from Yunnan into Myanmar.	1) Requires that the stratigraphic variations observed between eastern and western Sibumasu are so fundamentally different and incompatible as to need a suture zone between them. 2) A cryptic suture is located along the trend of the Pan Luang Fault in Myanmar, and the Three Pagodas-Ranong-Khlong	1) Sibumasu (Sibuma) reduced to very narrow continental sliver. 2) For incorrect reasons considers the metamorphics around Mogok to be separate (part of Sibuma) from rest of the metamorphic belt (part of the Irrawaddy Block). 3) No hard evidence for a (purely cryptic) suture (Luxi-Nujiang) on the

		Marui faults in Thailand. 3) That the Luxi-Nujiang Suture cuts across the Mogok Metamorphic belt north of Mogok.	eastern side of the Irrawaddy Block either in Myanmar or Thailand. 4) Requires unrealistic restoration of blocks onto Gondwana margin. 5) Incompatible with existence of Cathaysian fossils in Central Myanmar
<b>6) Western Myanmar Mogok Foreland</b> (Mitchell, 2018; Mitchell et al., 2015)	1) Permits emplacement of pre-Mid Cretaceous ophiolites from the east 2) Compared with Irrawaddy Block A model, the Mogok Metamorphic belt is considered as a single entity. 2) Explains the projection of the Luxi-Nujiang suture from Yunnan into Myanmar.	1) That the stratigraphic variations observed between eastern and western Sibumasu are so fundamentally different and incompatible as to require a suture zone between them. 2) A cryptic suture is located along the trend of the Pan Luang Fault in Myanmar, and the Three Pagodas-Ranong-Khlong Marui faults in Thailand. 3) That the Luxi-Nujiang Suture runs between the Mogok Metamorphic Belt and the Chaung Magyi formation.	1) No hard evidence for a (purely cryptic) suture (Luxi-Nujiang) on the eastern side of the Irrawaddy Block either in Myanmar or Thailand. 2) Incompatible with existence of Cathaysian fossils in Central Myanmar
<b>7) West Burma Platelet</b> (Rangin et al., 2013)		1) Treats Mt Victoria region as separate from the area under the Central Basin. 2) Requires a suture between Mt Victoria area, and the Central Myanmar.	1) Does not fit with findings of detrital zircon study of Sevastjanova et al. (2016). 2) Is only focused on origin of schists and Triassic clastics in eastern Indo-Burma Ranges, does not offer solution for Central Myanmar.
<b>8) Greater Sibumasu-Tengchong</b> (this study)	1) Compatible with detrital zircon data of Sevastjanova et al. (2016) 2) Accommodates a Meso-Tethys suture within Myanmar	1) Gondwana origin for block. 2) Rifting can explain the stratigraphic variations in the Carboniferous-Permian section.	1) Does not satisfactorily explain the location of the Myitkyina Ophiolite and arc-related rocks within the Tagaung-Myitkyina Belt.

## **Appendix A: NordSIMS Cameca 1280 Ion Probe Zircon U/Pb Geochronology Analytical Methodology**

Zircon U–Pb analyses on samples MY1, MY4 and MY9 was performed at the NordSIMS facility (Swedish Museum of Natural History, Stockholm) using a CAMECA IMS 1280 SIMS. Analytical procedures closely follow those of Whitehouse et al. (1999) and Whitehouse and Kamber (2005), using a ca. 6 nA O<sub>2</sub> primary ion beam to sputter an elliptic crater of ca. 20–25 µm. Secondary ions were measured at a mass resolution sufficient to resolve Pb ions from molecular interferences ( $M/\Delta M$  c. 5400) using a single ion-counting electron multiplier and a peak-hopping routine. All analyses were run in fully automated chain sequences. The U/Pb ratio calibration was based on regularly interspersed analyses of the 91500 zircon standard. Common lead corrections were made using the terrestrial Pb-isotope composition of Stacey and Kramers (1975) when the count rate of <sup>204</sup>Pb exceeded detection limit (3 × standard deviation of the detector background over the analytical session). Ages were calculated and presented using Isoplot v3.16; Ludwig (2004). Ages are presented at the 95% confidence (2σ) level and, when concordia ages are calculated, the quoted mean square of weighted deviates (MSWD) value is that of combined concordance and equivalence following the recommendation of Ludwig (2004).

## **Appendix B: Curtin GeoHistory Facility LA-(MC)-ICP-MS Split-stream U/Pb and Lu/Hf Geochronology Analytical Methodology**

Sample MY182 was analyzed for combined zircon U-Pb and Lu-Hf analysis through combined laser ablation inductively-coupled plasma mass

spectrometry (LA-ICP-MS) and multicollector mass spectrometry (MA-MC-ICP-MS) at the John de Laeter Centre, Curtin University. Zircon grains were ablated using a Resonetics RESolution M-50A-LR sampling system (incorporating a Compex 102 excimer laser) coupled to an Agilent 7700 ICP-MS. Following 15-20 seconds of background analysis, samples were ablated for 30 seconds at a 7 Hz repetition rate using a 33  $\mu\text{m}$  beam spot, and laser energy of 1.5 J/cm<sup>2</sup>. The sample cell was flushed by ultrahigh purity He (0.68 L min<sup>-1</sup>) and N<sub>2</sub> (2.8 mL min<sup>-1</sup>). Isotopic intensities were measured using an Agilent 7700s quadrupole ICP-MS, with high purity Ar as the plasma gas. In each scan of the mass spectrum, the dwell time for most elements was 0.01 s, with the exception of <sup>88</sup>Sr (0.02 s), <sup>139</sup>La (0.04 s), <sup>141</sup>Pr (0.04 s), <sup>204</sup>Pb, <sup>206</sup>Pb, <sup>207</sup>Pb, <sup>208</sup>Pb (0.03 s), <sup>232</sup>Th (0.0125 s), and <sup>238</sup>U (0.0125 s). International glass standard NIST 610 was used as the primary standard to calculate elemental concentrations other than Hf (using <sup>29</sup>Si as the internal standard element and an assumed 14.76 % Si content in zircon) and to correct for instrument drift. Hf in zircon samples was determined using standard zircon GJ-1 (Jackson et al., 2004) with <sup>90</sup>Zr as the internal standard element. Standard blocks were typically run after 20 unknown analyses. During the time-resolved analysis, contamination resulting from inclusions and compositional zoning was monitored, and only the relevant part of the signal was integrated. The trace element results for NIST 612 (secondary standard) using NIST 610 as the reference material and assuming 33.6 wt % Si, indicate that the accuracy was better than 3% for most elements with the exception of P (5%) and Fe (10%). The analytical precision was better than 10% for most elements.

### Appendix C: NIGL LA-MC-ICP-MS Lu-Hf Analytical Methodology

Samples MY1, MY4, MY9, MY106, MY34, MY37, MYYAD, and MY145 were analyzed at the NERC Isotope Geosciences Laboratory (NIGL) to measure their zircon Lu-Hf isotopic compositions using a Thermo Scientific Neptune Plus MC-ICP-MS coupled to a New Wave Research UP193UC excimer laser ablation system (see Spencer et al. (2015) for the full method description). Helium was used as the carrier gas through the 'TwoVol2' cell, and mixed with Argon at a Y-piece before the torch. Measurement comprised the masses:  $^{172}\text{Yb}$ ,  $^{173}\text{Yb}$ ,  $^{175}\text{Lu}$ ,  $^{176}\text{Hf}+\text{Yb}+\text{Lu}$ ,  $^{177}\text{Hf}$ ,  $^{178}\text{Hf}$ ,  $^{179}\text{Hf}$  and  $^{180}\text{Hf}$ , with a 1 second integration time during a 30 second ablation. A 35  $\mu\text{m}$  spot size was used, with a fluence of 7  $\text{j}\cdot\text{cm}^{-2}$ . Standard sample bracketing using reference material zircons Plešovice, Mud Tank and 91500 (Sláma et al., 2008; Woodhead and Hergt, 2005) allowed for the monitoring of precision and accuracy, correction for instrumental drift of the Lu/Hf ratio, and accuracy of the Yb ratio correction. Normalization of the laser ablation Hf isotope data was achieved with solution analyses of reference solution JMC475 (both un-doped and doped with up to 5 ppb Yb). The interference of  $^{176}\text{Yb}$  on the  $^{176}\text{Hf}$  peak was corrected using a  $^{176}\text{Yb}/^{173}\text{Yb}$  ratio calibrated for Hf mass bias using the Yb-doped JMC475 solutions (Nowell and Parrish, 2001). The  $^{176}\text{Lu}$  interference on the  $^{176}\text{Hf}$  peak was corrected using the measured  $^{175}\text{Lu}$  and an assumed natural ratio of  $^{176}\text{Lu}/^{175}\text{Lu}$  of 0.02653. Systematic uncertainties of Hf and Lu isotope ratios were propagated quadratically, incorporating the external variance of the reference material for each analytical session. The reproducibility of the  $^{176}\text{Hf}/^{177}\text{Hf}$  ratio of the reference materials ranges from 46 to 56 ppm, and the accuracy based on accepted values is <100 ppm. Lolite 2.5

(Paton et al., 2011) was used for data reduction. Full results of the samples and reference material are provided in the accompanying excel sheet. All uncertainties are reported at 2 sigma.

#### **Appendix D: NordSIMS Cameca 1280 Zircon O isotope analytical methodology**

Oxygen isotope analyses of samples MY1, MY4, MY106, MY145 were performed using a CAMECA IMS 1280 large geometry SIMS at the NordSIMS facility in Stockholm, Sweden following methods similar to those described by Whitehouse and Nemchin (2009). A critically focused Cs<sup>+</sup> primary beam with 20 keV impact was used to sputter the sample, and a low-energy electron flooding gun was used for charge compensation. The primary beam current was ca. 2 nA yielding a ca. 15 µm analytical spots, including a 10 µm raster to homogenize the beam. Each analysis consisted of an initial pre-sputter over a rastered 20 µm area to remove the gold coating, followed by centering of the secondary beam in the field aperture (field of view on the sample of 30 µm with 90x magnification transmission ion optics). The <sup>16</sup>O (ca. 2 x 10<sup>9</sup> cps) and <sup>18</sup>O ion beams were mass filtered at a mass resolution of ca. 2500 (M/ΔM) and analysed simultaneously using two Faraday detectors with amplifiers housed in an evacuated, temperature stabilized chamber. The secondary magnet field was locked at high stability using an NMR field sensor operating in regulation mode. All pre-sputter, beam centering and data acquisition steps were automated in the run definition. Typical internal precision obtained for individual run <sup>18</sup>O/<sup>16</sup>O ratios determined from 12 4-second integrations was ca. 0.1 ‰ (SE).



Fully automated sequences comprised two measurements of the reference zircon, Geostandards 91500 (Wiedenbeck et al., 2004) bracketing six measurements of unknown targets, over four analytical sessions. The regularly interspersed 91500 measurements were used to correct measured isotope ratios for any drift during the analytical session and for instrumental mass fractionation (IMF), assuming  $\delta^{18}\text{O}_{\text{V-SMOW}} = 9.86 \text{ ‰}$ . External precision on  $\delta^{18}\text{O}_{\text{V-SMOW}}$  was 0.14 ‰ (SD) and is propagated onto the internal precision to yield the overall uncertainty reported in Table 4. Six analyses of the Temora-1 zircon standard yield a weighted  $7.98 \pm 0.11 \text{ ‰}$  (SD), which is within error of the value of 7.93 ‰ reported by Valley (2003).

**Author Bios**

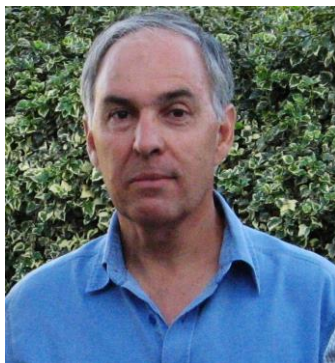
**Nick Gardiner** is a Research Fellow at Curtin University specializing in isotope geochemistry and geochronology. He has an undergraduate degree in geology from the University of Oxford, a MSc in geochemistry from the University of Leeds, and then returned to Oxford to complete a DPhil in isotope and metamorphic geochemistry. After a number of years working in the global commodities markets, he returned to Oxford (and academia) in 2013, and joined Curtin in 2015. His current research focuses on using geochemical tools to constrain magmatic–metamorphic processes, notably in: (a) petrogenetic controls on granite-hosted mineral deposits; (b) the growth and development of Earth's early continental crust; and (c) isotope systematics applied to crustal evolution studies.



**Mike Searle** is Professor of Earth Sciences at Oxford University. He has a PhD from the Open University, and has worked for over 30 years along the Oman - United Arab Emirates mountain belt. He has also worked along the Himalayan and Karakoram ranges and across the Tibetan Plateau carrying out fieldwork every year since 1985. For the last 10 years he has worked in SE Asia in Thailand, Vietnam and Myanmar, particularly in the Mogok Metamorphic Belt. He has authored over 220 papers, co-edited 5 Special Publications of the Geological Society, London, and authored 2 books, recently "Colliding Continents, a geological Exploration of the Himalaya, Karakoram, and Tibet" (OUP).



**Dr. Chris Morley** Mixed history of oil industry exploration and structural geology specialist for Amoco, Elf Aquitaine and PTTEP, coupled with teaching and research at Universiti Brunei Darussalam (Brunei), Aberdeen University (UK), Chulalongkorn and Chiang Mai Universities (Thailand). Has an extensive background in integrating outcrop geology, seismic and well data for both structural, regional geology, sedimentary and exploration projects (particularly in SE Asia and East Africa). Author of over 160 publications in international journals. Currently Program Director for International M.Sc. in Petroleum Geophysics at Chiang Mai University, Thailand.



**Laurence Robb** Before moving to the United Kingdom, Laurence Robb was Professor of Economic Geology in the School of Geosciences at the University of the Witwatersrand, South Africa, and between 2001-2005, Director of its Economic Geology Research Institute (EGRI). He is currently Visiting Professor in the Department of Earth Sciences at the University of Oxford. He has worked for over 30 years on many the great mineral districts of the African continent and is currently involved in research on the metallogeny of Myanmar/Burma and also Western Sahara.



**Professor Martin Whitehouse** is head of NordSIMS. His primary research interests are in applying radiogenic and stable isotopes to the evolution of the terrestrial planets, including the Earth. Specific questions include: the earliest evolution of the Earth-Moon system; the origin and nature of early crusts on the terrestrial planets and (on Earth) the transition from such protocrust to modern-style plate-tectonic recycling; the nature and evolution of the early surface reservoirs (atmosphere, hydrosphere); and evidence for early biogenic activity on Earth. These investigations are largely conducted using in situ microanalysis of both radiogenic and stable isotopes with the ion microprobe coupled with other in situ and bulk analytical methods.



**Nick Roberts** is a Research Scientist at the British Geological Survey, and is responsible for LA-SC-ICP-MS instrumentation as part of the NERC Isotope Geosciences Laboratory. Nick has expertise in applying geochronology and isotope geochemistry to a wide range of solid earth geoscience. Nick's specialist interests lie in understanding crustal evolution through Earth history and in collisional tectonics, particularly the Sveconorwegian and Himalayan orogenies. Nick has co-authored over seventy papers, edited four special volumes, and is currently an editor for the journals *Geology* and *Geoscience Frontiers*



**Chris Kirkland** is Associate Professor at Curtin University in Perth, Australia, and leader of the Timescales of Mineral Systems theme at Curtin CET node. He completed his PhD in isotope geology at University College Dublin investigating the geochronology of Arctic Norway. Following a post-doctoral fellowship at the Nordic ion microprobe facility, Swedish Museum of Natural History, he moved to Western Australia in 2008 to take up a position as Senior Geochronologist with the Geological Survey of Western Australia. In 2015 Chris moved to Curtin University and currently uses geochronology, stable and radiogenic isotopes to address a wide range of questions in the Earth Sciences.

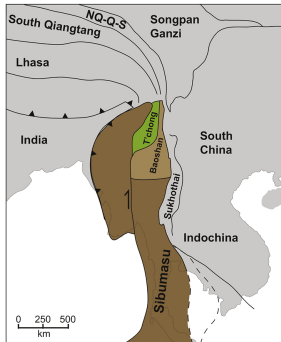
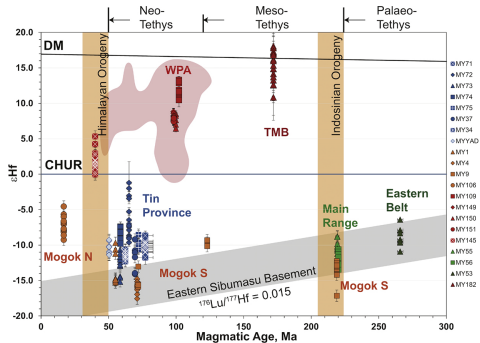




**Dr. Christopher Spencer** has been a research fellow at Curtin University since 2015. He received his BSc and MSc in Geological Sciences from Brigham Young University (USA) followed by a Ph.D. from the University of St Andrews (UK; completed 2014) and an isotopic apprenticeship from the NERC Isotope Geosciences Laboratory (NIGL) based at the British Geological Survey in Keyworth. He is an Associate Editor of *Geoscience Frontiers*, *Geosphere*, and *Geophysical Research Letters*. He is also the founder and editor-in-chief of *TravelingGeologist*. His research focuses on tectonochemistry to investigate orogenic processes and secular change of tectonic processes through Earth history.

## Highlights

- We present new zircon U-Pb, Hf and O isotope data from Myanmar
- isotopically characterising major magmatic belts informs on crustal architecture
- a tectonic model for Myanmar's Mesozoic-Cenozoic assembly is proposed



Graphics Abstract

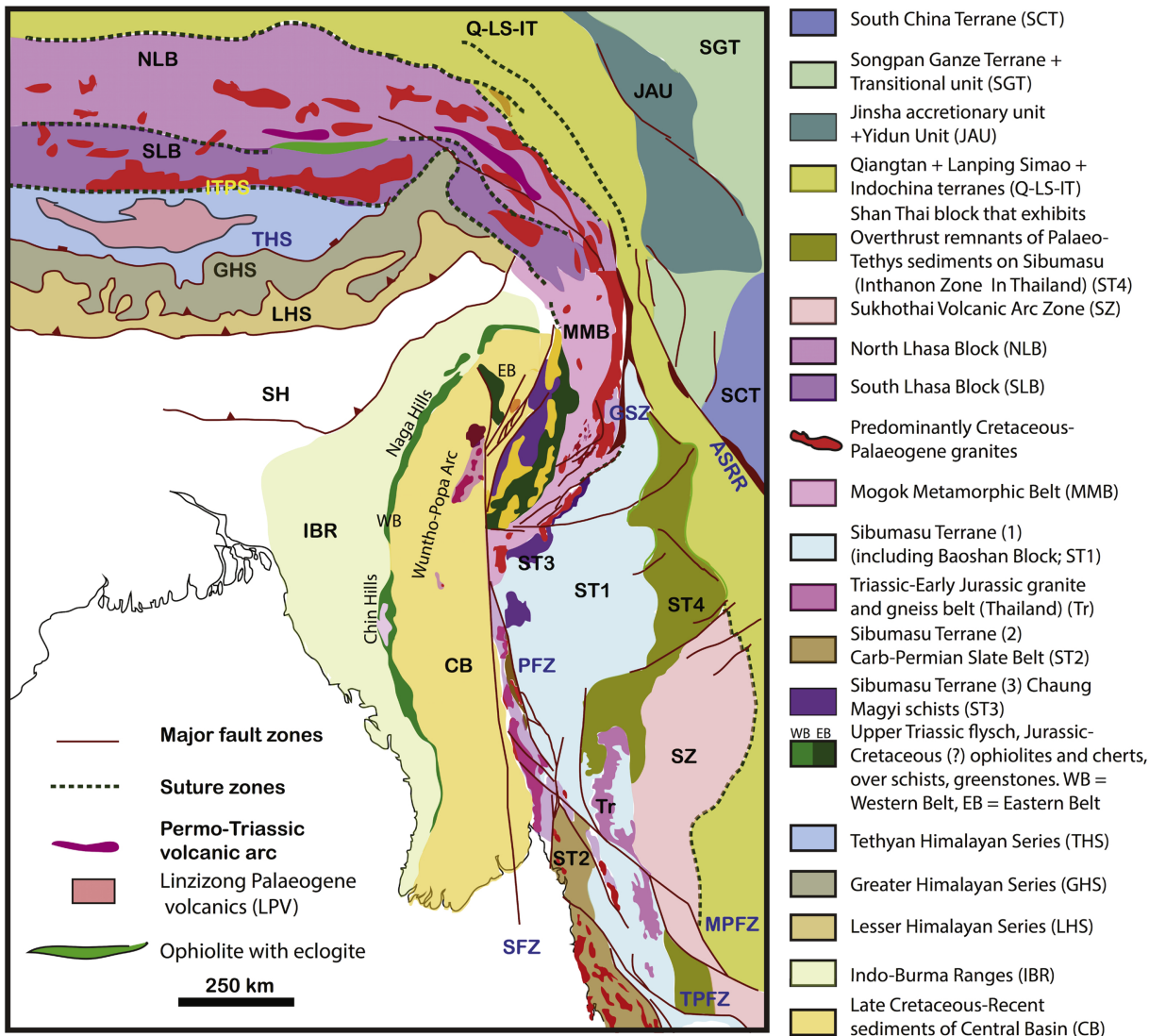


Figure 1

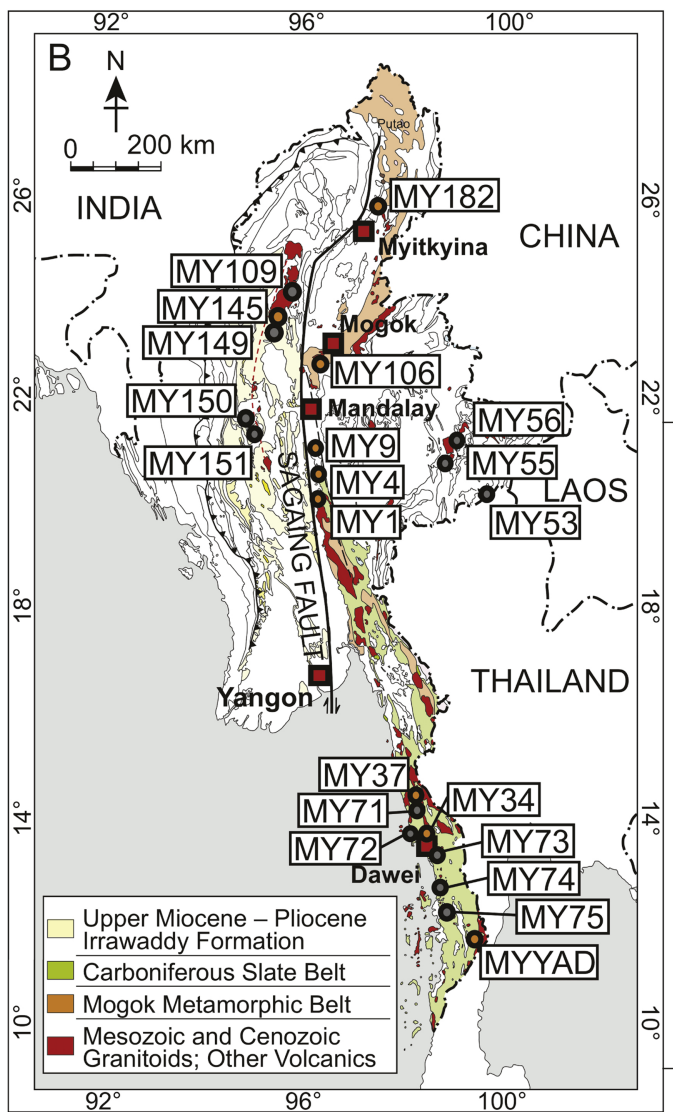
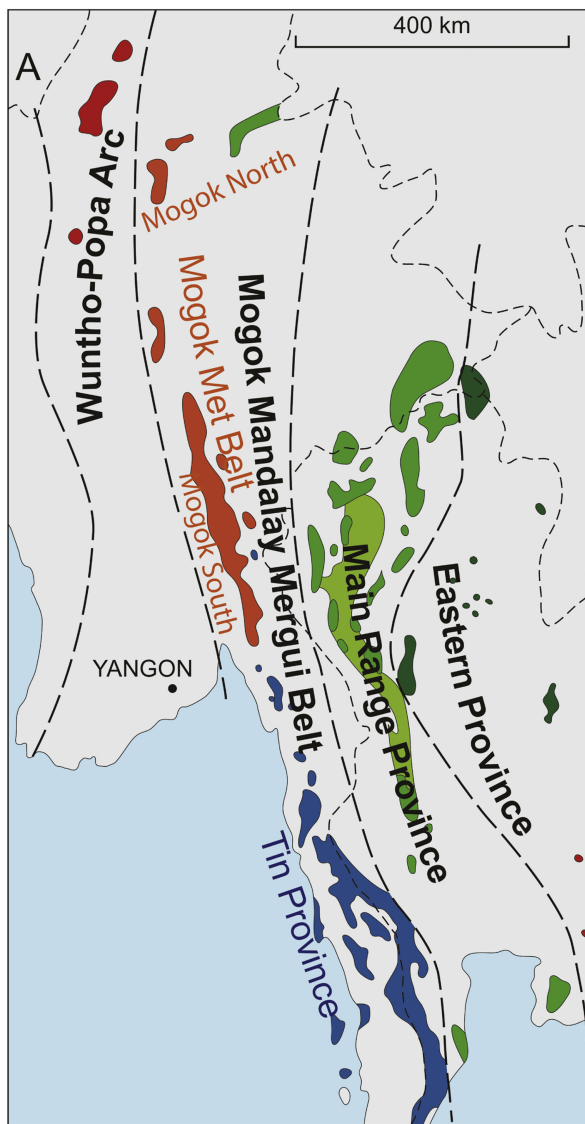


Figure 2

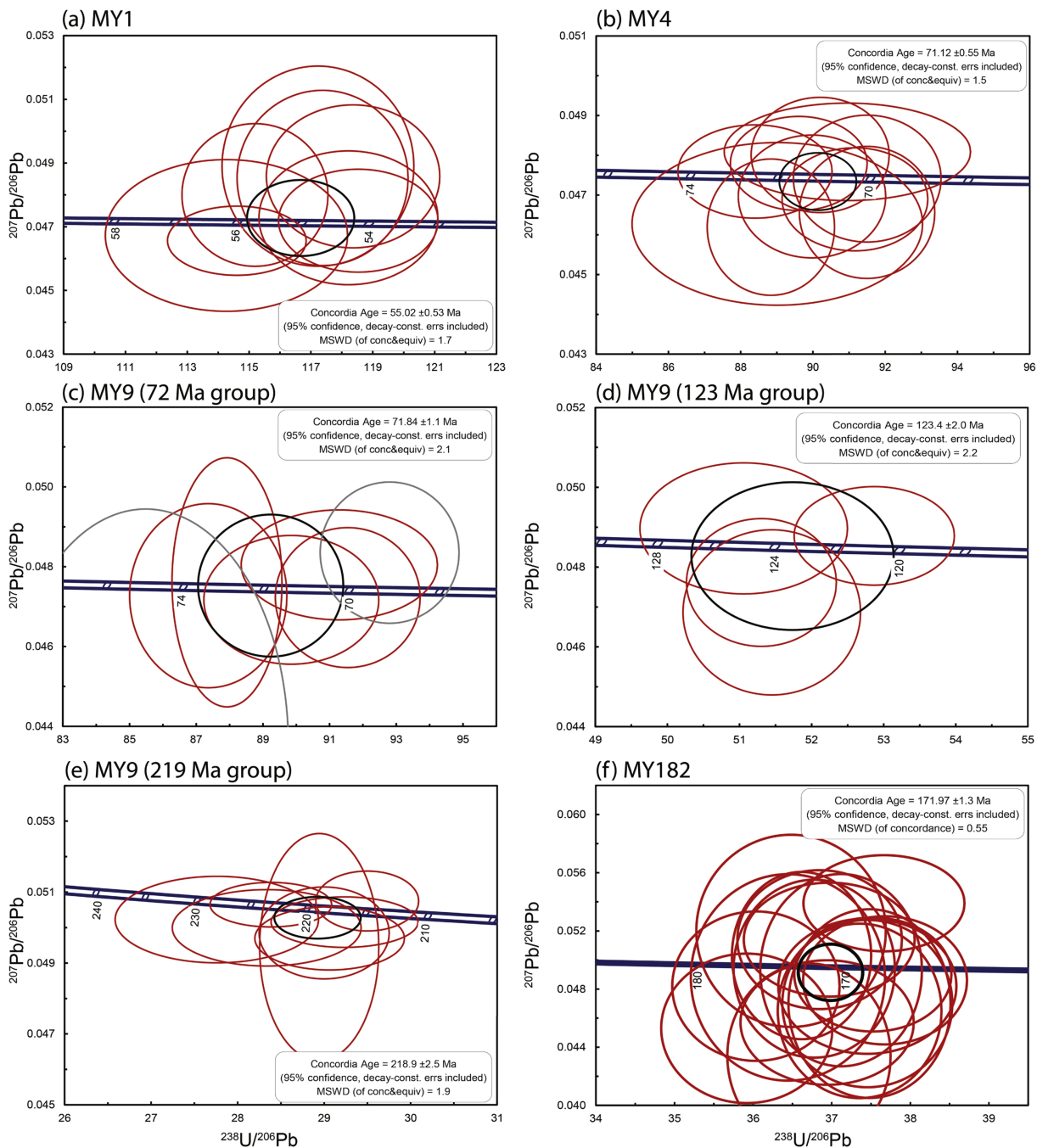


Figure 3



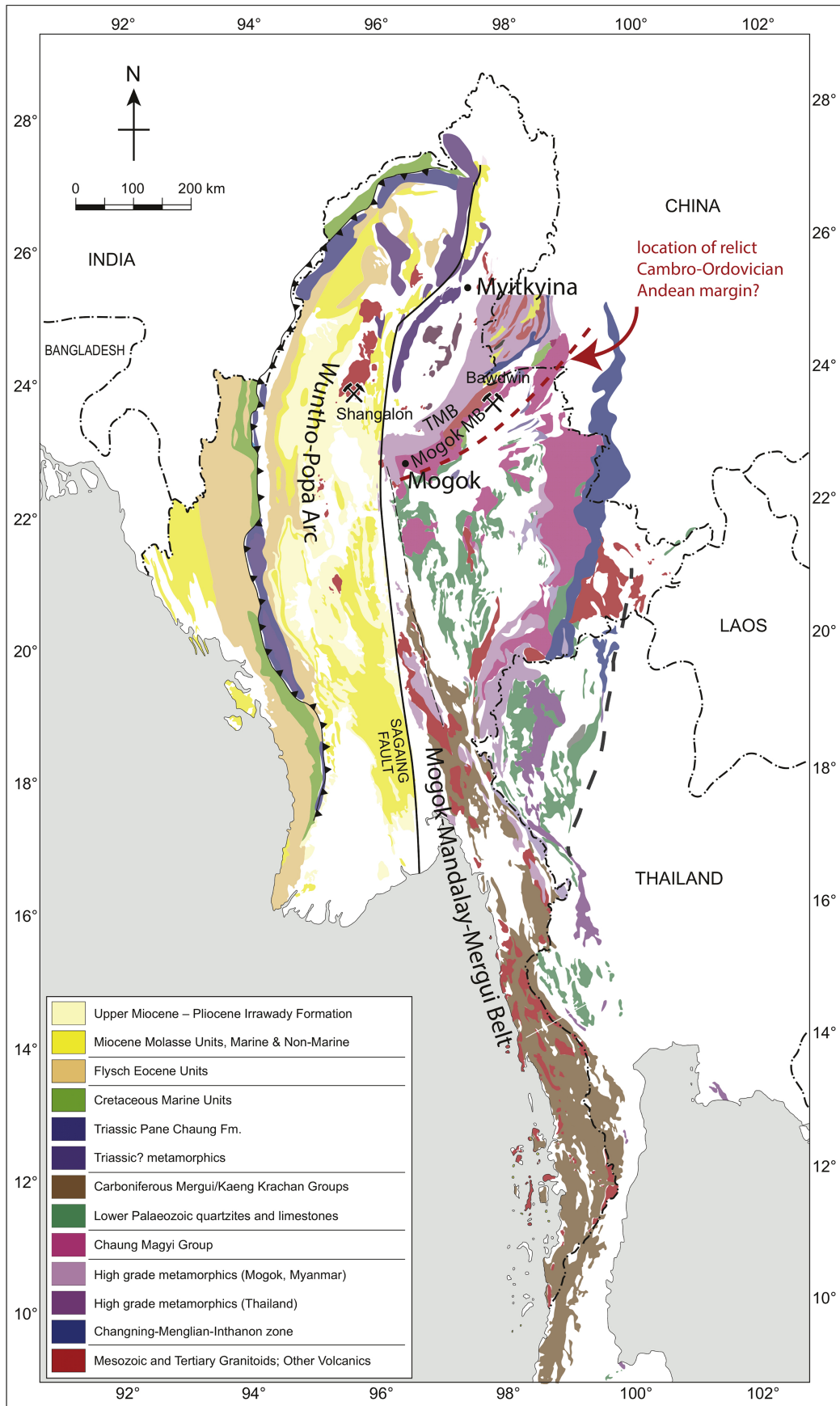


Figure 5



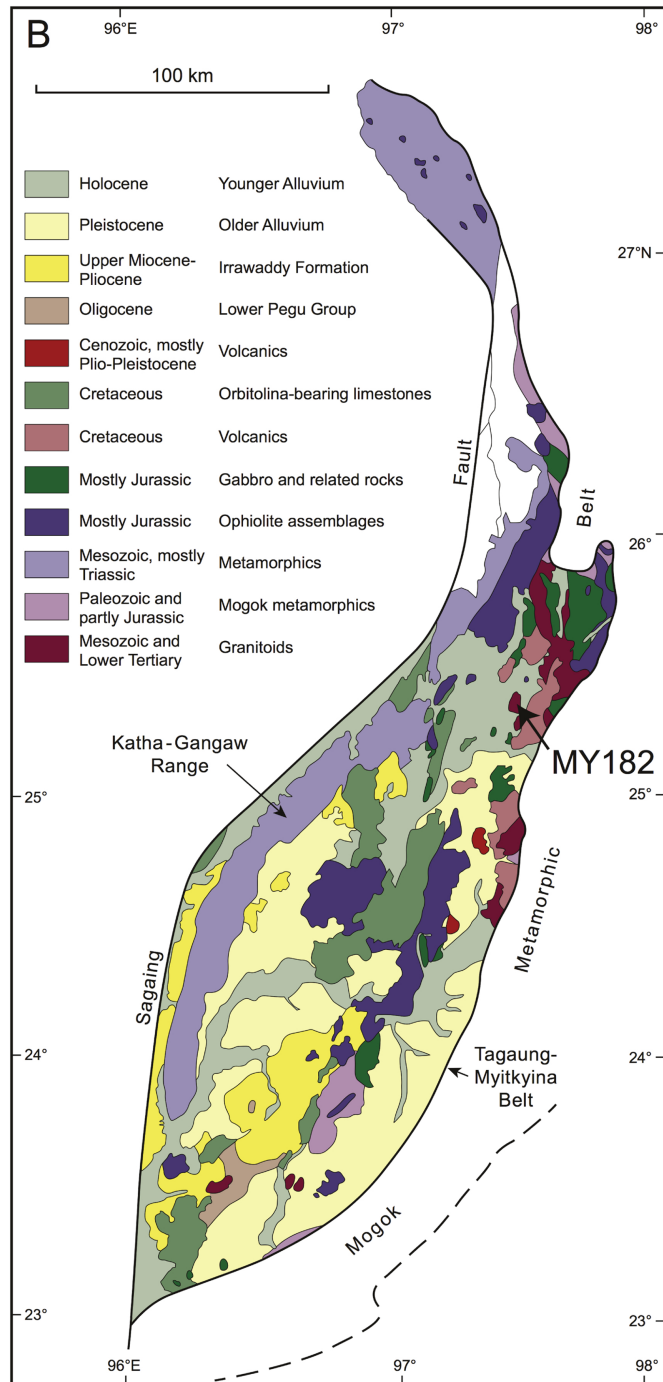
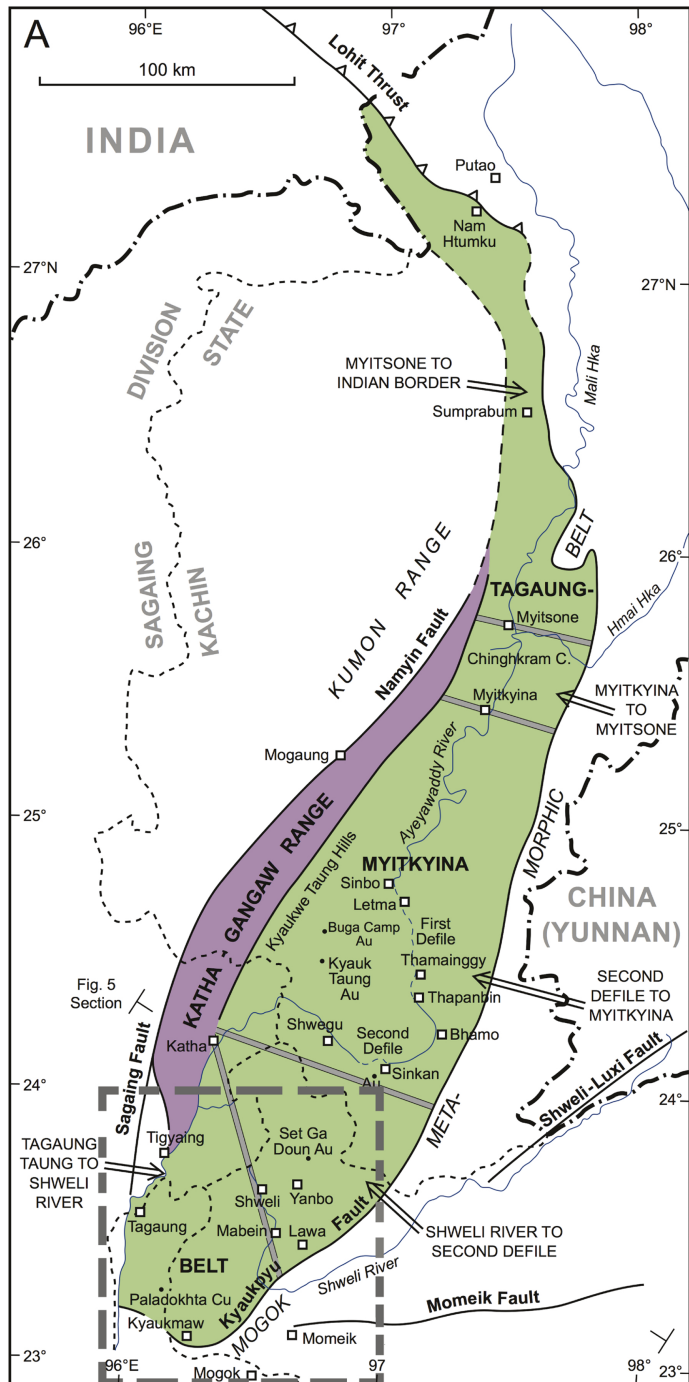


Figure 6

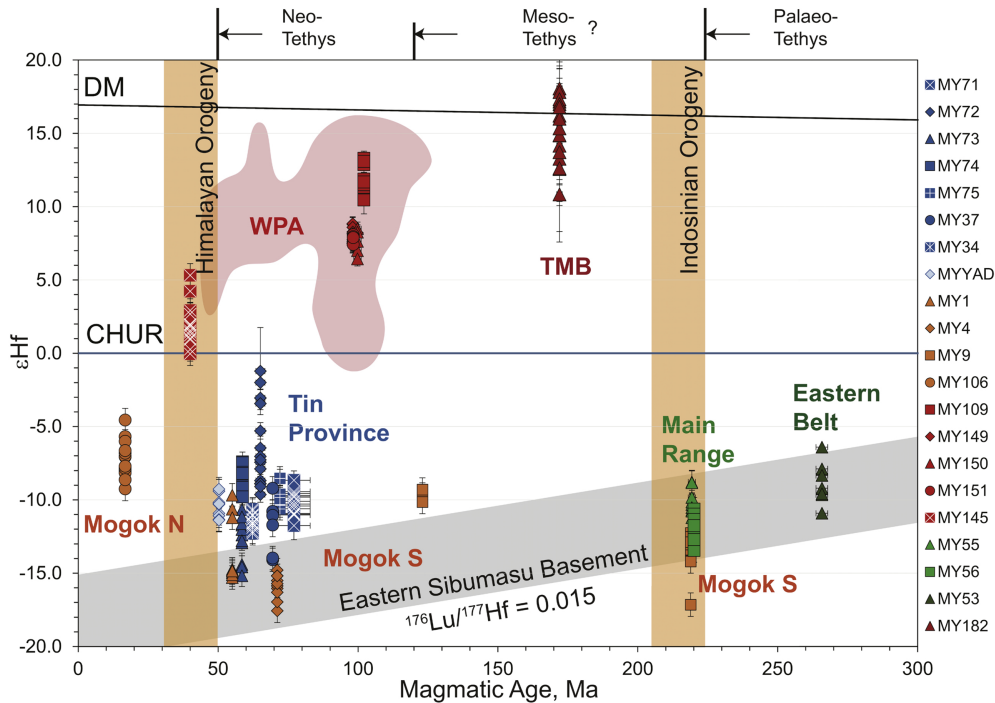


Figure 7

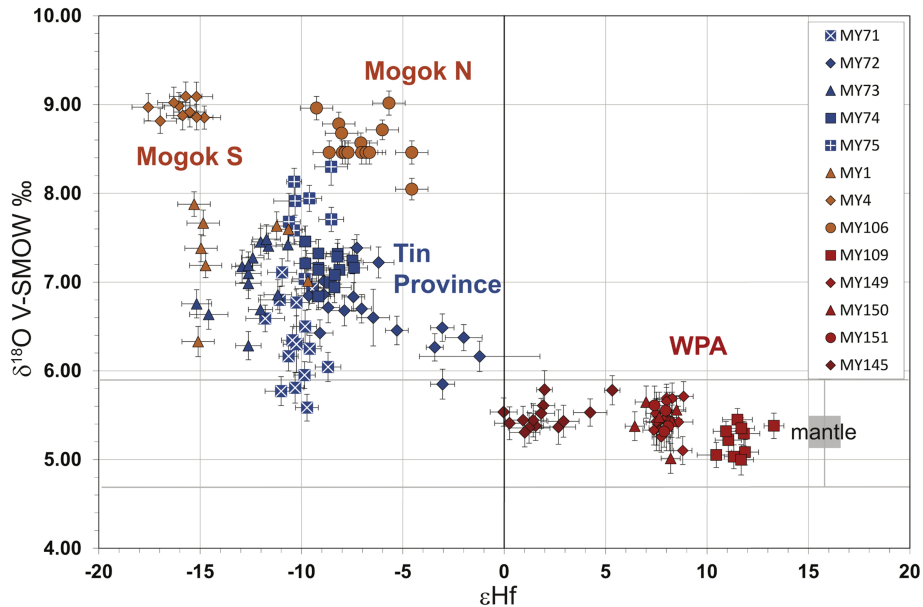


Figure 8

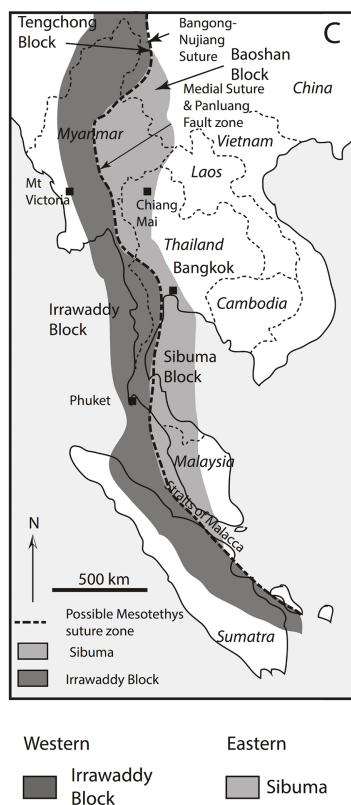
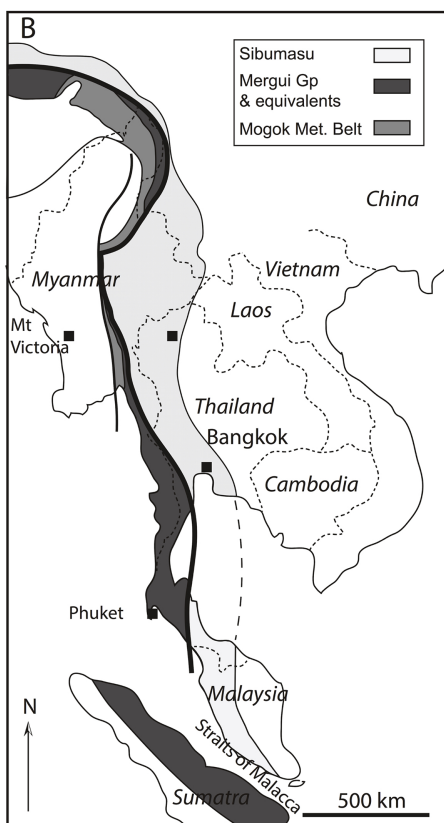
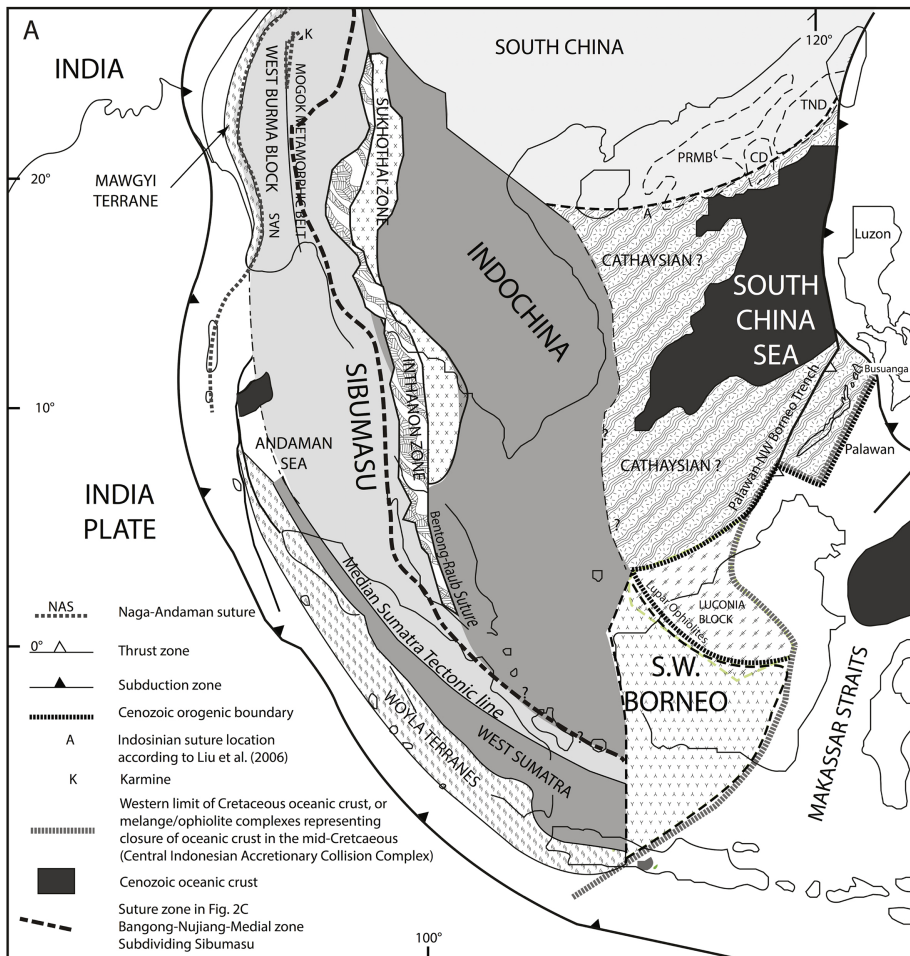


Figure 9

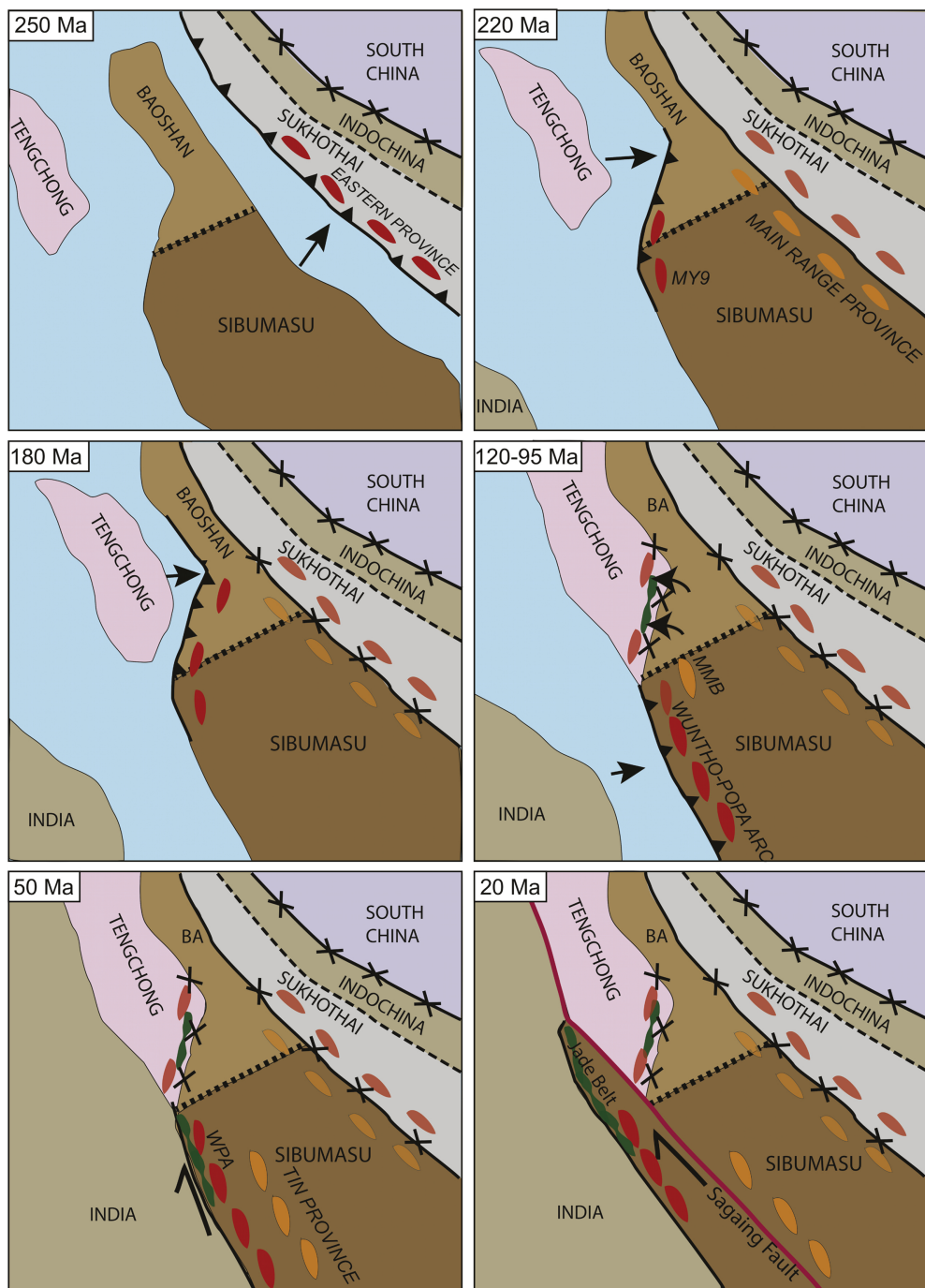


Figure 10

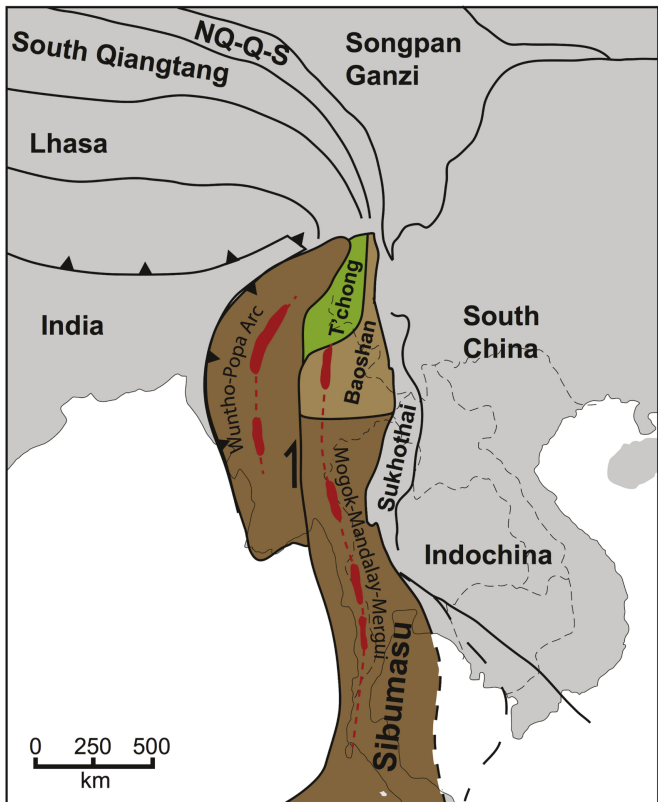


Figure 11



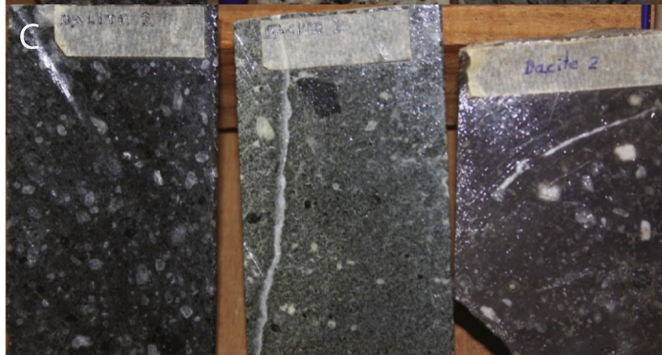
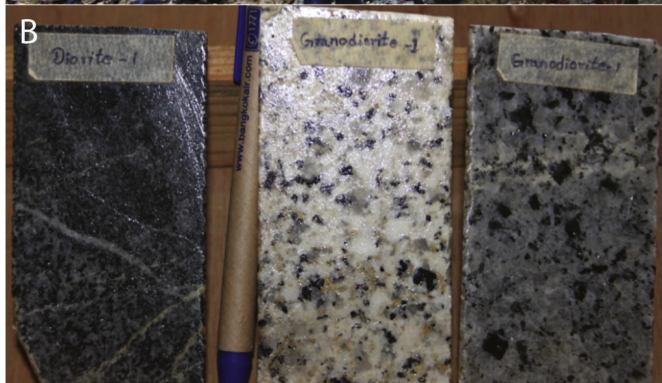
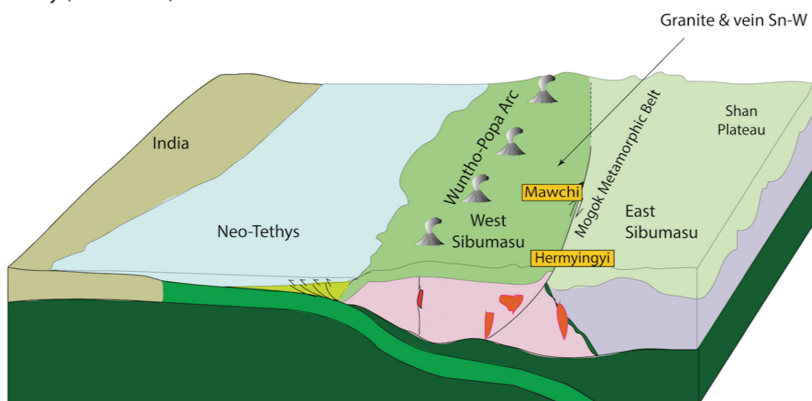
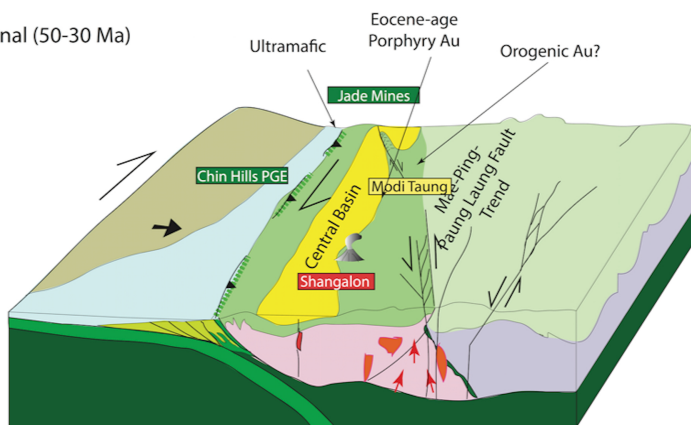


Figure 12

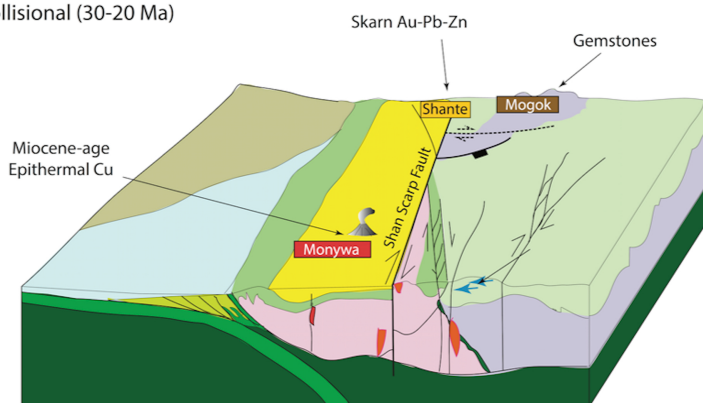
(a) Accretionary (100-50 Ma)



(b) Collisional (50-30 Ma)



(c) Late Collisional (30-20 Ma)



(d) Highly-Oblique Collisional (15-0 Ma)

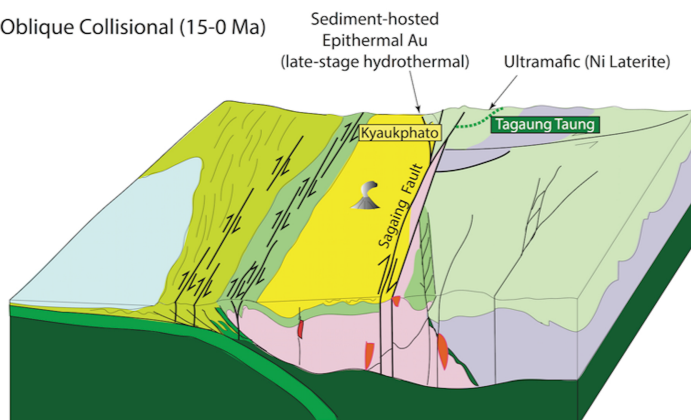


Figure 13



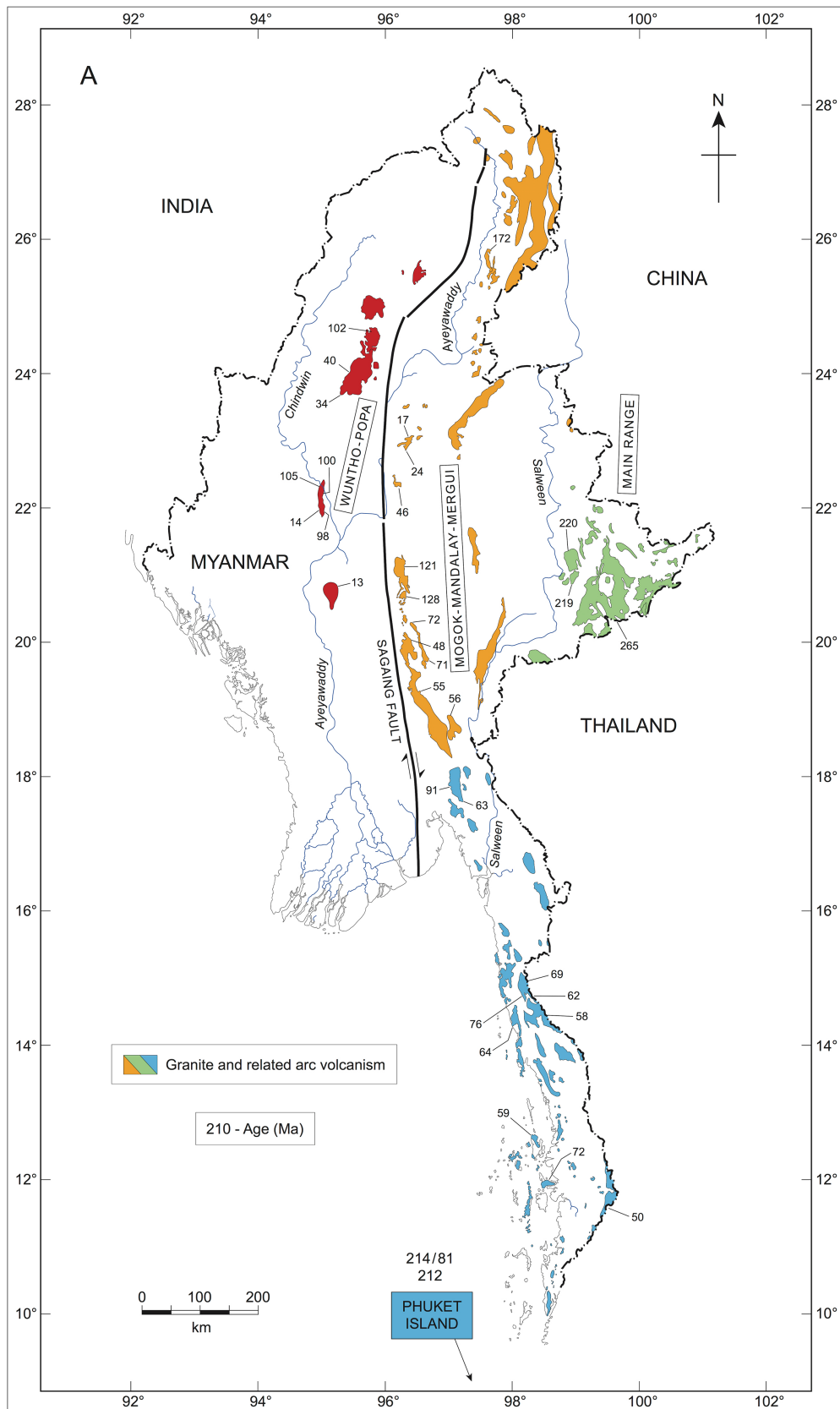


Figure 14a

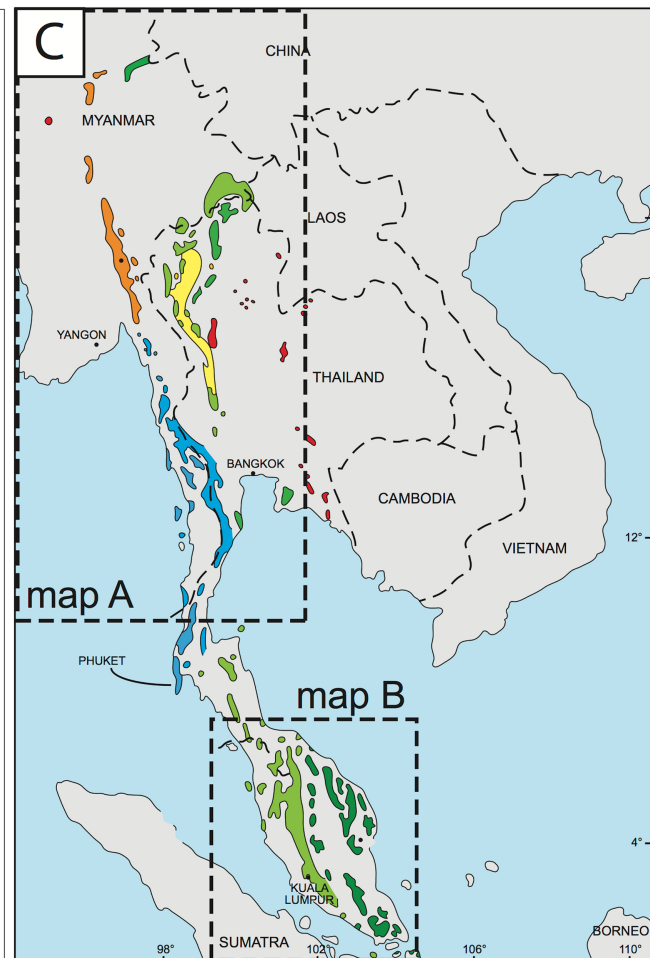
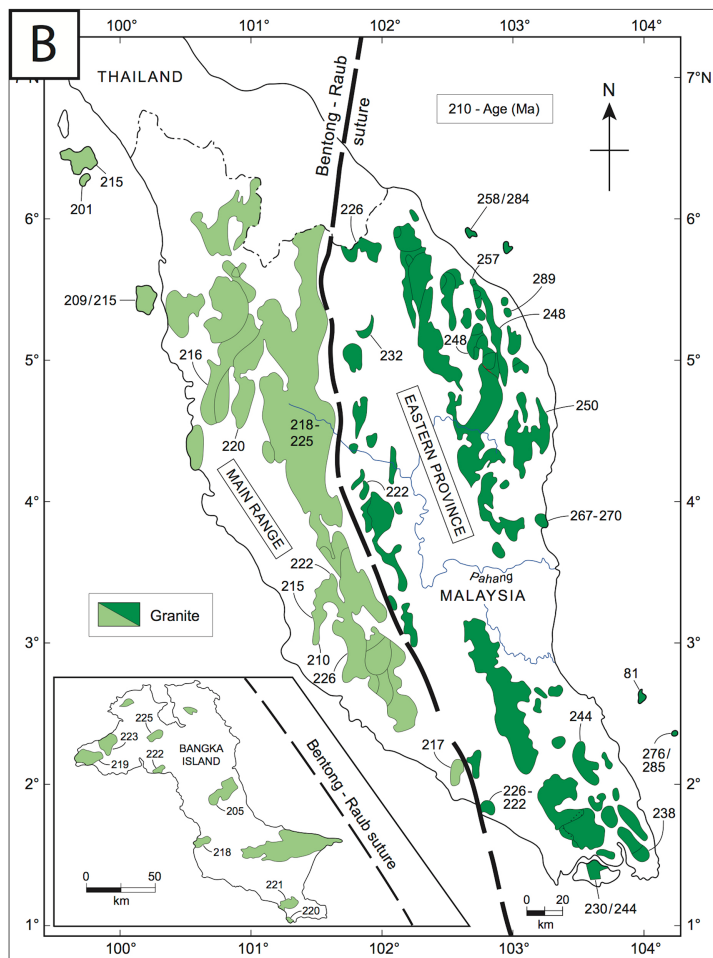


Figure 14bc

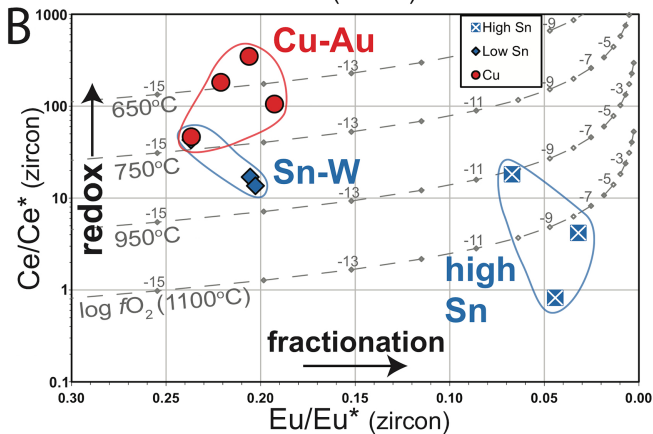
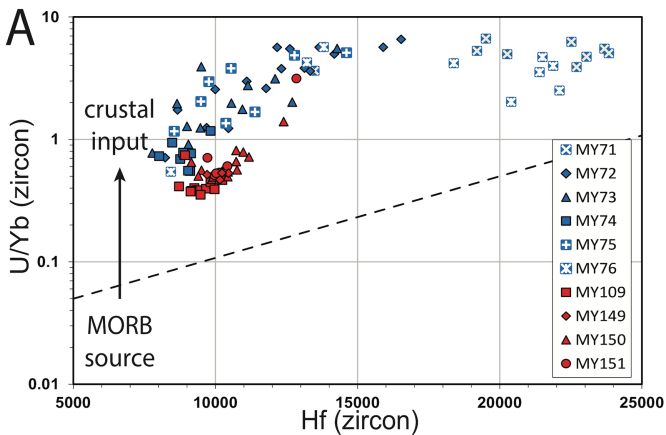


Figure 15